DESIGN AND CALIBRATION OF A X-RAY MILLIBEAM

A Thesis

Submitted to the Faculty

of

Purdue University

by

Joseph Walter Silvers

In Partial Fulfillment of the

Requirements for the Degree

of

Master of Science

December 2005

MAY 0 2 2006

REPORT DOCUMENTATION PAGE

Form Approved
OMB No. 0704-0188

1. AGENCY USE ONLY *(Leave blank)*	2. REPORT DATE	3. REPORT TYPE AND DATES COVERED
	29.Apr.06	THESIS

4. TITLE AND SUBTITLE
DESIGN AND CALIBRATION OF A X-RAY MILLIBEAM.

5. FUNDING NUMBERS

6. AUTHOR(S)
MAJ SILVERS JOSEPH W

7. PERFORMING ORGANIZATION NAME(S) AND ADDRESS(ES)
PURDUE UNIVERSITY

8. PERFORMING ORGANIZATION REPORT NUMBER
CI04-1772

9. SPONSORING/MONITORING AGENCY NAME(S) AND ADDRESS(ES)
THE DEPARTMENT OF THE AIR FORCE
AFIT/CIA, BLDG 125
2950 P STREET
WPAFB OH 45433

10. SPONSORING/MONITORING AGENCY REPORT NUMBER

11. SUPPLEMENTARY NOTES

12a. DISTRIBUTION AVAILABILITY STATEMENT
Unlimited distribution
In Accordance With AFI 35-205/AFIT Sup 1

12b. DISTRIBUTION CODE

13. ABSTRACT *(Maximum 200 words)*

DISTRIBUTION STATEMENT A
Approved for Public Release
Distribution Unlimited

14. SUBJECT TERMS	15. NUMBER OF PAGES
	130
	16. PRICE CODE

17. SECURITY CLASSIFICATION OF REPORT	18. SECURITY CLASSIFICATION OF THIS PAGE	19. SECURITY CLASSIFICATION OF ABSTRACT	20. LIMITATION OF ABSTRACT

DEDICATION

This thesis is dedicated to those who have most greatly impacted my life in preparation for and while attending Purdue University. To my nation and the United States Air Force, for selecting me into this challenging and gratifying academic program. To my fellow graduate students for their friendship and encouragement. To the Purdue faculty, and especially those in the School of Health Sciences. To my parents, [redacted], my Aunt [redacted] and the [redacted] Family. To my wife, [redacted], who has been my overwhelming supporter and best friend for almost 11 years. To my children, [redacted], who continue to provide a redeeming outlet and place of refuge. And to my loving Father in heaven, who has saved my life and brought me into the kingdom of the Son he loves. May He alone receive all glory, honor and praise.

"The views expressed in this article are those of the author and do not reflect the official policy or position of the United States Air Force, Department of Defense, or the U.S. Government"

ACKNOWLEDGMENTS

Many have had a profound effect on my life and education, but over the course of this project there were a few exceptional individuals who provided significant support and guidance. Without their help, I could not have imagined (much less completed) the details of this monumental and rewarding task.

I would like to thank Dr. James Schweitzer for assisting me with instrument calibrations and allowing me to use his laboratory and equipment for my research. I would like to thank Dr. Jian Li who provided me with the necessary lab space to conduct my experiments. I would like to thank Dr. George Sandison for his razor-sharp acuity and interest in my life and work. I'm thankful to Dr. Mike Ringor of Faith, Hope, and Love Cancer Care for opening up his schedule and helping me better understand various methods of detection and phantom configurations. I would especially like to thank Dr. Robert Stewart who has been instrumental in my education and one of the finest instructors and mentors I have ever met. Words cannot express my heartfelt gratitude for his investment in my life.

TABLE OF CONTENTS

Page

Page

LIST OF TABLES

Table Page

LIST OF FIGURES

Figure Page

Figure Page

ABSTRACT

Silvers, Joseph Walter. M.S., Purdue University, December 2005. Design and Calibration of an X-ray Millibeam. Major Professor: Robert D. Stewart.

It has been generally accepted that genetic damage is caused by the deposition of energy within the nucleus of a cell, and the extent of this damage is approximately proportional to the absorbed dose (the linear no-threshold dose-response model). However, recent experiments have shown that genetic alterations, cell death or transformation can occur in cells that receive no direct radiation at all – the so-called *bystander effect.* The goal of this project was to convert a broad-beam Hewlett-Packard (HP) 43855B Faxitron x-ray machine into a millibeam configuration that can target small sections of a cell culture dish with a precise dose of radiation. This millibeam provides novel capabilities for radiobiological studies into the mechanisms underlying bystander effects caused by *x*-rays, a low linear energy transfer (LET) radiation. Air kerma and absorbed dose calibration factors for the HP Faxitron were developed for use in Fricke dosimetry, parallel-plate ionization chambers, Lithium Fluoride thermoluminescent dosimetry (TLD), and EBT GafChromic film to characterize the spatial distribution and accuracy of the doses produced by the Faxitron. A new film scanning and analysis technique was developed using an off-the-shelf Canon 9950F 16-bit transmission scanner and the free ImageJ software from the National Institute of Health. A multi-layer shield composed of lead and steel was designed to convert the 26.035 cm Faxitron x-ray beam into a millibeam that targets 10 to 60% of the area on a 9-cm diameter cell culture dish.

ABSTRACT

Silvers, Joseph Walter. M.S., Purdue University, December 2005. Design and Calibration of an X-ray Millibeam. Major Professor: Robert D. Stewart.

It has been generally accepted that genetic damage is caused by the deposition of energy within the nucleus of a cell, and the extent of this damage is approximately proportional to the absorbed dose (the linear no-threshold dose-response model). However, recent experiments have shown that genetic alterations, cell death or transformation can occur in cells that receive no direct radiation at all – the so-called *bystander effect*. The goal of this project was to convert a broad-beam Hewlett-Packard (HP) 43855B Faxitron x-ray machine into a millibeam configuration that can target small sections of a cell culture dish with a precise dose of radiation. This millibeam provides novel capabilities for radiobiological studies into the mechanisms underlying bystander effects caused by *x*-rays, a low linear energy transfer (LET) radiation. Air kerma and absorbed dose calibration factors for the HP Faxitron were developed for use in Fricke dosimetry, parallel-plate ionization chambers, Lithium Fluoride thermoluminescent dosimetry (TLD), and EBT GafChromic film to characterize the spatial distribution and accuracy of the doses produced by the Faxitron. A new film scanning and analysis technique was developed using an off-the-shelf Canon 9950F 16-bit transmission scanner and the free ImageJ software from the National Institute of Health. A multi-layer shield composed of lead and steel was designed to convert the 26.035 cm Faxitron x-ray beam into a millibeam that targets 10 to 60% of the area on a 9-cm diameter cell culture dish.

1. INTRODUCTION

Many studies have been performed to examine the radiation response of cells at the molecular and cellular level. It has been generally accepted that genetic damage is caused by the deposition of energy by ionizing radiation within the nucleus of a cell (Preston 2004). Moreover, experiments have shown that the induction of many types of DNA damage, including double strand breaks (DSB), is proportional to the radiation absorbed dose (Frankenberg-Schwager 1990, Frankenberg *et al.* 1999). The linear no-threshold (LNT) relationship between absorbed dose and the amount of DNA damage produced in a cell suggests that biological responses arising from DNA damage, including possibly the induction of cancer, may be approximately proportional to the absorbed dose. However, the validity of LNT-based risk estimates for low- and intermediate doses of radiation is the subject of much ongoing debate (Preston 2003, Upton 2003, Higson 2004, Feinendegen 2005, Martin 2005, Trosko *et al.* 2005).

Although mechanistic and epidemiological studies provide some support for the application of LNT concepts in radiation protection (NCRP 2001), recent experiments have shown that genetic alterations, neoplastic transformations, apoptosis, and other effects can occur in cells that receive no direct radiation at all – the so-called *bystander effect* (Little 2000). The growing body results from low dose (Nagasawa and Little 1992), microbeam (Nelson *et al.* 1996, Hei *et al.* 1997, Prise *et al.* 1998), and medium transfer experiments (Mothersill and Seymour 1997) provide compelling evidence that cell-to-cell communication can enhance or suppress many of the biological events and processes involved in the development of cancer. Additional radiobiological studies are needed to better assess the potential impact on radiation responses of intercellular communication.

The goal of this project was to convert a broad-beam HP 43855B Faxitron x-ray machine into a millibeam configuration that can target small sections of a cell culture dish with a precise dose of radiation. This millibeam provides novel capabilities for future studies into the mechanisms underlying bystander effects caused by low doses of *x*-rays, a low-LET radiation.

The project scope includes the development of 130 kVp x-ray air kerma and absorbed dose calibration factors for use in Fricke dosimetry, parallel-plate ionization chambers, Lithium Fluoride (LiF) TLD, and EBT GafChromic film. The calibration factors that are traceable to National Institutes of Standards and Technology (NIST) radiation sources. The TLD-100, ionization chamber and Fricke dosimetry were used to investigate the operational characteristics of the HP Faxitron, and the GafChromic film was used to determine two-dimensional dose distributions across standard-sized cell culture dishes. A new film scanning and analysis technique was developed using an off-the-shelf Canon 9950F 16-bit transmission scanner and the free ImageJ software from the National Institute of Health (NIH). A multi-layer shield composed of lead and steel was designed to convert the 26.035 cm (10.25 inch) Faxitron x-ray beam into a millibeam that targets 10 to 60% of the area on a 9-cm diameter cell culture dish. Film and TLD measurements were performed to confirm that the dose outside the targeted area is negligible. The attenuation of x-rays within the cell culture medium and hardening of the beam by a 0.4 mm Cu filter were quantified.

This report is organized as follows. Chapter 2 provides an overview of the fundamental principles of radiation physics, dosimetry and shielding. The design and specifications of the HP Faxitron are also summarized in this chapter. Additional information about the HP Faxitron can be found in Appendix A. In Chapter 3, the operational characteristics and NIST-traceable calibration factors for the Fricke, TLD, ionization chamber, and GafChromic film are presented. Chapter 4 summarizes the results of a series of studies characterizing absorbed dose rates with and without the 0.4 mm Cu filter. Dose volume histograms (DVH) for cell culture dishes at prescribed locations within the x-ray beam,

with and without the 0.4 mm Cu filter and with and without the millibeam shield, are also presented in Chapter 4. The appendices provide detailed laboratory procedures related to the use of EBT film scanning and analysis system.

2. PRINCIPLES OF RADIATION PHYSICS AND DOSIMETRY

This chapter provides an overview of fundamental principles of radiation physics, dosimetry and shielding related to the HP Faxitron x-ray machine. The photon fluence (spectrum) and the half-value (HV) thickness of several common shield materials are reported for the HP Faxitron. A multi-layer shield composed of steel and lead is designed to attenuate the 130 kVp unfiltered Faxitron beam by a factor of 10^6. Holes in the shield were machined so that the x-ray beam can be focused to a beam that corresponds to 10 to 60% of the area of a standard 9-cm cell culture dish.

2.1. Radiation Physics

2.1.1. Ionizing and Non-Ionizing Electromagnetic Radiation

The wavelength, λ, and energy, E, of all types of electromagnetic radiation are related by:

$$E = \frac{hc}{\lambda}, \tag{2.1}$$

where h is Planck's constant (4.13×10^{-21} eV s) and c is the speed of light in a vacuum (3×10^8 m s^{-1}). Figure 2.1 shows the classification of electromagnetic radiation into ionizing and non-ionizing radiation. The elements with the lowest and highest ionization potential are cesium (3.89 eV) and helium (24.6 eV), respectively. Photons with energies less than 3.89 eV ($\lambda > 318.8$ nm) are non-ionizing radiation, photons with energies greater than 24.6 eV ($\lambda < 50.4$ nm) always have sufficient energy to cause ionization, and photons with energies between 3.89 eV and 24.6 eV may be either ionizing or non-ionizing radiation depending on the nature of the attenuating medium. Visible light corresponds to photons with energies from 1.77 eV ($\lambda = 700.6$ nm) to 3.10 eV ($\lambda = 400$

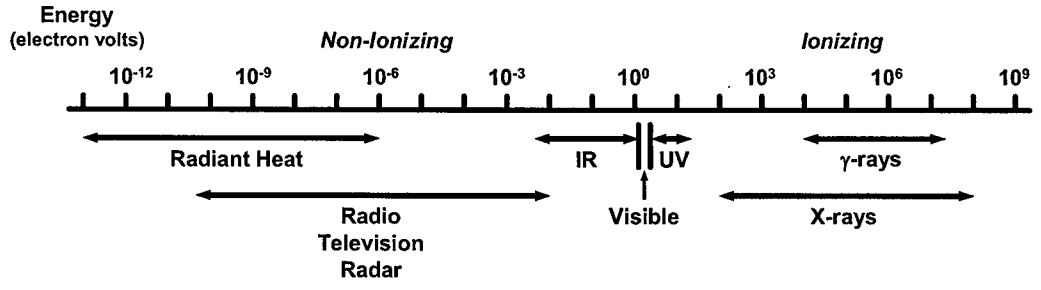

Figure 2.1. Classification of electromagnetic radiation into ionizing and non-ionizing radiation.

nm) and are thus non-ionizing electromagnetic radiation. Ultra-violet (UV) radiation spans the energy range from 3.10 eV (UV-A) to 12.4 eV (UV-C, $\lambda = 100$ nm). Because UV radiation, especially UV-C, exceeds the ionization energy of many of the elements, it is often considered ionizing radiation rather than non-ionizing radiation.

Although x-rays and γ-rays are both electromagnetic radiation, they arise from very different processes. Electromagnetic radiation is produced when charged particles are accelerated in the electromagnetic field surrounding the nucleus of an atom. Photons are also produced when electrons in high-energy states transition to lower energy states after ionization of an inner shell electron. The photons produced in these processes are collectively referred to as *x-rays*. Typical energy ranges for diagnostic x-rays (< 220 kVp) are from 10 keV ($\lambda = 0.124$ nm) to 220 keV ($\lambda = 5.64$ pm). In radiation therapy for the treatment of cancer, x-ray energies are often in the 6 MeV ($\lambda = 0.21$ pm) to 18 MeV ($\lambda = 0.069$ pm) range. In contrast to x-rays, γ-rays are monoenergetic photons emitted when the nucleus of an atom is left in an excited state after radioactive decay. The γ-ray is emitted with the nucleus transitions from the excited state to a ground state. Typical energies for γ-rays range from 2.46 keV (^{173}Er, $\lambda = 0.504$ nm) to 11.3 MeV (^{20}Na, $\lambda =$ 0.11 pm). Common γ-rays emitters include ^{60}Co (1.17 MeV, $\lambda = 1.06$ pm; 1.33 MeV, $\lambda =$ 0.93 pm) and ^{137}Cs/^{137m}Ba (0.662 MeV, $\lambda = 1.87$ pm).

2.1.2. Photon Interaction Mechanisms

Photon interactions are quantified by the linear attenuation coefficient μ or, equivalently, the mass attenuation coefficient, μ/ρ (ICRU 1980). The linear attenuation coefficient is the probability, per unit distance traveled, that a photon interacts with matter. Interaction coefficients for the elements and common biological and shielding materials are available through the NIST Physical Reference Data website (http://physics.nist.gov/PhysRefData). For photons with energies less than 10 MeV, the three principal photon interaction mechanisms are photoelectric absorption, Compton scattering, and pair production, i.e.,

$$\frac{\mu}{\rho} = \frac{\mu_{PE}}{\rho} + \frac{\mu_C}{\rho} + \frac{\mu_{pp}}{\rho}. \tag{2.2}$$

Here, μ_{PE}, μ_C and μ_{pp} denote the linear attenuation coefficients for photoelectric absorption, Compton scattering, and pair production, respectively.

Photoelectric absorption occurs when a photon is absorbed and an electron is ejected (refer to Figure 2.2), usually from the K, L, or M shells of an atom. The majority of the photon's energy is transferred to the electron, although a small fraction of the energy may be transferred to the "recoil" atom. For the photoelectric effect to occur, the energy of the incoming photon must exceed the binding energy of the orbital electron. The maximum kinetic energy (T_e) of a photoelectron is given by the formula

$$T_e = E - BE_e, \tag{2.3}$$

where E is the energy of the incident photon and BE_e is the binding energy of the electron.

When electrons from higher-energy orbitals fill vacancies created by the ejection of the photoelectron, characteristic x-rays or Auger electrons are emitted. The mass attenuation coefficient for photoelectric absorption cross section per atom is proportional to the fourth power of the atomic number (Z) for the atom and inversely proportional to the third power of energy for the photon, i.e., $\mu_{PE}/\rho \propto Z^4 / E^3$. Thus, low-energy photons

are much more prone to interact with high-Z absorbers through photoelectric absorption than low-Z materials.

As illustrated in Figure 2.3, Compton scattering, also referred to as incoherent scattering, occurs when an incoming photon transfers some of its kinetic energy to an orbital electron. In Compton scattering, the transfer of energy from the photon to the electron is governed by conservation of energy and linear momentum. When the binding energy of the electron to the nucleus is neglected, the energy of the photon with energy E_i that scatters through angle θ_s will have an energy (E_f) that is determined by the formula:

$$\frac{1}{E_f} - \frac{1}{E_i} = \frac{1}{m_e c^2}(1 - \cos\theta_s), \tag{2.4}$$

The maximum energy transferred to the recoil electron, $E_i - \frac{m_e c^2}{2}$, is the maximum energy lost by the photon, $E_i - E_f$, and occurs when $\theta_s = 180°$.

Pair production is an energy-to-matter transformation wherein a photon is absorbed within the nucleus of an atom and a positron-electron pair (e^+ *and* e^-) with kinetic energy equal to

$$T_{e^+} + T_{e^-} = E_\gamma - 2m_e c^2. \tag{2.5}$$

Here, E_γ is the energy of the incident photon and $m_e c^2$ is the rest mass energy of an

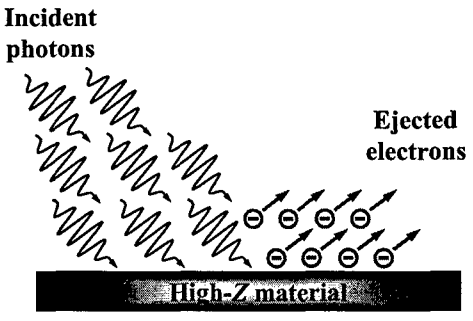

Figure 2.2. Idealized schematic illustrating the photoelectric effect.

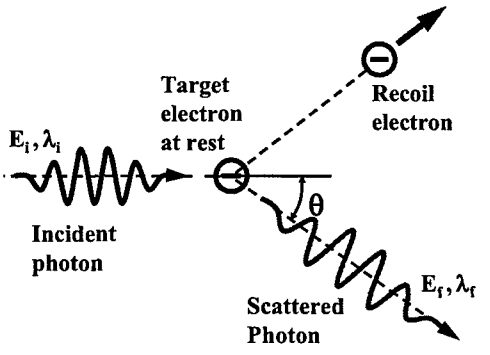

Figure 2.3. Idealized schematic illustrating Compton scattering of a photon from a free electron.

electron (511 keV). Photons with energies less than 1.02 MeV do not interact through pair production because they do not impart sufficient energy to create a positron-electron pair.

As illustrated in Figure 2.4 for copper, photoelectric absorption and Coherent scattering are the two main interaction mechanisms below about 150 keV (0.15 MeV). Coherent scattering, which occurs when a photon interacts with the entire atom, competes with photoelectric absorption, but is a relatively unimportant energy deposition mechanism compared to the photoelectric effect. For higher-Z materials such as copper, steel and lead, Compton scattering is the most important interaction mechanism between about 150 keV and 5 MeV. In low-Z materials such as water, Compton scattering is an important interaction mechanism for photons with energies as low as 10 keV (Figure 2.5). The 130 kVp HP Faxitron produces x-rays with a peak energy of 130 keV. For common (beam hardening) filters and shielding materials, photoelectric absorption is the dominate interaction mechanism below 130 keV. For water and cell culture media, Compton scattering is the dominate interaction mechanism below 130 keV.

2.1.3. Electron Interaction Mechanisms

As photons traverse matter, they produce energetic secondary electrons through processes such as Compton scattering and photoelectric absorption. Charged particles interact continuously with essentially all of the atoms along their path, and thousands of interactions are typically required before the initial kinetic energy of the electron is completely transferred to the surrounding medium. The transfer of energy from a charged particle to the surrounding medium is quantified by the stopping power, $S = -dE/ds$, where dE is the differential amount of kinetic energy lost along a small path ds. Typical units for the stopping power are keV/μm.

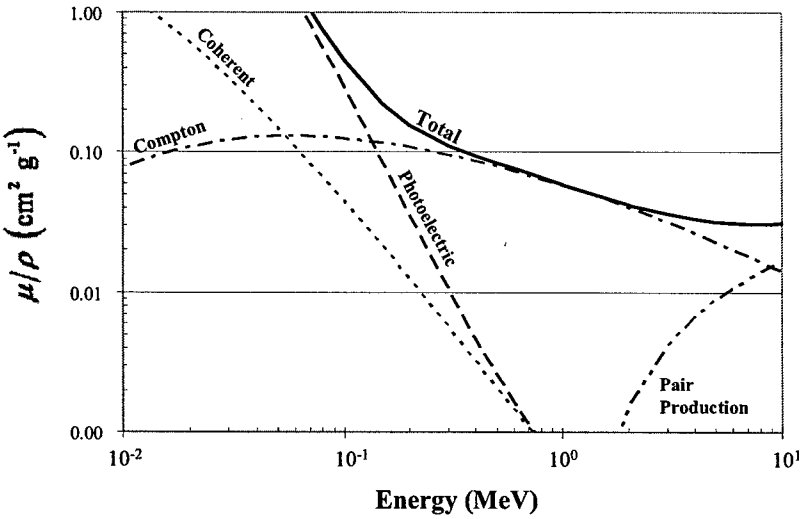

Figure 2.4. Mass attenuation coefficient in Cu for photons (NIST 2005).

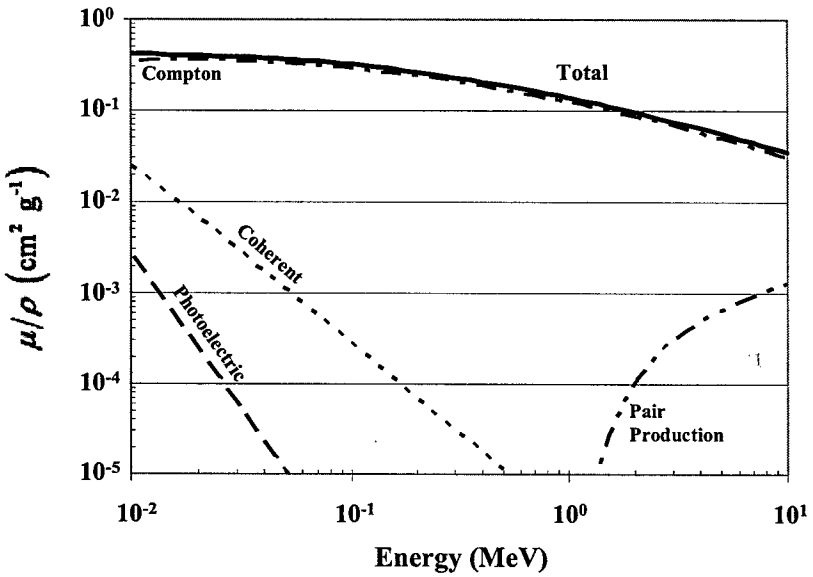

Figure 2.5. Mass attenuation coefficient in water for photons (NIST 2005).

For electrons, total stopping power is the sum of the collisional stopping power S_{coll} and the radiative stopping power S_{rad} (ICRU 1984), i.e., $S = S_{coll} + S_{rad}$. The collisional stopping power describes energy loss due to Coulombic interactions, and, for electrons with energies 0.01 to 10 MeV, can be expressed as

$$S_{coll} = \rho\left(\frac{Z}{A}\right) f(I,\beta), \tag{2.6}$$

where ρ is the density of the stopping medium, Z/A is the ratio of the medium's atomic number to the mass number, and $f(I,\beta)$ is a generally complicated function of the effective ionization potential of the medium, denoted I, and the speed of the electron relative to the speed of light, $\beta = v/c$. The radiative stopping power, which is related to the production of bremsstrahlung may be described by the formula (ICRU 1984):

$$S_{rad} = \left(\frac{\rho N_a}{A}\right)\left(T + m_e c^2\right) Z^2 F(E,Z). \tag{2.7}$$

Here, $\rho N_a/A$ is the atomic density of the absorber medium, T is the kinetic energy of the electron, $m_e c^2 = 511$ keV is the rest mass energy of the electron, Z is the atomic number of the absorber, and $F(E,Z)$ is a function that varies slowly with E for energies up to 1 MeV. Eq. (2.7) implies that the emission of bremsstrahlung is most important for energetic electrons in a high-Z medium.

The energy transferred to a small region of matter per unit distance traveled through that region is always greater than or equal to the actual energy deposited inside that region. The local energy deposition rate along the path of a charged particle is referred to as LET. The LET of a charged particle is proportional to the square of the charge and inversely proportional to the particle's kinetic energy, i.e., $LET \propto q^2 T^{-1}$. The relative biological effectiveness of ionizing radiation tends to increase with increasing LET. Electrons and photons (whose kinetic energy is transferred to electrons through photon interaction mechanisms) are considered low-LET radiation (< about 1-5 keV/μm). Energetic ions, such as α particles and protons, are usually considered high LET radiations. The total energy deposited by a charged particle along its path, LET_∞, is referred to as the unrestricted LET and this quantity is exactly equal to the stopping

power, *S*. The restricted LET (LET_{Δ}) only includes those energy deposits smaller than some threshold energy, Δ (ICRU 1970).

Electrons follow a tortuous path through matter because of multiple elastic and inelastic scattering events caused by Coulomb interactions. The maximum distance into a material that a charged particle can penetrate before losing all of its kinetic energy is called the range. Figure 2.6 shows the range of energetic electrons in water. The range of a 130 keV electron (i.e., the maximum possible energy that can be produced in the 130 kVp Faxitron) in water is 0.223 mm based on the continuous slowing down approximation (CSDA). The range of electrons in an absorber mainly depends on the electron density and, to a lesser extent, the *Z*-value. Low-Z materials are often used to shield beta radiation because they provide good absorption qualities while minimizing the production of bremsstrahlung.

2.1.4. Formation of X-rays

X-rays are composed of bremsstrahlung radiation and characteristic x-rays (fluorescence). Bremsstrahlung is produced when energetic electrons interact with the atomic nuclei of a target medium at distances on the order of 0.01 μm. The deceleration of the electron in the electromagnetic field of the nucleus results in the conversion of kinetic energy into electromagnetic radiation, as illustrated in Figure 2.7. Bremsstrahlung

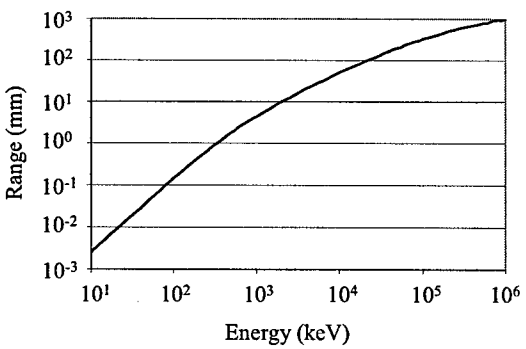

Figure 2.6. CSDA range of energetic electrons in water (NIST 2005).

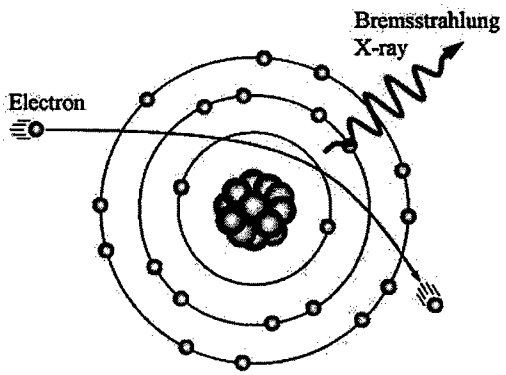

Figure 2.7. Idealized schematic showing the acceleration of an electron in the electromagnetic field of a nucleus to form bremsstrahlung.

interactions produce a continuous spectrum of x-ray energies because the electron-nucleus interaction may occur at different distances. The energy of the bremsstrahlung radiation is higher for close interactions than for more distant ones. In extremely rare instances, the incident electron transfers all of its energy to the nucleus to produce a bremsstrahlung photon with energy exactly equal to the kinetic energy of the electron. Low-energy photons contribute disproportionately to bremsstrahlung radiation because atoms are mostly empty space and interactions close to the nucleus (i.e., higher energy yield) have a low probability of occurrence (Bushberg 2002).

Figure 2.8 shows an idealized schematic of the processes responsible for the emission of characteristic x-rays. When an energetic electron interacts with an orbital electron, sufficient energy may be transferred to overcome the binding energy between the electron and the nucleus. The inner shell vacancy created by the ejection of the orbital electron is quickly filled by electrons from higher-energy orbitals. The excess energy released during these transitions is responsible for the emission of characteristic x-rays or, alternatively, an Auger electron. The energy of the characteristic x-rays corresponds to the difference between the binding energies of the electron shells involved in the transition (Bushberg 2002). The binding energies of the innermost orbitals in the Faxitron tungsten anode (denoted K, L and M in Figure 2.8) are 69.5, 11.5, and 2.5 keV, respectively. Electrons with energies greater than 69.5 keV can eject K-shell electrons (leaving an electron vacancy), and lower energy electrons may eject L- or M-shell electrons.

Because the atom is now energetically unstable, electrons from L, M, N, or O shells will readily transition to and fill the vacancy. When this transition occurs, a photon is created with energy equal to the difference in binding energies. As tube voltage is increased above the K-shell binding energy, characteristic x-ray production becomes a larger fraction of the x-ray spectrum. In tungsten, an electron that transitions from the L to K shell will produce a characteristic x-ray (K_α) with energy equal to 69.5 keV – 11.5 keV = 58.0 keV. K_β x-rays have energy equal to 69.5 keV – 2.5 keV = 67.0 keV. Figure 2.9

shows the notation commonly used for characteristic x-rays. Characteristic x-rays are unique to each element because electron-nucleus binding energies are unique to each element.

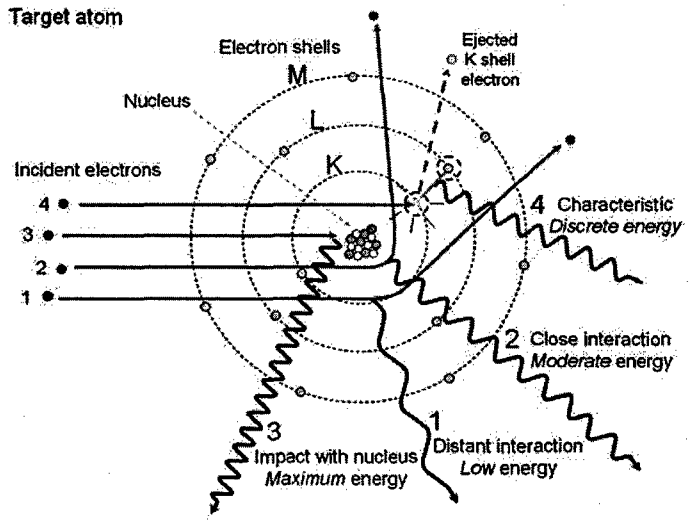

Figure 2.8. Idealized schematic showing how energetic electrons may interact with an atom to produce electromagnetic radiation, i.e., bremsstrahlung and characteristic x-rays (Seibert 2004).

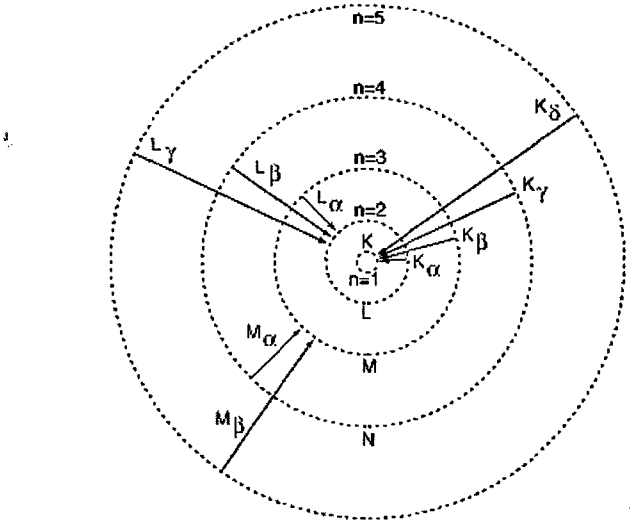

Figure 2.9. Idealized schematic identifying the notation often used for characteristic x-rays. K_α and K_β fluorescence occur when orbital electrons transition from the L to K and M to K orbitals, respectively.

2.2. Characteristics of the HP Faxitron X-ray Machine

This section provides a brief overview of the HP 43855B Faxitron x-ray machine. Additional information about the operating procedures and safety guidelines for the Faxitron x-ray machine are available in Appendix A.

2.2.1. Overview of X-ray System Components

X-ray machines are designed to provide both a containment system and the necessary energetics to produce a projected x-ray field through a target region of interest. Figure 2.10 shows an idealized schematic of a typical x-ray machine.

The first step for x-ray production requires free electrons to be available in the evacuated environment of the x-ray tube insert to allow electrical conduction between the electrodes. Activating the filament circuit causes intense heating of the filament due to its electrical resistance and releases electrons by a process known as thermionic emission (Seibert 2004). The second step involves the application of a high voltage, typically ranging from 50 to 220 kV, from the x-ray generator to the cathode and anode. Tube current, defined as the number of electrons traveling between the electrodes, is expressed

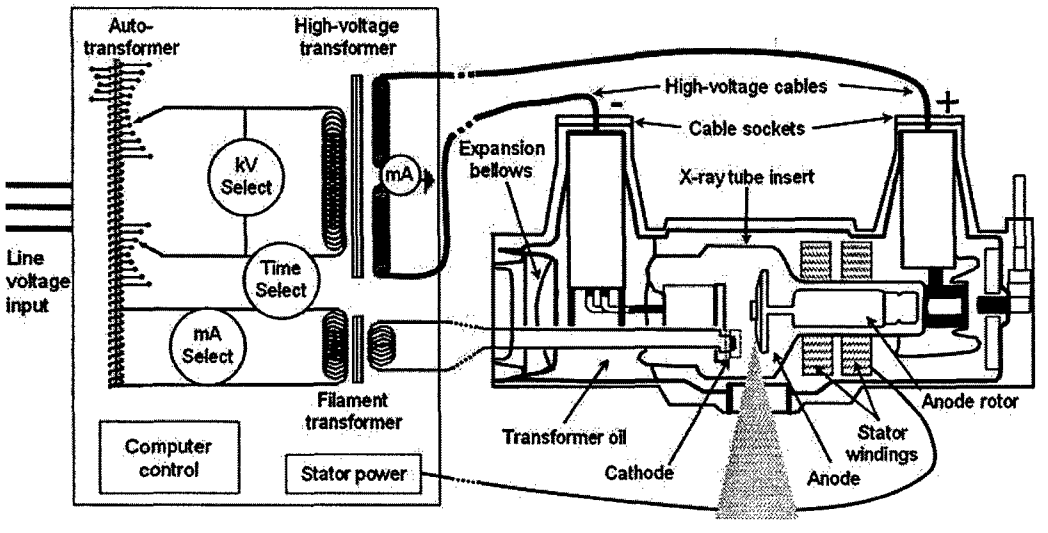

Figure 2.10. Idealized schematic of x-ray tube and generator (Seibert 2004).

in milliampere (mA) units (1 mA = 6.24×10^{15} electrons second^{-1}). Each electron attains a kinetic energy (in keV) equal to the applied tube voltage (kVp). The maximum x-ray energy (in keV) is equal to the applied voltage. As summarized in Section 2.1.4, the deceleration of electrons in a tungsten target (same as HP Faxitron) will result in the emission of bremsstrahlung radiation and characteristic x-rays. During operation, x-ray machines may operate at a slightly reduced voltage. This phenomenon is called the *ripple* and is calculated

$$ripple = \left(kVp_{nominal} - kVp_{operational}\right) / kVp_{nominal} . \quad (2.8)$$

2.2.2. Specifications of the Faxitron X-ray Machine

The HP Faxitron, which is shown in Figure 2.11, is a self-contained, shielded cabinet x-ray system that was designed to produce high-resolution radiographs of small objects. Possible applications include scientific and industrial x-ray inspection, quality control, failure analysis and other operations requiring non-destructive sample analysis. The Faxitron has the shape and appearance of a small oven and can be used in an occupied area without any additional shielding. The self-rectifying, thermionic x-ray tube is regulated at approximately 3 mA and has a continuously variable output voltage of 10 – 130 kVp. The Faxitron produces a uniform, circular beam emitted at a 30 degree angle through a 0.64 mm Beryllium window (see Figure 2.12). At the top irradiation shelf, the beam diameter is 26.035 cm, and the machine has a removable 0.4 mm copper filter to assist with beam hardening.

2.2.3. HP Faxitron X-ray Energy Spectrum

The HP Faxitron uses a tungsten anode for the production of x-rays. Figure 2.13 shows an example of the predicted x-ray energy spectrum produced when 70 and 130 keV electrons are decelerated in a tungsten target. The characteristic x-ray peaks in the 130 keV spectrum result from K_α (58.0 keV) and K_β (67.0 keV) fluorescence. These peaks are not observable in the 70 keV energy spectrum because only a small fraction of the incoming electrons have sufficient energy to eject orbital electrons and produce

characteristic x-rays. The mean energies of the 70 kVp and 130 kVp x-ray spectrums are 37.9 keV and 54.1 keV, respectively.

Low-energy or "soft" x-rays are relatively easy to absorb which presents a potential problem for dosimetry studies that require energy deposition in target mediums of varying thicknesses, e.g., culture medium in a Petri dish. To eliminate this problem, filters are used to "harden" the x-ray spectrum (absorb the soft x-rays). As illustrated in Figure 2.14, a 0.4 mm layer of Cu is effective at absorbing most photons in the 130 kVp Faxitron spectrum below 30 keV.

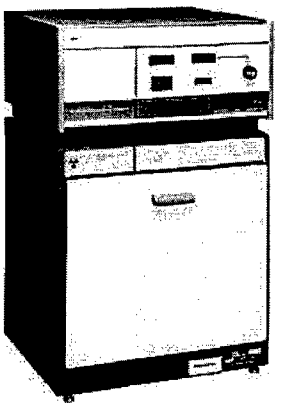

Figure 2.11. HP Faxitron 130 kVp variable output x-ray machine.

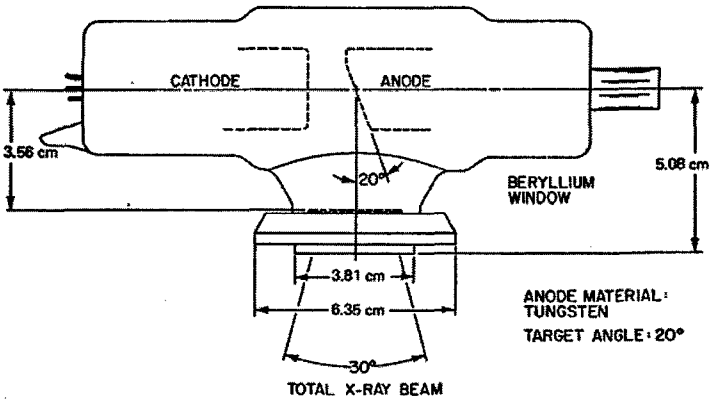

Figure 2.12. Design of the Faxitron anode and x-ray tube (HP 1986).

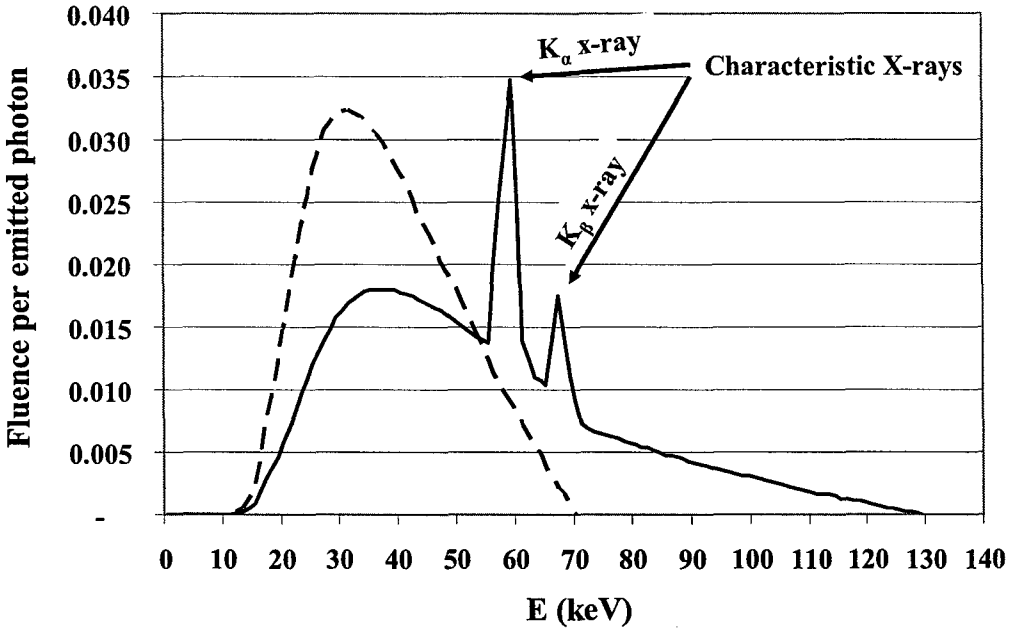

Figure 2.13. X-ray energy spectrum produced by 70 and 130 kVp x-ray machine with a tungsten anode, as calculated with the radiography spectrum generator available at www.edonnelly.com (see also Boone and Seibert 1997). The solid line shows the 130 kVp x-ray spectrum (1% ripple, 0.0 mm Al filtration) and dashed line shows the 70 kVp x-ray spectrum (0% ripple, 0.0 mm Al filtration).

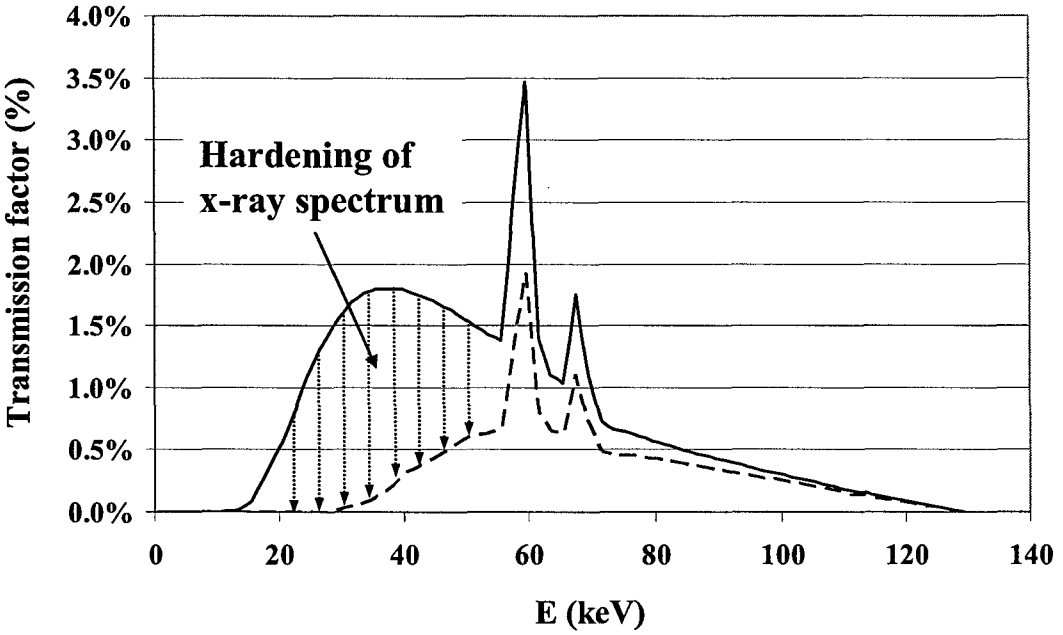

Figure 2.14. Hardening of a 130 kVp x-ray spectrum. The solid line shows the 130 kVp x-ray spectrum (1% ripple, 0.0 mm Al filtration) and dashed line shows the effect of a 0.4 mm Cu filter. The mean energies for the two spectrums are 54.1 keV and 69.2 keV, respectively.

2.2.4. Beam Formation and Heel Effect

The anode of the HP Faxitron, as well as most diagnostic x-ray tubes, is comprised of tungsten because of its high atomic number ($Z = 74$) and extremely high melting point (3,422 °C). These qualities are necessary for efficient x-ray production and tolerance of high temperatures, respectively. The area (actually a volume) on the anode responsible for stopping the energetic electrons and for the emission of x-rays is called the focal spot. Focal spots vary in size with projected image location and a balance is necessary to ensure good field coverage and optimal heat loading (Bushberg 2002). Since x-rays are emitted at various depths in the anode structure, photons directed toward the anode side of the beam are partially attenuated within the anode. As a result, the radiation intensity across the projected x-ray field varies from high-to-low in the cathode-to-anode direction. This is called the "heel-effect" (see Figure 2.15). The heel effect is eliminated when the beam is hardened by a 0.4 mm Cu filter because the remaining soft x-rays that were not absorbed in the anode are absorbed by the copper.

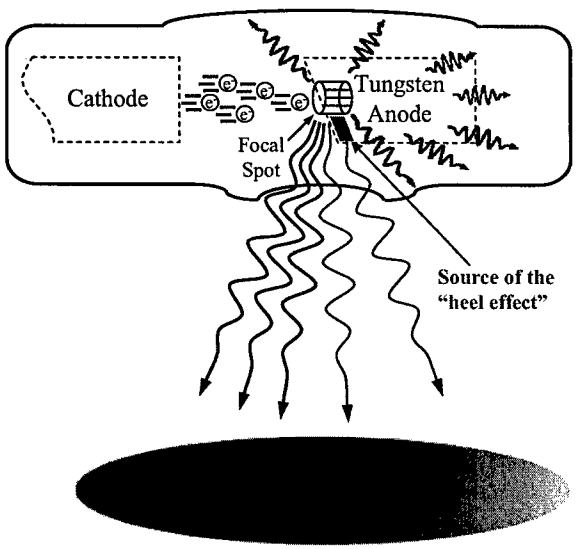

Figure 2.15. Idealized schematic demonstrating the heel effect. X-rays are emitted from the focal spot and partially attenuated by the thickness of the anode. The result is a lower x-ray intensity on the anode-side of the beam.

2.3. Radiation Dosimetry Quantities and Units

2.3.1. Particle Fluence

Particle fluence (Φ) is defined by the relation

$$\Phi = \frac{N}{A}. \tag{2.9}$$

Here, N is the number of particles passing through unit cross-sectional area, A. Fluence is typically specified in units of cm^{-2}. The related concept, fluence rate ($cm^{-2}\ s^{-1}$), is the derivative of the fluence with respect to time, i.e.,

$$\dot{\Phi} = \frac{d\Phi}{dt} \tag{2.10}$$

The energy fluence, ψ ($J \cdot cm^{-2}$) and energy fluence rate ($J\ cm^{-2}s^{-1}$) are defined as

$$\Psi = \Phi E \text{ and} \tag{2.11}$$

$$\dot{\Psi} = \frac{d\Psi}{dt}, \text{ respectively,} \tag{2.12}$$

where E is the kinetic energy. For a x-ray energy spectrum, the total energy fluence is the product of the number of photons at each energy times the photon energy integrated over all energies.

2.3.2. Local Deposition of Energy

Characteristic x-rays, Compton-scattered photons, annihilation photons and bremsstrahlung radiation produced during an interaction deposit their energy at points far removed from the original interaction site (Shultis 2002), and only a fraction, f, of the photon's energy is deposited locally (i.e., close to the interaction site). The linear energy transfer coefficient, denoted μ_{tr} (cm^{-1}), accounts for those interactions that transfer energy to charged particles and excludes the energy carried away by Compton scattered photons, annihilation photons and characteristic x-rays (bremsstrahlung radiation is included in μ_{tr}). The energy absorption coefficient, μ_{en}, excludes bremsstrahlung radiation as well as the photons created in other interactions, i.e., $\mu_{en} = (1-g)\mu_{tr}$. Here, g represents the

average fraction of the kinetic energy of secondary charged particles (produced in all interactions) subsequently lost in radiative (photon-emitting) energy-loss processes.

2.3.3. Kinetic Energy Transferred to Charged Particles (KERMA)

As a beam of photons passes through a medium, photons interact and transfer some or all of their energy to charged particles. Kerma is the sum of the initial kinetic energies of all the charged ionizing particles released by the interaction of indirectly ionizing radiation (ICRU 60), which may be expressed as the product of the energy fluence and the mass energy transfer coefficient, i.e.,

$$K = \Psi \frac{\mu_{tr}}{\rho} = 1.602 \times 10^{-10} \frac{\text{Gy}}{\text{MeV/g}} \times E\left(\frac{\mu_{tr}}{\rho}\right)\Phi . \tag{2.13}$$

2.3.4. Absorbed Dose

Absorbed dose, D, is defined as the energy deposited by ionizing radiation, E, per unit mass of material, m:

$$D \equiv \frac{E}{m}. \tag{2.14}$$

Absorbed dose is defined for all types of ionizing radiation, and its SI unit is the Gy. When bremsstrahlung interactions are negligible and electronic equilibrium is established, absorbed dose equals kerma, i.e., $D_{air} \cong K$. (Zoetelief 2001). Electronic equilibrium means that the net number of electrons (and the sum of their energies) entering and leaving the region of interest is zero. For situations in which charged particle equilibrium has been established, absorbed dose is the product of the energy fluence and the mass energy absorption coefficient, i.e.,

$$D = \Psi \cdot \frac{\mu_{en}}{\rho} = 1.602 \times 10^{-10} \frac{\text{Gy}}{\text{MeV/g}} \times E\left(\frac{\mu_{en}}{\rho}\right)\Phi . \tag{2.15}$$

For the x-ray energy spectrum produced by the HP Faxitron (Figure 2.13), the ratio of the absorbed dose in air to the air kerma is 0.99956 for the unfiltered beam (Figure 2.14, solid line) and 0.99959 for the Cu-hardened beam (Figure 2.14, dashed line), thus

$$\frac{\mu_{en}}{\rho} \cong \frac{\mu_{tr}}{\rho} \text{ and } D_{air} \cong K. \tag{2.16}$$

2.3.5. Exposure

Exposure, denoted by the symbol X, is the amount of electrical charge produced by ionizing photons in a given mass of air and is relevant for photons with energies less than about 3 MeV. Above this threshold, photons produce long-range secondary electrons and electronic equilibrium is seldom established. The traditional unit of exposure is the roentgen (R). The roentgen is defined as the quantity of radiation that produces, in air, precisely 2.58×10^{-4} coulomb of charge (of either sign) per kilogram of air, i.e., $1\,R = 2.58\times10^{-4}$ C kg^{-1} of air. Since the charge on a single ion is 1.602×10^{-19} C and because the average energy required to produce a single ion pair in dry air is 33.85 $\pm$ 0.15 eV (ICRU 1979), exposure may be written as

$$X = 114.5\frac{\mathrm{R}}{\text{C-eV}}\cdot\frac{\mu_{en}}{\rho}\Psi = 1.835\times10^{-8}\frac{\mathrm{R}}{\text{MeV/g}}\times E\left(\frac{\mu_{en}}{\rho}\right)\Phi. \tag{2.17}$$

From Eqs. (2.15) and (2.17), it follows that 1 Gy of absorbed dose in air equals 114.5R.

2.3.6. Fluence-to-Dose Conversion Factors for the HP Faxitron

To convert particle fluence, the direct measure of the number of photons passing through a region of interest, into a more biologically relevant quantity (i.e., absorbed dose), a conversion factor is needed (Shultis 2005). For the Faxitron x-ray spectrum, an appropriate fluence-to-dose conversion factor, $R(E)$ can be computed using

$$R(E) = \frac{D}{\Phi}\left(\text{Gy cm}^2\right) = 1.602\times10^{-10}\sum_{i=1}^{n} f_i E_i\left(\frac{\mu_{en}(E_i)}{\rho}\right), \tag{2.18}$$

where n is the number of energy bins, E_i is the photon energy (MeV) in the ith bin, and f_i is the fraction of fluence in the ith energy bin. Table 2.1 tabulates fluence-to-dose conversion factors for the 130 kVp Faxitron obtained with 1 keV energy bins (n = 130).

Table 2.1. Fluence-to-Dose Conversion Factors.
130 kVp tungsten x-ray, 1% ripple (pGy cm^2).

Medium	With 0.4 mm Cu filter	Without filter
Al (Z=13)	14.74	2.45
Fe (Z=26)	92.41	19.69
Cu (Z=29)	107.65	25.45
Pb (Z=82)	193.56	72.79
Water	2.80	0.54
Air	2.71	0.52
Tissue	2.59	0.50

The dose per unit fluence in the table above is about 4 to 6 times higher for the filtered (hardened) x-ray beam than for the unfiltered beam. The lower dose per unit fluence with the unfiltered beam is due to the lower average energy of the x-ray spectrum.

For conditions of electronic equilibrium, an estimate of the absorbed dose in one medium may be converted to an estimate of the absorbed dose in another medium using

$$D_1 = D_2 \cdot \frac{R(E)_1}{R(E)_2}. \tag{2.19}$$

Thus a 130 kVp x-ray that deposits some absorbed dose in air will deposit the following absorbed dose in water, for a filtered (0.4 mm Cu) and unfiltered beam:

$$D_{water} = D_{air} \cdot \frac{(D/\Phi)_{water}}{(D/\Phi)_{air}} = D_{air} \cdot \frac{2.80 \text{ pGy cm}^2}{2.71 \text{ Gy cm}^2} = 1.033\, D_{air}, \text{ and} \tag{2.20}$$

$$D_{water} = D_{air} \cdot \frac{(D/\Phi)_{water}}{(D/\Phi)_{air}} = D_{air} \cdot \frac{0.54 \text{ pGy cm}^2}{0.52 \text{ Gy cm}^2} = 1.038\, D_{air}, \text{ respectively.} \tag{2.21}$$

Absorbed dose in water (Gy) can also be related to exposure (in R). For the filtered and unfiltered 130 kVp x-ray, the appropriate conversion factors are:

$$D_{water} = 1.033\, D_{air} \cdot \frac{R}{114.5\, D_{air}} = 9.022 \times 10^{-3}\, R \tag{2.22}$$

$$D_{water} = 1.038\, D_{air} \cdot \frac{R}{114.5\, D_{air}} = 9.066 \times 10^{-3}\, R. \tag{2.23}$$

Figure 2.16 compares the contribution to the overall absorbed dose (in water) of x-rays in the 130 kVp Faxitron spectrum. X-rays with energies below the K_α peak (58 keV) are responsible for 32.2% and 74.5 % of the total dose in the filtered and unfiltered beam, respectively.

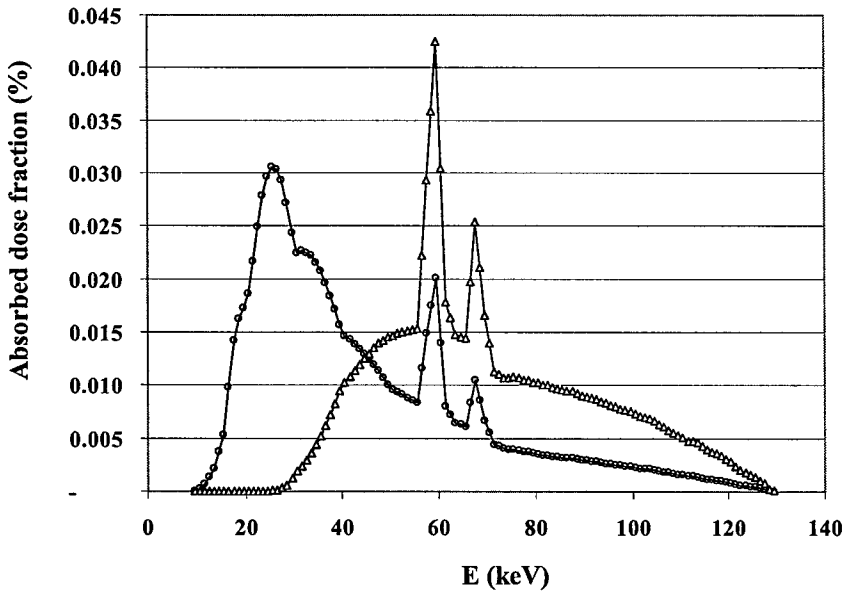

Figure 2.16. Absorbed dose fraction (in water) for a 130 kVp tungsten x-ray spectrum. Triangles denote the filtered (0.4 mm Cu) spectrum and circles denote the unfiltered energy spectrum. The area beneath the curves is unity.

2.4. Radiation Attenuation and Shielding

2.4.1. Attenuation of Photons in a Purely Absorbing Medium

For the Faxitron x-ray machine (i.e., photon energies at or below 130 keV), the dominant interaction mechanisms are Compton scattering in low-Z materials and

photoelectric absorption in high-Z materials. For the Faxitron x-ray energy spectrum, radiation shields composed of high Z materials may be considered a purely absorbing medium, i.e., $\mu \cong \mu_{PE}$. For a purely absorbing medium, the total photon intensity is well approximated by

$$I(l) = I(0)e^{-l}. \tag{2.24}$$

Here, l is the optical thickness of the attenuating material, $I(0)$ is the initial photon intensity (cm^{-2}) and $I(l)$ is the photon intensity after passing through optical thickness l (refer to Figure 2.17). For a radiation shield composed of m layers of different kinds of shield material, the optical thickness is given by

$$l = \sum_{j=1}^{m} \mu_j \Delta x_j , \tag{2.25}$$

where μ_j is the linear attenuation coefficient for the jth shield material and Δx_j is the thickness of the jth shield material. For a polyenergetic radiation source incident on a multi-layer shield, Eq. (2.24) becomes

$$I(l) = \sum_{i=1}^{n} f_i I_i(0) e^{-l_i} , \tag{2.26}$$

where f_i is the fractional intensity of photons in the ith energy bin and

$$l_i = \sum\nolimits_j \mu_j(E_i)\Delta x_j . \tag{2.27}$$

2.4.2. Attenuation Factor and Half Value Layer

For a polyenergetic radiation source, the absorbed dose attenuation factor (A_f) may be defined as

$$A_f = \frac{D(l)}{D(0)} = \frac{\sum_{i=1}^{n} f_i E_i \left(\frac{\mu_{en}(E_i)}{\rho} \right) I_i(l)}{\sum_{i=1}^{n} f_i E_i \left(\frac{\mu_{en}(E_i)}{\rho} \right) I_i(0)} . \tag{2.28}$$

Figure 2.18 shows the estimated attenuation factor for the unfiltered 130 kVp Faxitron x-ray energy spectrum and several materials commonly used in shielding applications. As expected, lead is much more effective at attenuating low energy x-rays than lower Z materials, such as aluminum, iron and copper. The results shown in Figure 2.18 indicate

that a 3 mm layer of lead will reduce the absorbed dose by more than 10^5 whereas 3 mm of aluminum, water, or air have a small or negligible effect on the absorbed dose.

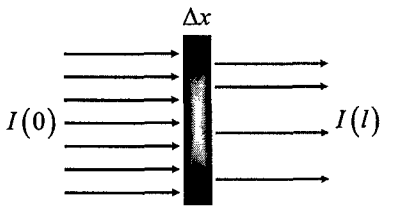

Figure 2.17. Exponential photon attenuation through a shield of thickness Δx.

The first and second half-value layer (HVL) is frequently used, along with the tube voltage, to specify the radiation quality of x-rays (Zoetelief 2001). The HVL is the shield thickness required to reduce the dose by ½, i.e, a $A_f = 0.5$. Table 2.2 summarizes the 1st and 2nd half-value thickness (mm of Al) for the 130 kVp HP Faxitron x-ray machine with and without the 0.4 mm Cu filter. Larger HVLs indicate a more penetrating x-ray spectrum. For both the filtered and unfiltered Faxitron x-ray spectrum, the 2nd HVL is substantially larger than the second HVL, which is indicative of beam hardening.

Table 2.2. First and second HVL for the 130 kVp Faxitron (mm Al), with and without 0.4 mm Cu filter.

Beam Filtration	1st HVL	2nd HVL
0.4 mm Cu	8.76	Not measured
None	0.66	2.31

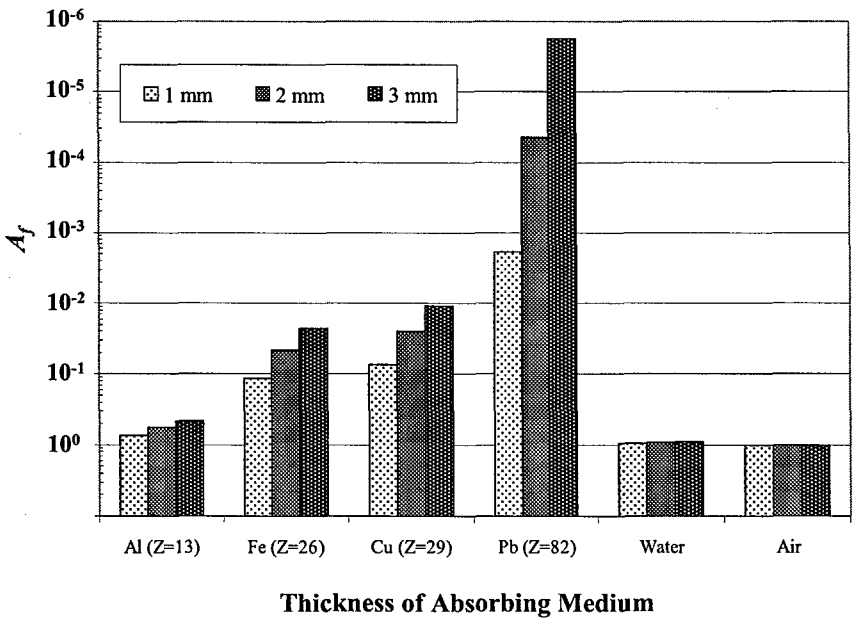

Figure 2.18. Estimated A_f for an unfiltered 130 kVp x-ray spectrum (based on a pure absorbing medium).

2.4.3. Design of the Millibeam Shield for Faxitron

The shield design in this project relies on principles of broad-beam attenuation, wherein it is assumed the x-ray source is located sufficiently far from the shielding slab so that the radiation reaches the wall in nearly parallel rays (Shultis 2005). Similarly, the attenuation in the air is considered negligible compared to attenuation within the shield.

Two methods were used to predict the shield thickness required to reduce absorbed dose from the Faxitron 130 kVp x-ray by a factor of 10^6, i.e., $A_f = 10^{-6}$. The first method used Eq. (2.28) and assumes the shield is a pure absorbing medium (i.e., photoelectric absorption is the dominant interaction mechanism for low-energy photons in high Z materials). For comparison, attenuation factors were also computed with the empirical relation (Shultis 2005)

$$A_f = \left[\left(1+\frac{\beta}{\alpha}\right)e^{\alpha\gamma x} - \frac{\beta}{\alpha}\right]^{-1/\gamma}, \tag{2.29}$$

where x is the shield thickness. The attenuation factor, A_f, depends on the nature and thickness of the shielding, the source energy characteristics, and the angle of incidence. Relevant values for α, β, and γ are listed in Tables 2.3 and 2.4 for lead and steel, respectively (Simpkin 1995). Table 2.5 provides a comparison of the predicted shield thicknesses needed to achieve an attenuation factor of 10^{-6} for each of the two methods (i.e., Eq. 2.28 and Eq. 2.29). This comparison was performed for a 120 and 140 kVp tungsten x-ray filtered with 2.8 mm of Al. Linear-linear interpolation was accomplished to estimate the required shield thickness to achieve 10^{-6} attenuation.

Table 2.3. Lead attenuation parameters (broad beam geometry with 2.8 mm Al filtration, Simpkin 1995).

Parameter	120 kVp	140 kVp
α	2.246	2.009
β	8.95	5.916
γ	0.5873	0.4018
β/α	3.9849	2.9447

Table 2.4. Steel attenuation parameters (broad beam geometry with 2.8 mm Al filtration, Simpkin 1995).

Parameter	120 kVp	140 kVp
α	0.2336	0.1724
β	1.797	1.328
γ	0.8116	0.8458
β/α	7.6926	7.7030

Table 2.5. Estimated thickness (in mm) to obtain a shield reduction of 10^{-6}. *Linear-linear interpolation of the 120 and 140 kVp shield thicknesses.

Shielding Material	120 kVp	140 kVp	130 kVp	
	(Eq. 2.29)	*(Eq. 2.29)*	*(Eq. 2.29)**	*(Eq. 2.28)*
Pb	4.93	5.19	5.06	3.30
Steel	47.74	65.30	56.52	37.1

The 130 kVp interpolated values from Eq. (2.29) provide the most conservative shielding estimates for Pb and steel (i.e., 5.06 mm and 56.52 mm, respectively). However, the pure lead composition would not be rigid enough to provide consistent beam collimation, and the pure steel composition would weigh almost 100 lbs! For this reason, a composite shield was selected to provide the necessary attenuation (see Figure 2.19).

The estimated shield attenuation factors for the composite shield are:

- $A_f(130\ \text{kVp}) = 1.13 \times 10^{-7}$ (Eq. 2.28)
- $A_f(130\ \text{kVp}) = 9.82 \times 10^{-6}$ (Eq. 2.29)

Both of the predicted values are close enough to the desired 10^{-6} criterion that the shield design was considered acceptable. Follow-up experiments with calibrated TLD pellets and GafChromic film confirm that the shield design (Figure 2.19) reduced the dose from the Faxitron beam to background levels (at least a factor of 3.3×10^3 reduction in dose; measurement of the attenuation factor was limited by the sensitivity of the TLD chip).

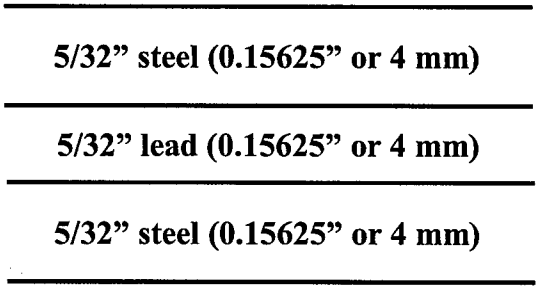

Figure 2.19. Composite design of a 12" x 12" shield. Constructed to reduce the effective absorbed dose of a 130 kVp x-ray by a factor of 10^6. Total weight: 22 lbs.

3. PRINCIPLES OF DETECTION AND MEASUREMENTS

This chapter provides an overview of radiation detection systems used to characterize the absorbed dose distribution within the HP Faxitron x-ray beam with and without the 0.4 Cu filter. The detection principles, calibration requirements for the HP Faxitron x-ray machine, and limitations and applicability of Fricke dosimetry, ionization chambers, TLD chips, and radiochromic film are summarized.

3.1. Detection Principles

3.1.1. Required Accuracy of Dosimetry Measurements

In many radiobiology experiments and in radiation therapy for the treatment of cancer, a 10% change in the absorbed dose will produce easily observable differences in biological response (Zoetelief et al. 2001 and references therein). Accurate dosimetry is a necessary requirement for the detection of subtle radiobiological effects and for ongoing efforts to develop quantitative models to predict the effects of radiation *in vitro* and *in vivo*. The International Commission on Radiological Units (ICRU) criteria for uniform irradiation requires a combined standard uncertainty less 5.2% (ICRU 1979), and this criterion has been adopted for efforts to commission the HP Faxitron x-ray machine.

3.1.2. Detector Response and Calibration Factors for Air and Water

Radiation dosimeters are designed to measure absorbed dose in a medium of interest. When investigating the effects of radiation in biological systems, the medium of interest is tissue (*in vivo*) or water (*in vitro*), and an important feature of a radiation detector is thus tissue or water equivalence. Although the direct measurement of absorbed dose in tissue-equivalent materials is possible (e.g., with calorimetry), many

radiation detectors quantify a physical quantity such as ionization in air rather than absorbed dose in water or tissue. For detectors such as these, a calibration factor is required to convert the detector response to an estimate of the absorbed dose in the desired medium.

Four radiation measurement systems were selected for the effort to commission the HP Faxitron system: (1) Fricke dosimetry, (2) an ionization chamber, (3) LiF TLD chips, and (4) EBT GafChromic film. To ensure high-quality radiation dosimetry, the ionization chamber and LiF TLD chips were sent to the University of Wisconsin (UW) Accredited Dosimetry Calibration Laboratory for exposure in NIST traceable 120 kVp and 80 kVp x-ray beams. The ionization chamber and a subset of the TLD chips were also irradiated by γ-rays from ^{137}Cs and ^{60}Co sources. The dose estimates reported by the UW calibration laboratory are for air kerma, which was converted to absorbed dose estimates in water using the methodology outlined in Chapter 2, Section 2.3.6. A summary of the relevant conversion factors needed to obtain the absorbed dose in water from air kerma are provided in Table 3.1 for the 130 keV x-ray energy range. The details of the methods used to generate calibration factors for each radiation measurement system are summarized in Sections 3.2 through 3.5.

Table 3.1. Kerma to Absorbed Dose Conversion Factors for the 130 kVp HP Faxitron x-ray.

Conversion	With Cu Filter	Without Filter
To convert from K to D_{air}	0.99959	0.99956
To convert from D_{air} to D_{water}	1.033	1.038

3.2. Fricke Dosimeter

3.2.1. Principles of Operation

The Fricke (ferrous sulfate) dosimeter is the best studied and most widely used liquid chemical dosimeter (Klassen 1999). It is capable of 0.1% precision for high-energy x-rays (i.e., > 100 keV) and is valued for its accuracy, reproducibility, and linearity. The principle of detection, like other chemical dosimeters, is based upon free-radical oxidization. When exposed to ionizing radiation, free radicals are produced through interactions with the chemical system (Attix 1966). The free radicals subsequently induce chemical reactions, and the number of products involved in these reactions is related to the absorbed dose in the system.

Fricke dosimeters consist of a ferrous sulfate ($FeSO_4$) solution. The following reactions occur when radiation interacts with the water in this solution:

$$\gamma + H_2O \rightarrow OH\cdot + H\cdot \tag{3.1}$$

$$H\cdot + H\cdot \rightarrow H_2 \text{ (gas)} \tag{3.2}$$

Afterwards, free radicals oxidize ferrous ions:

$$OH\cdot + Fe^{2+} \rightarrow Fe^{3+} + OH^- \tag{3.3}$$

The number of ferric (Fe^{3+}) ions can be measured by spectrophotometry according to the following equation:

$$OD = log_{10}\left(\frac{I_0}{I}\right), \tag{3.4}$$

where:

OD = Optical density

I_0 = Intensity of incoming light

I = Intensity of transmitted light

The absorbed dose is directly proportional to the optical density and can be determined by the formula:

$$D(\text{Gy}) = \frac{\Delta OD}{\varepsilon_M l \rho G(x)}, \tag{3.5}$$

where:

ΔOD = Increase in OD at 303 nm

ε = Extinction coefficient at 303 nm; $\varepsilon = \varepsilon_{Fe^{3+}} - \varepsilon_{Fe^{2+}} = 219.6 \text{ m}^2 \text{ mol}^{-1}$

l = Photometer path length; $l = 0.01$ m

ρ = Density of Fricke solution; $\rho = 1024 \text{ kg m}^{-3}$

$G(x)$ = Radiation chemical yield of ferric ion; $G = 1.50 \times 10^{-6} \text{ mol J}^{-1}$

After substitution of these values, Eq. (3.5) becomes

$$D(\text{Gy}) = 3373 \Delta OD . \tag{3.6}$$

3.2.2. Laboratory Procedures

To prepare the Fricke solution, 27 mg of ferrous sulfate and 2.2 mL sulfuric acid are dissolved in a 100 mL volumetric flask of distilled water. In addition, 6 mg of NaCl is added to quench organics. Next, the solution is transferred by pipette into seven irradiation dishes, i.e., 52.5 mm diameter Petri dishes. The minimum volume of water required to create a thin liquid layer is 4 mL, which corresponds to a layer of water 1.85 mm thick. The relationship between the thickness of water in the culture dish, x (in mm) and the volume of medium is given by

$$x = \frac{4000\ V}{\pi d^2}, \tag{3.7}$$

where V is the volume of water added to the culture dish (mL) and d is the inside diameter of the dish (mm).

A Shimadzu UV-Visible Recording Spectrophotometer (Purdue # 861781) Model UV-160U was used to obtain the *OD* measurements (see Figure 3.1). Glass cuvette cells were triple-rinsed with deionized (DI) water, and wiped dry with chemical wipes. The reference cell was filled with 3mL of DI water. The sample cell was rinsed with 1 mL of the respective Fricke dosimeter, and subsequently filled with the remainder of the 4 mL Fricke solution. Before and after each measurement, the sample cell was rinsed and filled with DI water, and then the spectrophotometer was zeroed. Spectrophotometer readings were documented, and later used to calculate the energy absorbed by the dosimeter.

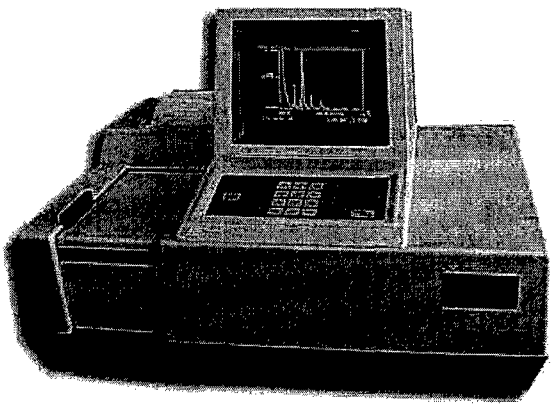

Figure 3.1. Shimadzu UV-Visible Recording Spectrophotometer Model UV-160U.

3.2.3. Calibration

The Fricke dosimeters were sequentially placed in the center of the Faxitron x-ray machine on the top shelf and irradiated for 0, 60, 90, 120, 180, 240, and 300 minutes. The x-ray was set to 130 kVp and delivered a 3 mA current. A 0.4 mm copper filter was used to harden the beam. A repeat experiment was accomplished without the 0.4 mm Cu filter. Figure 3.2 shows a plot of the relationship between ΔOD and the absorbed dose estimated using Eq. (3.6). The slope of the linear regression shown in Figure 3.2 is referred to as the sensitivity of the Fricke dosimeter (Klassen 1999). The same sensitivity of the Fricke dosimeter was the same with and without the 0.4 mm Cu filter, i.e., 296.5 Gy ΔOD^{-1}.

Figure 3.3 shows a plot of the absorbed dose plotted as a function of the irradiation time. Linear regression of the data shown in this plot gave an estimated dose rate of 3.76 Gy hr^{-1} and 90.85 Gy hr^{-1} for the filtered and unfiltered HP Faxitron x-ray spectrum, respectively. The 24-fold reduction in dose rate is primarily due to attenuation of the low energy component of the 130 kVp Faxitron x-ray spectrum (refer to Figure 2.14).

3.2.4. Limitations Applicability, and Sources of Error

Table 3.2 summarizes the major sources of uncertainty in Fricke dosimetry under careful conditions of preparation, irradiation, and analysis (Landolt 1992). To obtain the most reliable results from the Fricke dosimeter, sulfuric acid concentrations should not be less than 50 mM (Schulz et al 1990). Due to the accuracy, reproducibility, and linearity of response of the Fricke dosimeter, it is used in several standards laboratories (Ma et al 1993). Fricke dosimeters are especially useful because they are near-tissue equivalent (ρ=1.024 g cm^{-3}), and a good surrogate for water in a cell culture dish. One significant limitation of the Fricke dosimeter is spatial resolution which is due to the relatively large volumes necessary to obtain *OD* measurements. To wit, a standard spectrophotometer cuvette requires a minimum of 4 mL solution.

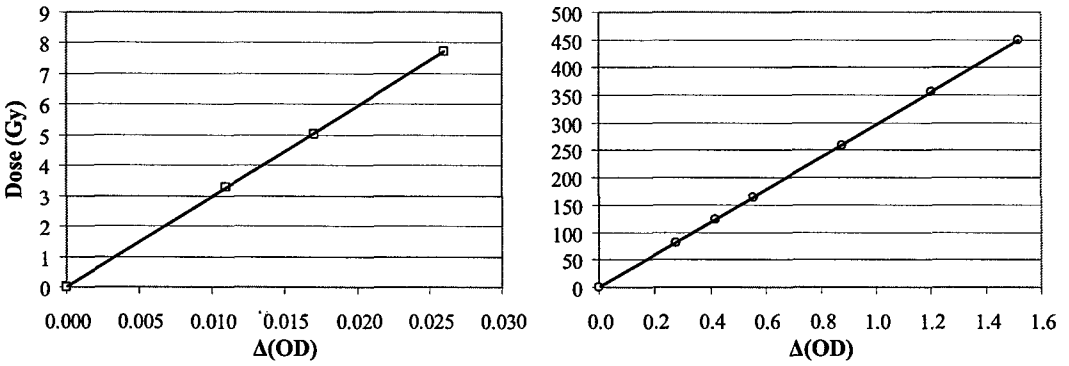

Figure 3.2. Fricke dosimeter calibration curves (130 kVp x-ray). Left panel: Filtered beam, 0.4 mm Cu. Right panel: Unfiltered beam. Slope of the regression line is 296.5 Gy ΔOD^{-1}.

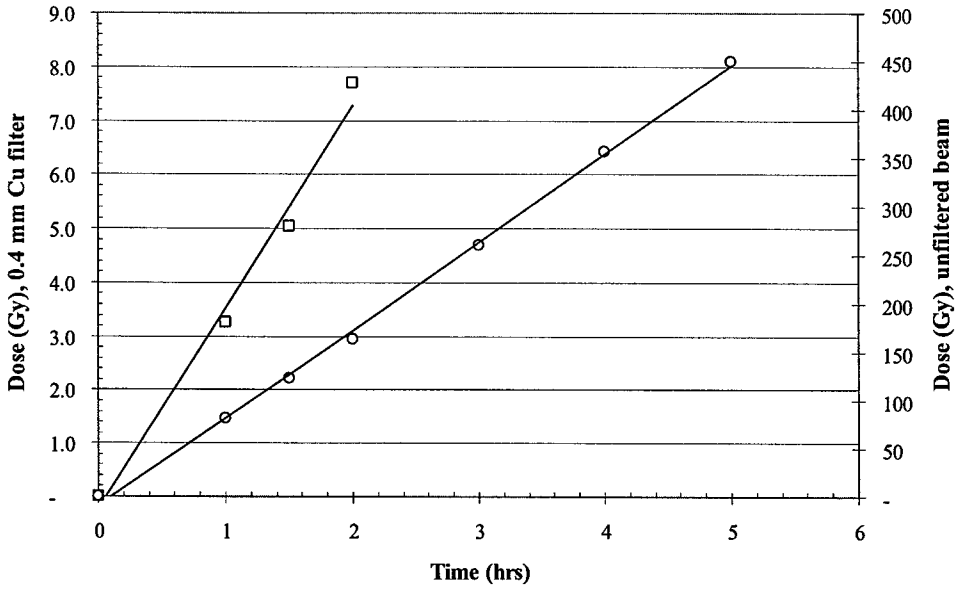

Figure 3.3. Fricke dosimeter irradiation curve (130 kVp x-ray). Squares denote the filtered (0.4 mm Cu) beam with slope 3.76 Gy h^{-1}. Circles represent unfiltered beam with slope 90.85 Gy h^{-1}. Linearity: r^2=0.986 and r^2=0.999, respectively.

Table 3.2. Sources of Error, Fricke Dosimeter.

Source of Error	Error (%)
Difference in *OD*	0.10
Spectrophotometer calibration	0.20
Reference value of εG	0.50
Storage effects of Fricke solution	0.05
Conversion factor Fricke solution-water	0.05
Perturbation correction for container walls	0.30
Total Error	*0.63*

3.3. Ionization Chamber

3.3.1. Principles of Operation

The air-filled ionization chamber is the simplest detector that responds to absorbed energy (Shapiro 1990). Normally, air is not a good conductor of electricity; however, high-energy x-rays and γ-rays produce the necessary ionizations to make this possible. The ion pairs that result from this phenomenon are collected inside the chamber (see Figure 3.4), and a sensitive electrometer is used to measure the current, $\Delta\dot{Q}\left(\mathrm{C\ s^{-1}}\right)$.

The flow of electric current is sustained by a voltage difference between the chamber wall and inner electrode. Based on the current measurement, as well as knowledge of the detection medium and sensitive volume, the exposure rate can be calculated:

$$\dot{X} = \frac{\Delta\dot{Q}}{\rho V}, \tag{3.8}$$

where $\dot{X}\left(\mathrm{R}\right)$ is the exposure rate in air, ρ is the density of air, and V is the sensitive volume in the chamber.

An important element of the chamber design is maintaining electronic equilibrium. Air-equivalent material is therefore used for the walls whose thickness approximates the maximum range of the ionized electrons. For low-kilovoltage (less than 100 kVp) x-ray beams, parallel-plate ionization chambers are used to determine absorbed dose at the surface of a tissue (Austerlitz 2003). These chambers have a doughnut-shaped sensitive volume embedded into tissue-equivalent walls.

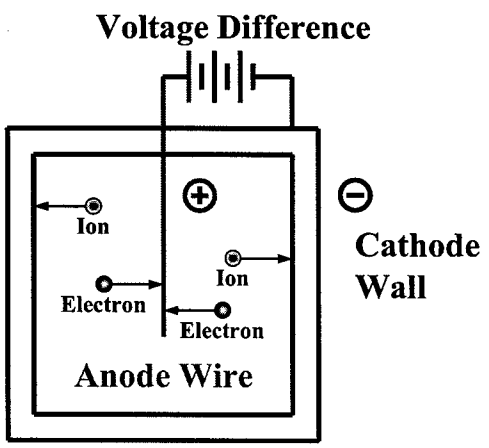

Figure 3.4. Simple ionization chamber design.

3.3.2. Calibration

The chamber selected for this project was the RadCal 3036 (see Figure 3.5). Two external chambers, the 30×6-11 and 10×5-180, were also used. Both are parallel-plate ion chambers with a 11 cm^3 and 180 cm^3 sensitive volume, respectively. All instruments otherwise have the same specifications (see Table 3.3). The RadCal 30×6-11 and 10×5-180 were calibrated on 8 Aug 2005 by the UW Accredited Dosimetry Calibration Laboratory (see Appendix C).

Table 3.3. RadCal 3036 Specifications.

Range – Rate Mode	0.001 to 1200 R/min (0.01 to 1000 mGy/min)
Range – Exposure Mode	0.0001 to 670 R (0.0001 to 5900 mGy)
Range – Pulse Mode	600 mR/min threshold
Accuracy	± 5%
Energy Response	± 5% , 1.5 to 14 mm Al HVL

The chambers were calibrated to the UW120-M and UW80-M beam code standard, and the systematic coefficients of variation (i.e., calibration factors) were found to be 0.979 R response^{-1} and 0.997 R response^{-1} for the 30x6-11, and 9.583×10^{-4} R response^{-1} and 9.739×10^{-4} R response^{-1} for the 10×5-180, respectively. The corrected exposure reading can be used to solve for the absorbed dose in air, with and without the Cu filter, by manipulating Eq. (2.17),

$$D_{water}(\text{Gy}) = 1.033\times\frac{X_{\text{air}}}{114.5} = 9.022\times10^{-3}\ X_{\text{air}}, \text{ and} \tag{3.9}$$

$$D_{water}(\text{Gy}) = 1.038\times\frac{X_{\text{air}}}{114.5} = 9.066\times10^{-3}\ X_{\text{air}}, \text{ respectively.} \tag{3.10}$$

Figure 3.6 shows dose response curve obtained with the RadCal 3036 ionization plotted as a function of the irradiation time.

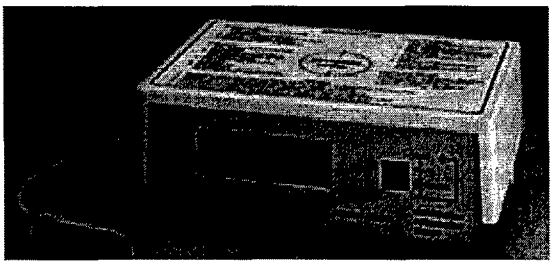

Figure 3.5. RadCal 3036 (S/N: 36-0412) ionization chamber with 30x6-11 external chamber (RadCal Corporation, Monrovia, CA).

3.3.3. Sources of Error

The manufacturer of the RadCal 3036 specifies the instrument is ± 5% accurate within its measurable range, and ± 5% energy independent across a range of x-ray energy spectrums (1.5 to 14 mm Al HVL). Table 3.4 provides a summary of potential sources of uncertainty (Landolt 1992).

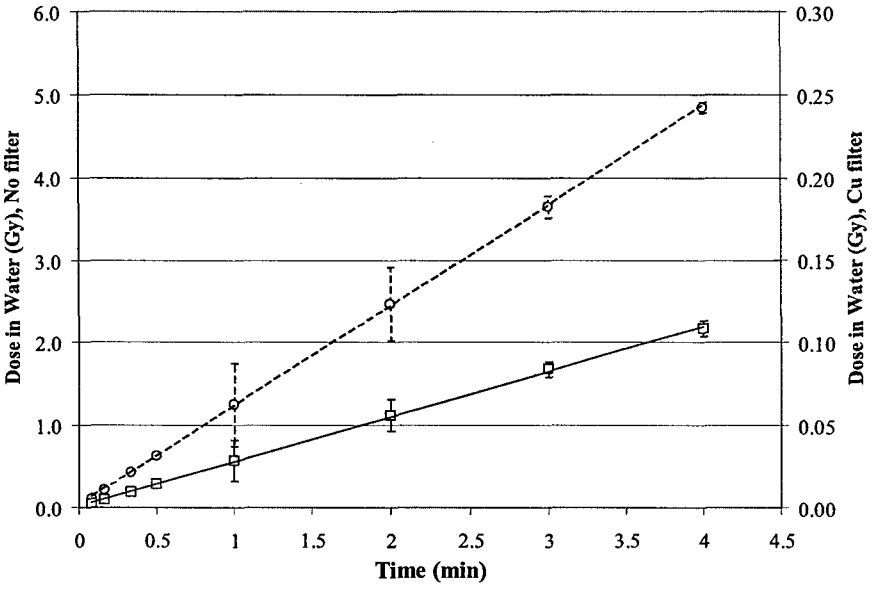

Figure 3.6. Absorbed dose rate (in water) for the Faxitron 130 kVp x-ray, determined using the RadCal 30×6-11 ionization chamber. Squares are with 0.4 mm Cu filter (slope is 1.638 Gy/h with r^2=0.9995), circles are without filter (slope is 72.546 Gy/h with r^2=0.9999).

Table 3.4. Sources of Error, Ionization Chamber.

Source of Error	Error (%)
Measurement of the sensitive volume	
- Chamber diameter	0.05
- Chamber depth	0.05
Correction for collecting electrode not at ground	0.02
Correction for electrical field inhomogeneity	0.02
Measurement of charge	
- Capacitance for charge measurement	0.05
- Voltage measurement	0.02
- Correction for incomplete ion collection	0.10
- Correction for humidity of air	0.05
- Correction for electron backscatter differences	0.05
W/e (for dry air)	0.20
Stopping power ratio	0.40
Perturbation correction factor	0.15
Total Error	*0.50*

3.3.4. Limitations and Applicability

Nearly energy independent, a calibrated ionization chamber provides an absolute method of radiation dosimetry that can readily measure x-ray exposure in air, and provide a close approximation to energy absorption in tissue (Mayneord 1938). Ionization chambers are relatively insensitive to environmental factors, such as temperature and humidity; however, they do require periodic calibrations. Ionization chambers respond linearly with exposure (see Figure 3.6), and can measure small increments over a wide exposure range (refer to Table 3.3) in an accurate and reproducible manner. They are also relatively inexpensive and easy to use.

3.4. Thermoluminescent Dosimeter

3.4.1. Principles of Operation

The TLD is a small crystalline dielectric device containing suitable impurities to make it perform as a thermoluminescent phosphor (McKeever 1984). When a TLD is exposed to radiation (i.e., absorbs energy), electrons are ionized and migrate to positively-charged impurities in the conduction band. Similarly, the holes that are left behind migrate to negatively-charged impurities in the valence band. Under normal conditions, the binding energy in these holes must be high enough to prevent recombination. Later, the TLD is deliberately heated to allow for electron-hole recombination at the luminescent centers, which is accompanied by the release of a light photon (Frame 2004). TLD readers are used to heat the phosphor and built-in photomultiplier tubes are used to measure the light output as a function of temperature. The reader records the radiation dose information in the form of a glow curve (Guo 2004).

3.4.2. Laboratory Procedures

Thermo electron TLD-100 lithium fluoride chips (Qty: 32; Dimensions: 3.2mm x 3.2mm x 0.38mm) and pellets (Qty: 57; Dimensions: 3.2mm x 3.2mm x 0.89mm) were used for this project in conjunction with a Harshaw 4000 TLD reader. The reader is manually operated, and features planchet-type heating with a programmable linear ramp time temperature profile (see Figure 3.7).

Glow curves were recorded using a maximum temperature of 300°C and a heating rate of 15°C s^{-1}. The anneal process immediately followed the glow curve measurement, and was configured for maximum recombination at 400°C for 30 seconds. TLDs were handled using either teflon-tipped vacuum tweezers or forceps, and were placed in the center of the planchet during heating (see Figure 3.8).

3.4.3. Calibration

Homogeneity testing was accomplished on chips and pellets prior to calibration to ensure TLDs consistently met performance specifications individually and as a group (discussed in Section 3.4.4). The chips performed poorly in the group homogeneity tests with a 9.02% standard error; however, individual chips were useful in some studies (i.e., beam uniformity). The pellets performed much better (4.55% SE), but 21 of the pellets failed the individual reproducibility tests (i.e., >5% relative error). The remaining 36 pellets all had a relative error below 3%, and were grouped according to their mean response (see Table 3.5 and Figure 3.9). All pellets in each group vary no more than 5% from the centerline of each group, and usually this variation was much less (i.e., 1 to 2%).

Table 3.5. TLD Pellet Homogeneity Groups.

Group	# of Pellets	Mean Response (uC)	% RE
A	9	11.49	1.01
B	19	11.05	1.18
C	8	10.46	1.66

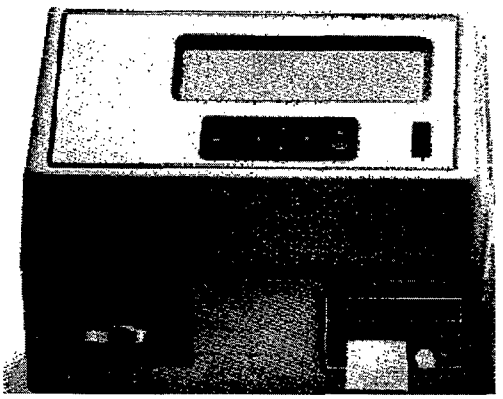

Figure 3.7. Harshaw 4000 TLD system reader (Harshaw TLD, Solon, OH).

Figure 3.8. TLD placement in planchet of reader.

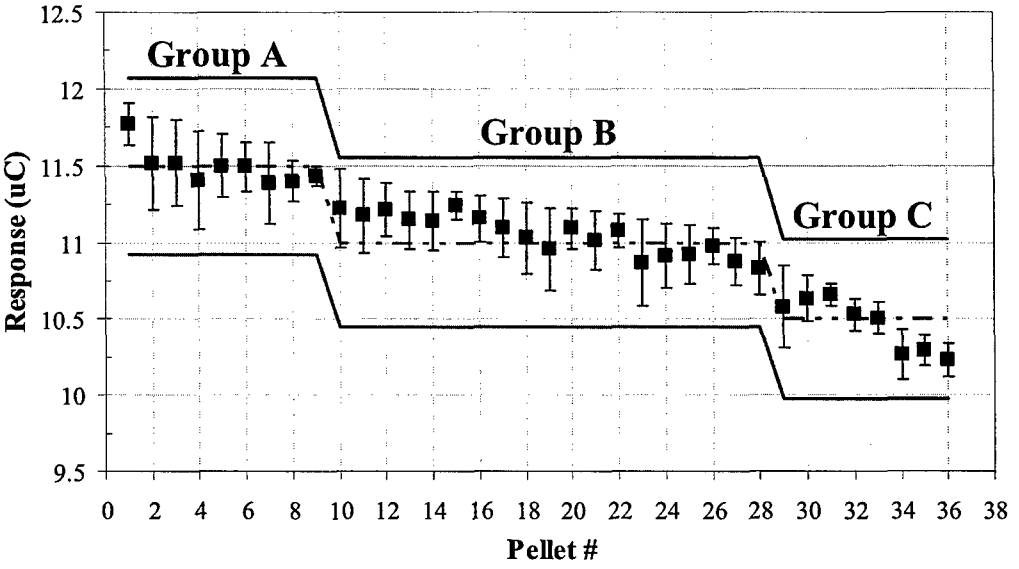

Figure 3.9. TLD Homogeneity Groups. The maximum relative error of each pellet is 3%; the maximum deviation from the mean (within each group) is 5%.

The UW Accredited Dosimetry Calibration Laboratory (ADCL) has created a series of X-ray beam qualities which were selected to match the beam qualities offered by the National Institute of Standards and Technology (NIST). The number indicates the x-ray tube voltage at constant potential, and the letter M indicates moderate filtration. UW matches these beam qualities with an advanced x-ray constant potential generator by setting the same kV as the NIST beam quality and adjusting the additional filtration to appropriate NIST beams (see Table 3.6). Inherent filtration for the UW-ADCL x-ray unit is 3.0 mm of beryllium, resulting in larger HVLs than those in Table 2.2.

Relying on the UW-ADCL, TLD pellets were calibrated to a 1 Gy dose of radiation (air kerma) according to the source specifications in Table 3.7.

Table 3.6. Selected UW Beam Codes (tungsten anode)

Beam Code	1st HVL (mm Al)	2nd HVL (mm Al)
UW80-M	2.96	4.35
UW100-M	4.98	6.92
UW120-M	6.96	8.92
UW150-M	10.2 (0.68 mm Cu)	11.72

Table 3.7. TLD Pellet Calibration Groups (air kerma).
One TLD pellet was used as a control in each group.

Source	Group	# of Pellets	CF (μC/Gy)
UW100-M	B1	5	21.40
UW120-M	B2	8	20.91
UW150-M	B3	5	20.16
Co-60	A	8	10.25
Cs-137	C	7	10.53

3.4.4. Sources of Error

The TLDs and TLD reader both contributed to potential uncertainty and were thus analyzed separately. Thermoelectron TLD chips and pellets consistent with those used for this project possess the sources of intrinsic error listed in Table 3.8 (Velbeck 1999).

Although the manufacturer advertises a batch homogeneity that is within 15% (compare with 11% and 9% in Table 3.8), this value was unacceptable for the requirements of this project. Experimental data was collected to verify these figures, and homogeneity uncertainty for pellets and chips was found to be 4.55% and 9.02%, respectively. By further grouping the TLDs into smaller subsets we were able to reduce this to <1.66% (pellets only). Finally, total uncertainty for pellets and chips was re-computed, and found to be 4.64% and 10.24%, respectively (see Table 3.9).

Additional sources of uncertainty associated with the Harshaw 4000 TLD reader are listed in Table 3.10 (Muniz 1995):

Table 3.8. Sources of Error, TLD Pellets and Chips.

Source	% Error, Pellet	% Error, Chip
Reproducibility	0.9	1.7
Homogeneity	≤ 11	≤ 9
Light Sensitivity (Dark conditions vs. 10 lux fluorescent lamp, 24 hrs)	0.99	0.88
Climate (90% humidity, 30 days)	4.12	4.48
Total Error	*11.82*	*10.23*

Table 3.9. Adjusted Sources of Error, TLD Pellets and Chips.

Source	% Error, Pellet	% Error, Chip
Reproducibility	0.9	1.7
Adjusted Homogeneity	1.66	9.02
Light Sensitivity (Dark conditions vs. 10 lux fluorescent lamp, 24 hrs)	0.99	0.88
Climate (90% humidity, 30 days)	4.12	4.48
Adjusted Total Error	*4.64*	*10.24*

Table 3.10. Sources of Error, TLD Reader.

Source of Error	Error (%)
Calibration of system	0.70
Determination of group mean value	0.20
Determination of f_e	0.30
Determination of f_s	0.50
Determination of absolute dose against reader algorithm	0.15
Total Error	0.94

3.4.5. Limitations and Applicability

TLDs are the most widely used detectors in personal radiation dosimetry (Weinstein 2003 and Zoetelief 2001). One of the most common phosphors, LiF, is considered tissue equivalent (compare $Z_{eff,\,LiF} = 8.2$ to $Z_{eff,\,tissue} = 7.4$) when combined with impurities such as magnesium, copper, and phosphorus (Gamboa-deBuen 1998). The advantages of TLDs include their capability of being reused several times, the small detector size (spatial resolution on the order of millimeters), and wide linear dose range from <1 μGy to a few Gy (Zoetelief 2001). In contrast, the main drawback for TLDs is related to annealing of the detector after readout, i.e., reproducibility. TLDs are not direct-reading detectors; however, readings can be obtained quickly with on-site readout systems.

Figure 3.10 compares the energy dependence of TLDs with different compositions, i.e., TLD-100 LiF chips vs. pellets. Above 100 keV, TLDs are generally energy independent, but below this value TLDs tend to over respond.

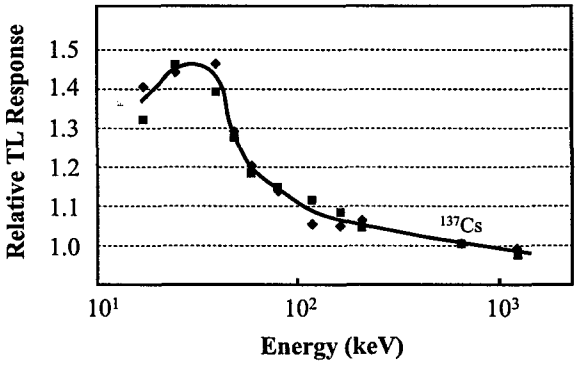

Figure 3.10. Energy response of TLD-100 chips (♦) and pellets (■); relative to 137Cs (Velbeck 1999).

3.5. Film Dosimetry and Scanning Film Digitizers

3.5.1. Principles of Operation

Film dosimetry is a relative radiation detection method that "took off" as a result of the urgent need to monitor Manhattan District workers during World War II (Frame 2004). One capability unique to film dosimetry is that dose distributions can be measured simultaneously over an entire plane. In addition, the high spatial resolution is limited only by the grain size of the film and by the size of the detector aperture of the densitometer (Mack 2003). The two most popular film types currently used for radiation dosimetry are silver halide radiographic films and self-developing radiochromic films. Table 3.11 provides a brief comparison of these two film types.

Table 3.11. Radiographic vs. Radiochromic Film.

	Radiographic	Radiochromic
Technology	Silver halide	GafChromic
Dose range	mGy – Gy	cGy – 10 Gy
Energy dependence	High	Low
Processing	Wet chemistry	Self developing
Size	Various	< 11"
Read method	Densitometer	Light-sensitive densitometer

Radiographic film (see Figure 3.11) employs a physical support (i.e glass plate, paper, or cellulose acetate) coated on one or both sides with a photographic emulsion (Frame 2004). The emulsion consists of silver bromide crystals suspended in a gelatinous matrix. Exposure to radiation promotes some of the electrons to impurities in the crystals where they reduce the silver. Later, during the development of the film, these specks of metallic silver speed up chemical reduction of the crystals. It is the resulting

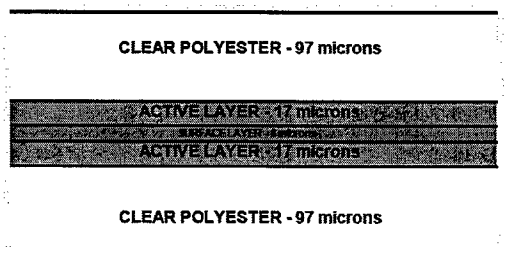

Figure 3.11. Composition of GafChromic EBT film (International Specialty Products, Wayne, NJ).

conversion of silver halide to metallic silver that gives the film its dark color. After the film is removed from the developer, it is washed and transferred into a fixative that dissolves the unreduced silver bromide. After the residual fixative is washed off, the film can safely be exposed to light and analyzed.

GafChromic dosimeters, unlike radiochromic dye films, have radiosensitive layers which contain microcrystals of a monomer. Ionizing radiation causes partial polymerization of the monomer into a blue (λ_{max} = 636 nm) polymer (Klassen 1997), which can be measured as a change in *OD* and used to compute the absorbed dose. EBT GafChromic film (used for this project) was designed for absorbed dose measurements in high-energy photon beams. As quoted by the manufacturer, the film has a useful dose range from 0.01 to 8 Gy, and an atomic composition of H (39.7%), C (42.3%), O (16.2%), N (1.1%), Li (0.3%), and Cl (0.3%). The structure of the EBT film consists of two sensitive layers, each having a thickness of 17 μm and separated by a 6 μm surface layer (refer to Figure 3.11) all sandwiched between two 0.97 μm clear polyester sheets (Devic 2005).

GafChromic EBT film can be measured with transmission densitometers, scanning film digitizers (SFD), or spectrophotometers. Maximum absorption within the active component of the film occurs at λ = 636 nm. Consequently, the response of EBT film will be enhanced by measurement with red light (ISP 2005). Measured absorption values (i.e., pixel intensity) are used to calculate *OD* according to Eq. (3.4). Absorbed dose is proportional to *OD*, and the two can be related by a calibration curve.

SFDs, or film scanners, are capable of digitally scanning an entire film image, and thus provide *OD* and absorbed dose values at every location on a 2D grid. A few distinguishable qualities of SFDs are the type of densitometry, the spatial resolution, and the number of bits per pixel (i.e., scanner output). While traditional office scanners rely on reflection densitometry, film scanners generally provide transmission optical densitometry. The latter produces a greatly increased range of *OD* values, and is

important for broad-beam dosimetry studies where the beam intensity may vary significantly with respect to location and absorbed dose.

Spatial resolution is especially important when trying to study dose deliveries to small groups of cells. Resolution is typically given as the number of pixels per unit length (dpi), which is squared to define an area (i.e., 200 dpi correlates with 40,000 pixels in^{-2}). Thus, a nominal 1200 dpi SFD scans with a resolution of 1.44×10^{6} pixels in^{-2}, which is equivalent to 0.0022 pixels μm^{-2} according to the following equation:

$$\text{Spatial Resolution} = \frac{(1200)^2 \text{ pixels}}{(\text{in})^2} \times \frac{\text{in}^2}{\left(2.54\times10^{4}\mu\text{m}\right)^2} = 0.0022 \text{ pixels } \mu m^{-2}. \quad (3.11)$$

By inverting this result (448.0 μm^2 $pixel^{-1}$) and assuming a cellular cross-sectional area of 100 μm^2, the expected number of cells per pixel (assuming a minimum volume of interstitial space) can be determined:

$$\text{Cellular Resolution} = \frac{448.0\mu\text{m}^2}{\text{pixel}} \times \frac{\text{cell}}{100\ \mu\text{m}^2} = 4.48 \text{ cells pixel}^{-1} \quad (3.12)$$

For radiation dosimetry applications, scan output is as important or more important than spatial resolution. Scan output is usually reported in bits per pixel, and relates to the number of shades of gray that are stored with the pixel information. The number of shades of gray can be calculated:

$$\#\ of\ Shades = 2^n - 1. \quad (3.13)$$

For example, a 2-bit grayscale image contains three ($2^2 - 1 = 3$) shades of gray per pixel, whereas a 16-bit grayscale image contains 65,535 ($2^{16} - 1 = 65,535$) shades of gray per pixel (see Table 3.12 for a summary of common scan outputs).

There are two related reasons why scan output is critical to achieving useful values of *OD*. First, absorbed dose varies as a function of *OD* and so a large number of shades are necessary to distinguish between slight variations in dose. An 8-bit scanner has 255 shades and cannot provide these slight variations, i.e., the mean difference between

computed dose values is 0.18 Gy. A 16-bit scanner, on the other hand, can produce 65,535 unique dose values with a mean difference of 0.002 Gy. Consequently, SFDs with high scan outputs provide superior analysis of irradiation patterns.

Second, to identify abnormal medical findings clinicians rely on even the slightest perturbations in grayscale threshold (these often occur in *OD* regions >2.5). 8-bit SFD technology cannot provide *OD* values in this range. Many of the SFDs currently used in clinical applications (i.e., Lumysis laser scanning system, Vidar VSR-16 Digitizer, etc.) rely on 16-bit scan output, and can achieve *OD* values above 4.0. In this "near-black" region (i.e., $OD > 2.5$), 207 additional shades of gray are available. Table 3.12 provides a summary of common scan outputs along with their corresponding number of shades.

Table 3.12. Common Scan Outputs.

Scanner Output	# of shades per pixel	# of shades in near-black region
8-bit	255	0
12-bit	4,095	12
16-bit	65,535	207
24-bit	16,777,215	53,054

The SFD used in this project was a commercial flatbed 16-bit film scanner manufactured by Canon (see Figure 3.12). The CanoScan 9950F provide 4800 × 9600 dpi optical resolution, and 48-bit 3-channel color output, i.e., 16-bit output per channel.

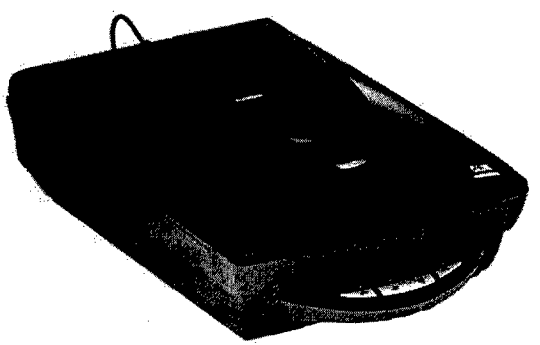

Figure 3.12. Canon CanoScan 9950F 16-bit flatbed transmission scanner (Canon USA).

3.5.2. Laboratory Procedures

Film samples were handled in accordance with recommendations outlined in the AAPM TG-55 report. The film sheets were only removed from their light-protective envelope during

irradiation and readout to reduce the effects of ambient light. Detailed lab procedures are provided in Appendix B.

3.5.3. Calibration

OD has been defined (Stevens 1996 and Cai 2003) as:

$$OD = log_{10}\left(\frac{S_0}{S}\right), \tag{3.14}$$

where S_0 is the mean pixel intensity of unexposed films, and S for exposed films. The *OD* response to *D* was further described as:

$$ln(OD) = ln(a) + \alpha \cdot ln(D), \tag{3.15}$$

where *ln(a)* is the y-intercept and α is the slope of the linear regression fit when *ln(OD)* is plotted against *ln(D)*.

A batch of EBT radiochromic film (ISP, Lot No. 35076-002AI, Exp. Date: March 2007) was irradiated in accordance with the calibration procedures in Appendix B. The Faxitron x-ray machine had the following configuration:

- Shelf height: Top
- Plexiglass template: Inserted
- Filtration: 0.4mm Cu and none.
- kVp: 130 kVp

Films used in the filtered and unfiltered beam were calibrated to the RadCal 30×6-11 parallel-plate ionization chamber (traced to the UW 1 Gy air kerma standard), which indicated an absorbed dose rate (in water) of 1.724 Gy hr^{-1} and 75.678 Gy hr^{-1}, respectively, at the center of the Faxitron x-ray beam.

Table 3.13. Selected irradiation times (s), Cu filtered beam.				
0	30	150	480	2100
5	40	180	600	2400
10	50	210	900	2700
15	60	240	1200	3000
20	90	300	1500	3300
25	120	360	1800	3600

Table 3.14. Selected irradiation times (s), unfiltered beam.				
0	30	60	150	240
5	35	75	165	255
10	40	90	180	270
15	45	105	195	285
20	50	120	210	300
25	55	135	225	315

Solving for Eq. (3.15), the values for α and $ln(a)$ were found to be 0.9066 and -2.0582 for filtered beam and 0.6701 and -1.9691 for unfiltered beam, respectively. Figure 3.13 shows that the logarithm of the optical density is directly proportional to the logarithm of absorbed dose.

By rearranging Eq. (3.15) to solve for D, we obtain:

$$D(\text{Gy}) = e^{\frac{ln(OD)-ln(a)}{\alpha}}. \tag{3.16}$$

By further substituting the corresponding constants for each study, a calibration curve can be obtained for the EBT film (see Figures 3.14).

The absorbed dose can be estimated with the EBT film by measuring the OD in a region of interest and solving the following equations for each study, respectively:

$$\text{0.4 mm Cu filtered beam: } D(\text{Gy}) = e^{1.1ln(OD)+2.27}, \text{ and} \tag{3.17}$$

$$\text{Unfiltered beam: } D(\text{Gy}) = e^{1.5ln(OD)+2.94}. \tag{3.18}$$

Warm-up and other artifacts associated with the scanner produced some inconsistencies in dose estimates determined with the EBT film. To increase the accuracy and reliability of the results obtained with the EBT film, dose estimates derived from Eqs. (3.17) and (3.18) at the center of the Faxitron beam were re-normalized to reproduce ionization chamber measurements at the center of the beam. Table 3.15 lists the calibration factors used to re-normalize dose estimates derived from Eqs. (3.17) and (3.18) so that they agree with the ionization chamber measurements. The fact that the calibration factors are near identical in the presence or absence of a Cu hardening filter indicates that both the film and ionization chamber are energy independent. Additional details of the artifacts caused by the Canon 9950F scanner are discussed in the next session, Sources of Error.

Table 3.15. Calibration factors used to normalize EBT GafChromic film to RadCal 30×6-11 parallel plate ionization chamber dosimetry standard.

	With 0.4 mm Cu filter	Without filter
Broad beam	1.512	1.514
Millibeam	1.234	1.107

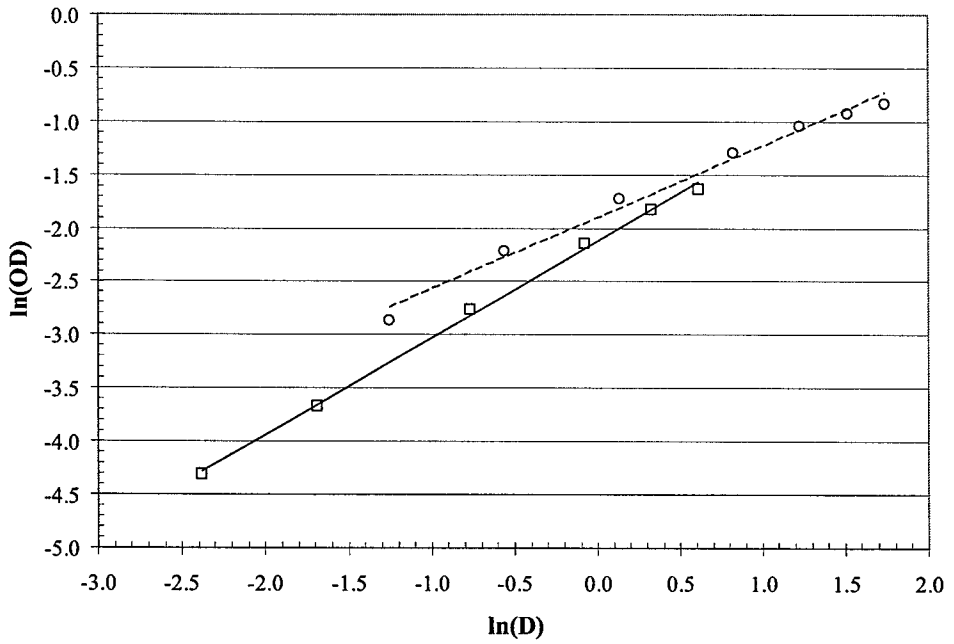

Figure 3.13. Determination of α and *ln(a)* for a filtered beam (squares, α=0.9066; *ln(a)*=-2.2792; r^2=0.998) and an unfiltered beam (circles, α=0.6669; *ln(a)*=-2.0735; r^2=0.988).

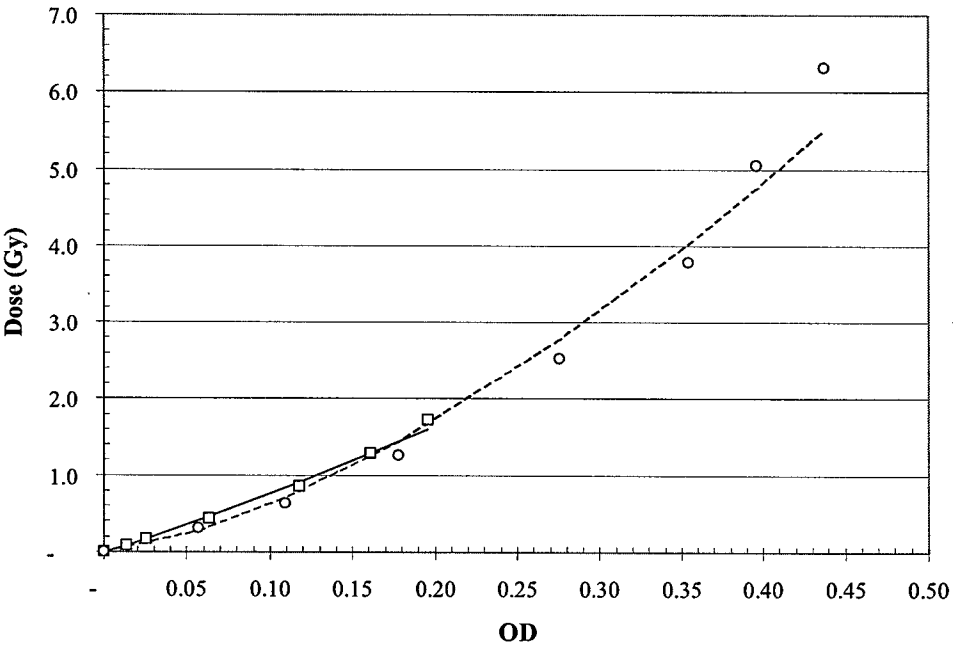

Figure 3.14. EBT film dose-response curve (absorbed dose in water) for a filtered beam (α=0.9066; *ln(a)*=-2.2792) and an unfiltered beam (α=0.6669; *ln(a)*=-2.0735). The squares and circles represent the corresponding ionization chamber data for the filtered and unfiltered beam, respectively. The solid and dashed lines represent the fit of Eq. 3.17 and 3.18, respectively.

3.5.4. Sources of Error

Sources of uncertainty were determined for the EBT GafChromic film and CanoScan 9950F. EBT film has a preferred orientation and will produce as much as 10% variation if scanned in landscape mode vs. portrait mode (ISP 2005). It's therefore important to consistently scan the film along the same axis. Tables 3.16 lists those sources of error associated with EBT GafChromic (Cheung 2005 and Butson 2006).

Studies have found (Mersseman 1998 and Devic 2005) that film scanners provide repeatable results to within 0.2%. Two significant sources of error related to the CanoScan 9950F include warm-up effects (5 – 10% variability if not warmed up for ~10 minutes) and edge effects (up to 20% variability) along the upper half (side nears the hinge) of the scanner. Other sources of error are listed in Table 3.17 (Mersseman 1998 and ISP 2005).

In one study, the overall uncertainty for EBT film in conjunction with an Agfa Arcus II scanner was found to be 5% (Devic 2005). The Arcus II scanner is an older model film scanner capable of 12-bit grayscale scans and an optical resolution of 600 × 1200 dpi.

After several experiments with the Canon 9950F transmission scanner, it was noted that the measured pixel intensity in the first 37 mm adjacent to the hinge of the scanner lid was found to have an average relative error (s.d./mean) of 20.17% $\pm$0.17% over a series of seven scans. The next 37 mm (away from the scanner lid) produced a relative error of 5.51%. Subsequent measurements taken at 37 mm intervals towards the front of the scanner produced average relative errors of 2.48%, 1.12%, 0.78%, and 0.89%, respectively. Clearly, the back 1/3 of the scanner (nearest the hinge of the scanner lid) produces the greatest variation. This did not appear to be related to the warm-up effect, and strictly seemed a product of the position of the film on the scanning bed.

Table 3.16. Sources of Error, EBT GafChromic Film.

Source of Error	Error (%)
Batch composition/uniformity	<5
Energy dependence (125 kVp x-ray)	<7
Post irradiation stability	6 – 9
Film thickness	Negligible
Sensitivity to indoor lighting	Negligible
Temperature (highly sensitive, otherwise)	negligible, lab
Storage effects	Negligible
Scan direction (must remain consistent)	10
Surface smudges (wear gloves, handle carefully, gently clean with lens cleaner rag)	Negligible
Total Error	*15.0*

Table 3.17. Sources of Error, SFDs.

Source of Error	Error (%)
Warm-up effects, requires 20 min warm up	0.12
Noise	0.20
Geometric accuracy (i.e., variability of resolution)	<0.2
Effect of horizontally scattered light (i.e., edge effects)	2
Total Error	*2.02*

3.5.5. Limitations and Applicability

EBT GafChromic film was selected for this project because of its: i) ability to self develop; ii) compatibility with a transmission technology scanner; iii) near-tissue equivalence (compare $Z_{eff,\,EBT} = 6.98$ to $Z_{eff,\,tissue} = 7.4$); iv) high sensitivity over a wide dose range (i.e., 0.01 – 8 Gy); and v) relative energy independence compared to radiographic film and other radiochromic film designs, i.e., <7% variance (Butson 2006). Other advantages common to film dosimetry in general include unrivaled spatial

distribution, 2-D dose distribution with single exposure, and variable detector size. Limitations of EBT film include: 1) *OD* increases gradually with time; 2) temperature dependent during and after irradiation; 3) sensitivity may vary somewhat across film; 4) preferred scan direction of film; and 5) *OD* may increase in UV light.

In recent years, the SFD is becoming the film reader of choice given the appropriate choice of channel and color adjustment. SFDs are superior to densitometers with respect to economy, sensitivity and measurable dose ranges and to spectrophotometers with respect to spot measurement (Cai 2003). Common artifacts of SFDs include:

- Drift in *OD* from warm-up effect of fluorescent lamp (corrective action: use first 20-30 minutes as warm-up time)
- Scanner spatial distortion
- Interference at the interface of film and glass plate from multiple reflection due to changes in the index of refraction (corrective action: use diffused glass or anti-reflective coated glass)
- Poor signal-to-noise ratio from temporal electronic and spatial noise (corrective action: reduce digitizing speed, use optimal resolution, average multiple scans, and/or apply linear signal processing techniques).

4. RESULTS

This chapter reports the results of a series of studies designed to assess the accuracy and reproducibility of the absorbed doses and absorbed dose rates achievable with the filtered and unfiltered 130 kVp HP Faxitron x-ray machine (i.e., with and without the 0.4 mm Cu filter). Tables of the estimated absorbed dose as a function of beam time are reported for cell culture dishes located at selected locations within the Faxitron beam. Absorbed dose estimates are reported with and without corrections for the effects of attenuation in thin layers of water, which is used as a surrogate for cell culture medium. GafChromic film was used to quantify the spatial distribution of absorbed dose within a 9-cm Petri dish for the broad beam and millibeam configurations of the Faxitron x-ray.

4.1. Operational Characteristics of the HP Faxitron

4.1.1. Accuracy and Reproducibility of Absorbed Dose Rates

To test the accuracy and reproducibility of the Faxitron x-ray, fluence repeatability and peak kVp tests were performed. The principal sources of uncertainty associated with the operational characteristics of the HP Faxitron x-ray machine are summarized in Table 4.1.

A Radiation Measurements Model 230 (SN 1154) was used to verify the maximum kVp output of the Faxitron x-ray. A prior calibration was performed on Aug 9, 2005, and a certificate is provided in Appendix C. With the Faxitron kVp manual adjustment tuned to 130 kVp, an output of 129 kVp was measured with the Model 230 instrument. Five repeat tests were performed, and all measurements were identical. These results were consistent with the kVp output display on the Faxitron x-ray, which over several 1-

minute tests was found to consistently report 128 to 129 kVp. This small (< 1%) drop, known as the ripple, is a common response of single-phase fixed anode x-ray machines, and can be calculated from Eq. (2.8).

Additional tests were performed to compare the x-ray production with and without an uninterrupted power supply (UPS). Using the RadCal 30×6-11 parallel-plate ionization chamber, comparison exposures with and without the UPS indicated a 0.245% negligible difference over a 4-minute irradiation. The accuracy of the solid-state timer used to control the irradiation time was also tested. Repeat measurements indicated the timer loses 2-seconds during a 59 minute and 59-second exposure (i.e., 0.056% loss).

Fluence repeatability tests were accomplished with the RadCal 3036 parallel-plate ionization chamber (refer to Chapter 3, Section 3). Figure 4.1 shows that the % relative error in the estimated dose rate decreases as the irradiation time increases. To wit, the relative error can be reduced to 3% for an irradiation time of 8 seconds. Ionization chamber measurements (Figure 4.2) demonstrate that the absorbed dose is proportional to the irradiation time up to at least 4 minutes. Measurements performed with Fricke dosimetry (Figure 3.3) indicate that the absorbed dose is proportional to irradiation time up to 59 minutes and 59 seconds (i.e., the maximum irradiation time in a single shot). The results of these linearity tests imply that fluctuations in the absorbed dose rate are negligible for the irradiation times possible with the Faxitron.

Table 4.1. Sources of Error, Faxitron X-ray.

Source of Error	Error (%)
Repeatability ($t \geq 8$ seconds)	< 3
Startup surge	1
kVp adjustment, manual fine tuning	1
Filter and/or shield orientation	Negligible
Total Error	*3.31*

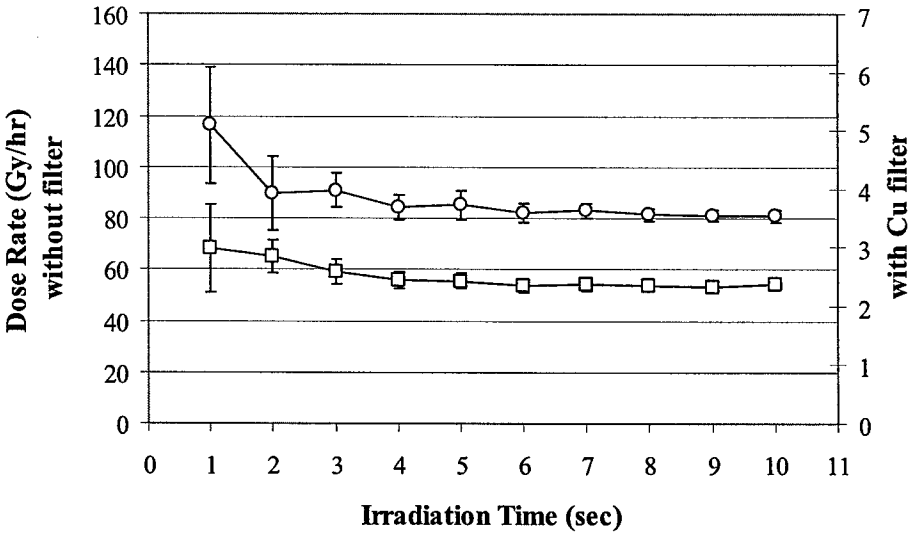

Figure 4.1. Absorbed doses delivered at the center of the 130 kVp x-ray beam. Squares denote insertion of 0.4 mm Cu filter; circles are without filter. Measurements were performed with the RadCal 3036 parallel-plate ionization chamber. Below 5 seconds, the relative error (%) is >5.5% and >6.7% respectively.

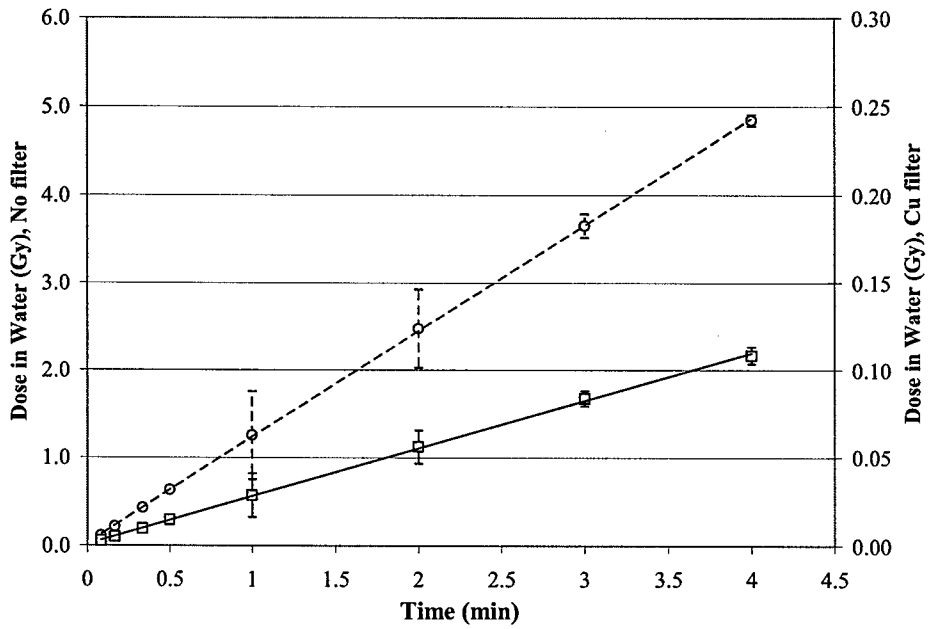

Figure 4.2. Absorbed dose as a function of irradiation time (0 to 4 minutes). Squares denote insertion of 0.4 mm Cu filter; circles are without filter. Measurements were performed with the RadCal 3036 parallel-plate ionization chamber. Error bars are not shown for irradiations below 1 minute to avoid merging data points.

4.1.2. Uniformity of the Faxitron Irradiation Field

While operating the Faxitron x-ray machine, it's important to take steps to minimize the impact of rack height and beam uniformity. There are two irradiation shelves that are accessible in the upper cabinet of the Faxitron x-ray machine. All measurements associated with this project were accomplished using the top irradiation shelf.

A beam uniformity study was performed to determine the variability in beam intensity across the field of interest (i.e., 26.035 cm diameter broad beam). Figure 4.3 shows the uniformity of the filtered beam, and Figure 4.4 shows the uniformity of the unfiltered beam.

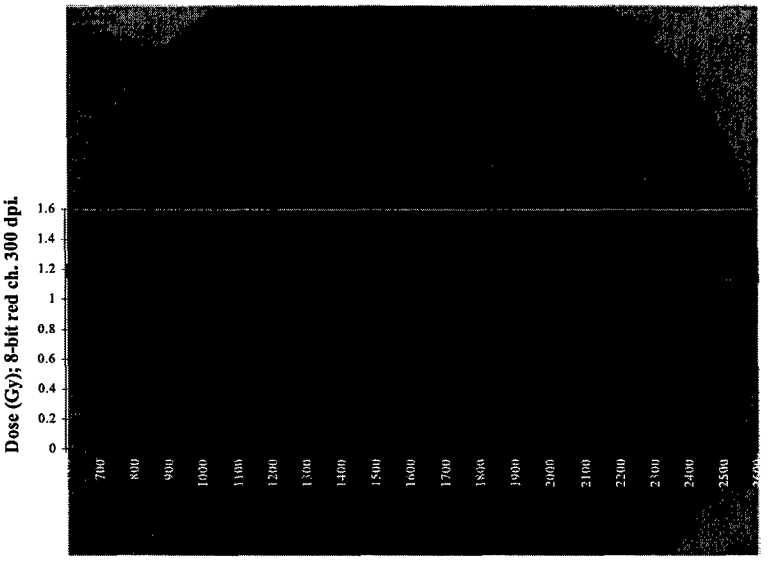

Figure 4.3. Absorbed dose distribution within the 130 kVp Cu-filtered x-ray beam (nominal 1 Gy dose). The area of the beam is 532.4 cm^2. The maximum dose is 1.42 Gy and the minimum dose is 0.77 Gy (ratio of maximum to minimum is 1.84).

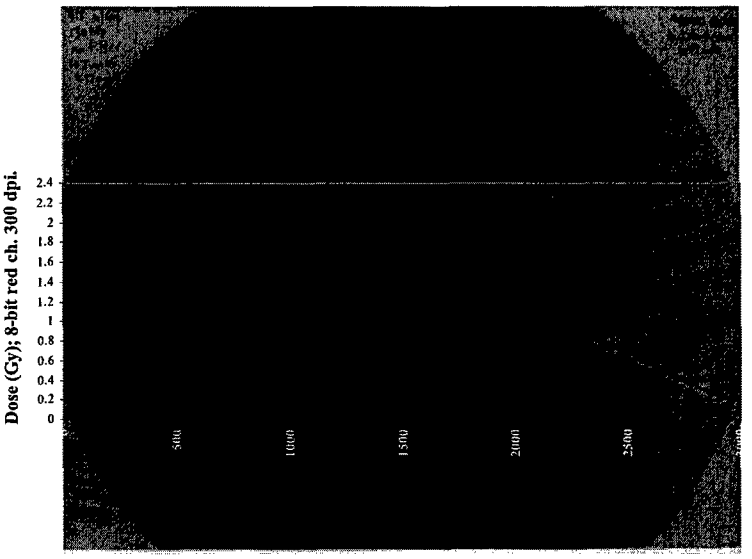

Figure 4.4. Absorbed dose distribution within the 130 kVp unfiltered x-ray beam (nominal 1 Gy dose). The area of the beam is 532.4 cm^2. The maximum dose is 2.26 Gy and the minimum dose is 0.18 Gy (ratio of maximum to minimum is 12.42).

Beam uniformity results are summarized in Table 4.2, and are given as the maximum and minimum absorbed dose across the horizontal axis of the beam. The relative error associated with uniformity along the y-axis was found to be less than 1 percent for both the filtered and unfiltered beam. Without the filter, there is a 3.79% relative error in absorbed dose from edge-to-edge along the x-axis of a 9 cm Petri dish centered on the beam. For the filtered beam, the relative error is 13.89% along the x-axis of a 9-cm Petri dish. Petri dishes on the anode side of the beam (right side of beam) experience a larger variation (~20%) than those on the cathode side (refer to Figure 4.4). The large field variation without the filter is a consequence of the heel effect (discussed at length in Chapter 2, Section 2.2.4).

Table 4.2. Absorbed dose distribution along the x-axis of the Faxitron 130 kVp filtered and unfiltered x-ray beam.		
Region of Interest	0.4 mm Cu filter	No filter
26.035 cm broad beam		
– Maximum *D* in water (Gy)	1.42	2.26
– Minimum *D* in water (Gy)	0.77	0.18
– Ratio of Max./Min.	1.84	12.42
9 cm Petri dish (centered on broad beam)		
– Maximum *D* in water (Gy)	1.42	2.00
– Minimum *D* in water (Gy)	1.20	1.05
– Ratio of Max./Min.	1.18	1.91

4.1.3. Absorbed Dose Rate at Surface of Water in 9 cm Petri Dish

Energy deposition studies were accomplished with 4-mL Fricke dosimeters (Chapter 3, Section 3.2), calibrated parallel-plate air wall ionization chamber (Chapter 3, Section 3.3), and calibrated LiF TLD-100 pellets (Chapter 3, Section 3.4). TLD pellet group B2 (air kerma calibration factor: 4.842 ± 0.2 cGy μC^{-1}) was used for both the filtered and unfiltered beam. Irradiation times ranged from 10 seconds to 4 hours. The Faxitron cabinet and operational settings were as follows:

- Shelf height: Top
- Chamber position: Center of beam
- Filtration: 0.4mm Cu (1st study) and none (2nd study)
- 130 kVp
- 3 mA

Ionization chamber measurements indicate that the absorbed dose rate at the water surface is constant for irradiation times as long as 5 minutes (0.144 Gy) for the filtered (0.4 mm Cu) beam (Figure 4.5) and up to 10 minutes (12.613 Gy) for the unfiltered beam (Figure 4.6). As expected, the dose rate with the filter in place is much lower (30× lower) than without the filter, a result of the attenuating effects of 0.4 mm of copper. The useful

range of the Fricke dosimeter is 20 to 400 Gy (ASTM 2005), which corresponds to an irradiation time of 13 – 133 hours for the filtered beam and 0.5 to 5.5 hours for the unfiltered beam. The former was not obtainable due to power interruptions in the lab electrical system.

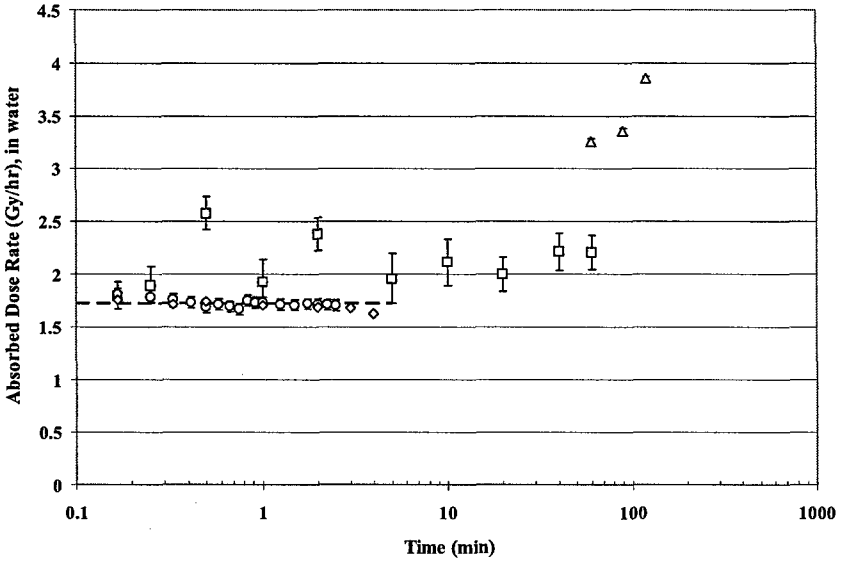

Figure 4.5. Absorbed dose rate in a thin layer of water (Gy/h), Cu filtered 130 kVp Faxitron spectrum, top center irradiation shelf,. Diamonds and circles are the 11 cm^3 and 180 cm^3 ionization chambers, respectively (1.724 Gy h^{-1} $\pm$ 0.0747 Gy h^{-1}). Squares and triangles denote TLD and Fricke dosimeter measurements, respectively.

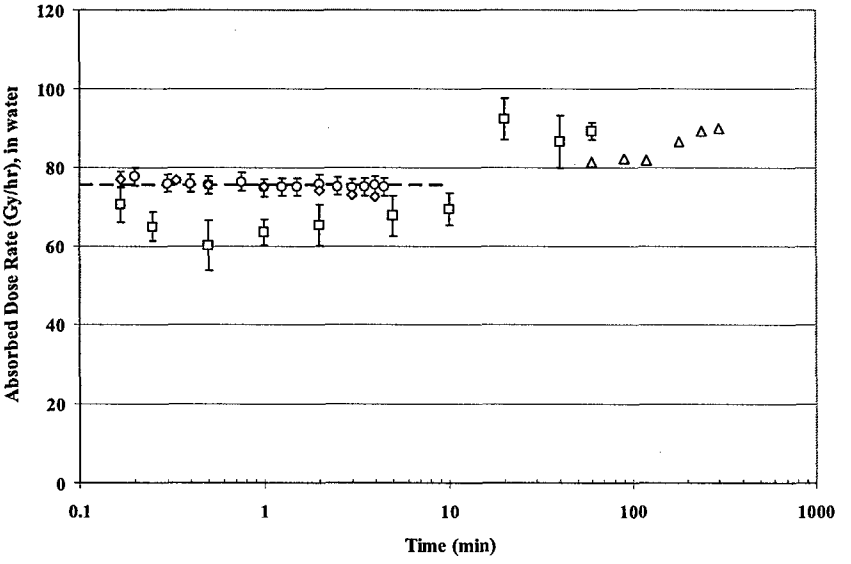

Figure 4.6. Absorbed dose rate in a thin layer of water (Gy/h), unfiltered 130 kVp Faxitron spectrum, top center irradiation shelf,. Diamonds and circles are the 11 cm^3 and 180 cm^3 ionization chambers, respectively (75.68 Gy h^{-1} $\pm$ 2.60 Gy h^{-1}). Squares and triangles denote TLD and Fricke dosimeter measurements, respectively.

4.1.4. Effect of Water Thickness on Faxitron Absorbed Dose Rates

Attenuation in water is a function of energy (see figure 4.7), and is highest for low-energy photons like those present in the unfiltered 130 keV spectrum (see Chapter 2, Figure 2.13).

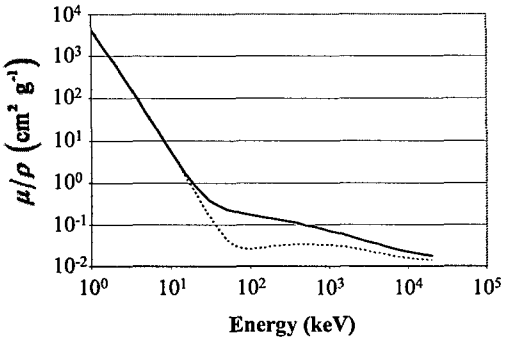

Figure 4.7. Mass attenuation coefficient (solid line) and mass energy absorption coefficient (dashed line) for water.

A study was completed to determine the effect of water thickness on absorbed dose for a 130 keV tungsten x-ray (0.64 mm intrinsic Beryllium filtration).

The relative reduction in dose was determined with the RadCal 30×6-11 parallel-plate ionization chamber. The sensitive volume was placed in the center of the beam (top shelf) under a 9-cm diameter cell culture dish filled with varying thicknesses of water. For these experiments, a minimum threshold of deionized water is necessary (5 mL) to cover the base of the Petri dish and overcome water tension.

A linear-quadratic function is used to fit the data for the unfiltered beam, and provides a method to estimate the reduction in dose rate as a function of the thickness of the cell culture medium, e.g.,

$$\frac{D(x)}{D(0)} = ax^2 + bx + c. \tag{4.1}$$

By substituting Eq. (3.7) into Eq. (4.1), we can directly obtain the dose reduction factor, $D(x)/D(0)$, given the volume (V) of the water or culture medium in mL and the inside diameter of the Petri dish (d) in mm:

$$\frac{D(x)}{D(0)} = a\left(\frac{4000\ V}{\pi d^2}\right)^2 + b\left(\frac{4000\ V}{\pi d^2}\right) + c. \tag{4.2}$$

Values for *a*, *b*, and *c* have been determined empirically as a best-fit 2nd order polynomial for the unfiltered beam. The filtered beam can be adequately fit by a straight line (i.e., $y=bx+c$)

Results for the filtered and unfiltered beam are provided in Figure 4.8. For the filtered beam, values for *b* and *c* are -0.0092 $mm^{-1}$and 0.9978, respectively. For the unfiltered beam, values for *a*, *b*, and *c* are 0.0280 mm^{-2}, -0.2121 mm^{-1}, and 0.8261, respectively.

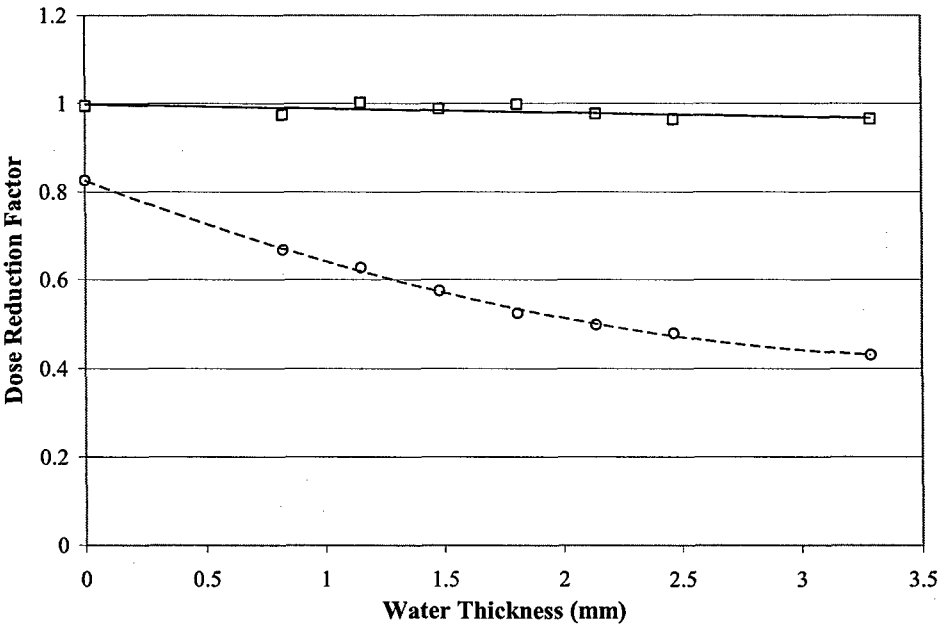

Figure 4.8. Reduction in the absorbed dose at the bottom of a Petri dish due to attenuation in cell culture medium (water). Squares and circles represent the filtered (0.4 mm Cu) and unfiltered beam, respectively. The value at 0 mm represents is less than unity because of attenuation within the lid of the Petri dish (0.6% and 17.5% for the filtered and unfiltered beams, respectively).

4.2. Absorbed Dose Distributions for the Faxitron Broad Beam and Millibeam

This section provides the operational configuration of the millibeam, and the absorbed dose patterns relevant to each millibeam. The latter is reported as a dose-volume histogram (DVH). The DVH is used extensively for 3-dimensional radiation treatment

planning. The general shape and area under the DVH curve is helpful in determining homogeneity of dose in the target volume (Drzymala *et al* 1991, Kutcher *et al* 1991).

4.2.1. Millibeam Configuration

Several millibeam studies were needed to ascertain the attenuation (and resultant absorbed dose) effected on the broad parallel x-ray beam by a series of system components (i.e., filtration, shielding, culture dishes and water medium). Table 4.3 provides a summary of the irradiation configurations used in these studies. The laboratory setup and orientation of the dishes inside the Faxitron cabinet is shown in Figures 4.9 and 4.10, respectively. Table 4.4 lists the dimensions of the millibeam, as well as the percent of dish (9 cm Petri) irradiated.

Table 4.3: Irradiation Configurations used for Faxitron Millibeam Studies

Configuration	*Filtration*	*Shielding*	*Absorption Medium(s)*
A	None	None	None
B	None	4 mm Pb & 8 mm steel	None
C	None	4 mm Pb & 8 mm steel	9 cm Petri dish w/lid
D	None	4 mm Pb & 8 mm steel	Dish with 1.64 mm water
E	0.4 mm Cu	None	None
F	0.4 mm Cu	4 mm Pb & 8 mm steel	None
G	0.4 mm Cu	4 mm Pb & 8 mm steel	9 cm Petri dish w/lid
H	0.4 mm Cu	4 mm Pb & 8 mm steel	Dish with 1.64 mm water

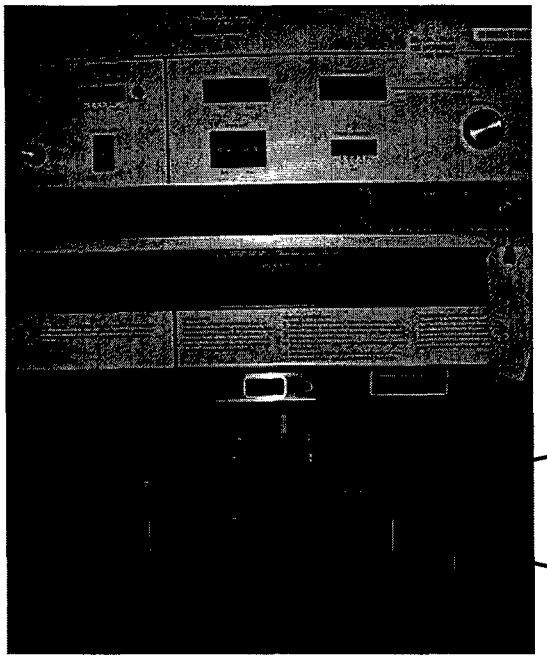

HP Faxitron Operator's Panel
- Peak Voltage: 130 kVp
- Irradiation time: 2 minutes

Millibeam Configuration in Faxitron X-ray Cabinet
- Top shelf
- Composite shield (4 mm Pb and 8 mm steel) with four holes to focus the x-ray millibeams
- Plexiglass template with wells to hold four 9 cm (outer diam.) pietri dishes

Figure 4.9. Millibeam configuration inside Faxitron.

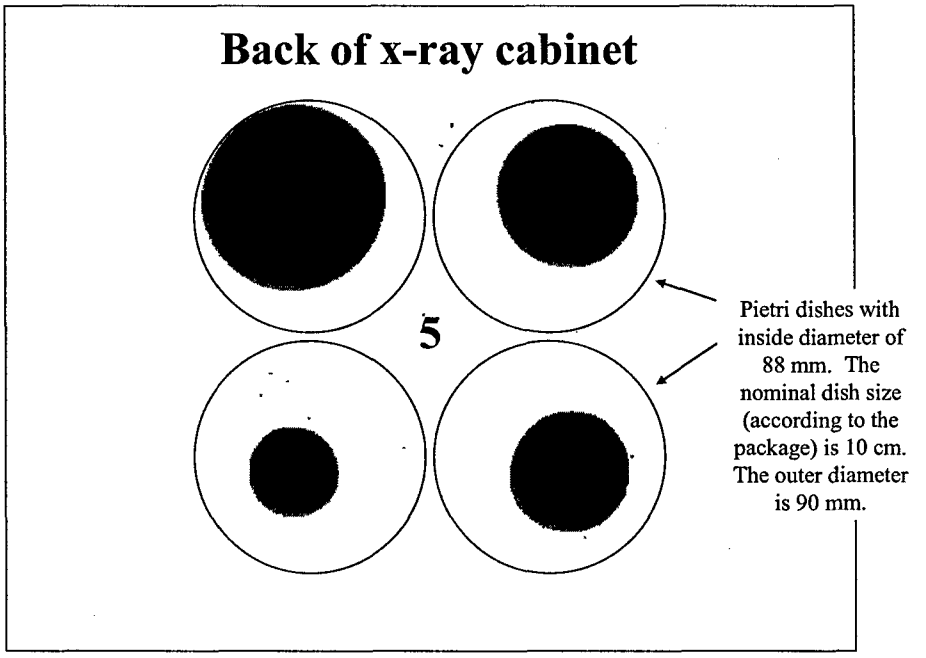

Figure 4.10. Orientation and millibeam targeting positions in Faxitron x-ray cabinet. Large circular discs represent relative size of 9 cm Petri dishes relevant to the millibeam x-ray fields. Position 5 is the center of the x-ray beam.

Table 4.4: Dish and Millibeam Dimensions.

Dish		*Millibeams*					
Inside diam. *mm*	Dish Area mm^2	Millibeam *Position #*	Pixels *Avg Count*	Beam Area mm^2	Diam *mm*	Diam *in*	% of dish irradiated *%*
88	6082.12	1	134500	3856.62	70.07	2.759	63.41%
88	6082.12	2	79100	2268.10	53.74	2.116	37.29%
88	6082.12	3	55200	1582.79	44.89	1.767	26.02%
88	6082.12	4	29000	831.54	32.54	1.281	13.67%

4.2.2. Dose-Volume Histograms

DVH plots were employed to describe the spatial pattern of dose delivery to the radiochromic film for configurations A (Figure 4.11 and 4.12), D (Figure 4.13 and 4.14), E (Figure 4.15 and 4.16), and H (Figure 4.17 and 4.18) as described in Table 4.3. The DVH for the remaining configurations (i.e., B, C, F, and G) are provided in Appendix D.

DVHs efficiently show the energy deposition characteristics within a given region of interest. Each DVH below is normalized to absorbed dose (in water) values obtained with the calibrated parallel-plate ionization chamber. A perfectly uniform beam would have a single bar indicating no variation in dose. Many bars indicate variation and overall lack of uniformity.

The DVH plots below are constructed to estimate the dose (in water) to the film. Regardless of the thickness of the medium, cells seeded at the bottom of the culture dishes will always receive 17.42% more dose than the film for the unfiltered beam. For the filtered beam, the cells will always receive 0.59% more dose than the film.

Configuration A: DVH for the unfiltered 130 kVp broad beam (no culture medium)

Figure 4.11 shows the response of EBT film to a broad beam irradiation conducted without the 0.4 mm Cu filter, without the millibeam shield, and without the culture medium (water). Figure 4.12 summarizes the absorbed dose distribution

delivered to the volume of interest (a 5.5 cm x 5.5 cm square region sampled inside the darker regions shown in Figure 4.11).

The image and plot below show the lack of uniformity of the broad parallel beam x-ray. The energy deposited in the four darker regions of the film was only attenuated through air while the remaining lighter region of the film experienced significant attenuation from the plexiglass insert used to support the millibeam shields and Petri dishes. The insert does not attenuate the beam prior to energy deposition in the Petri dish and was a result of film placement underneath the insert.

Positions 1 and 4 receive a larger dose than positions 2 and 3 because of the heel effect. The heel effect significantly increases the width of the DVH (refer to Figure 4.12) and is associated with a large standard deviation across the Petri dish.

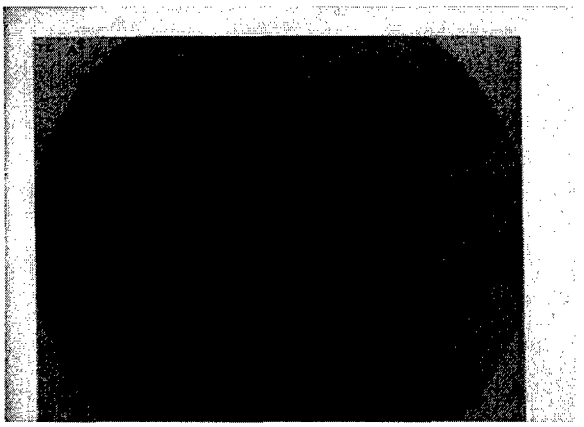

Figure 4.11. Irradiation patterns produced on the EBT film by the 130 kVp beam with no filtration (Configuration A, no shield or culture medium) during a 2-minute irradiation.

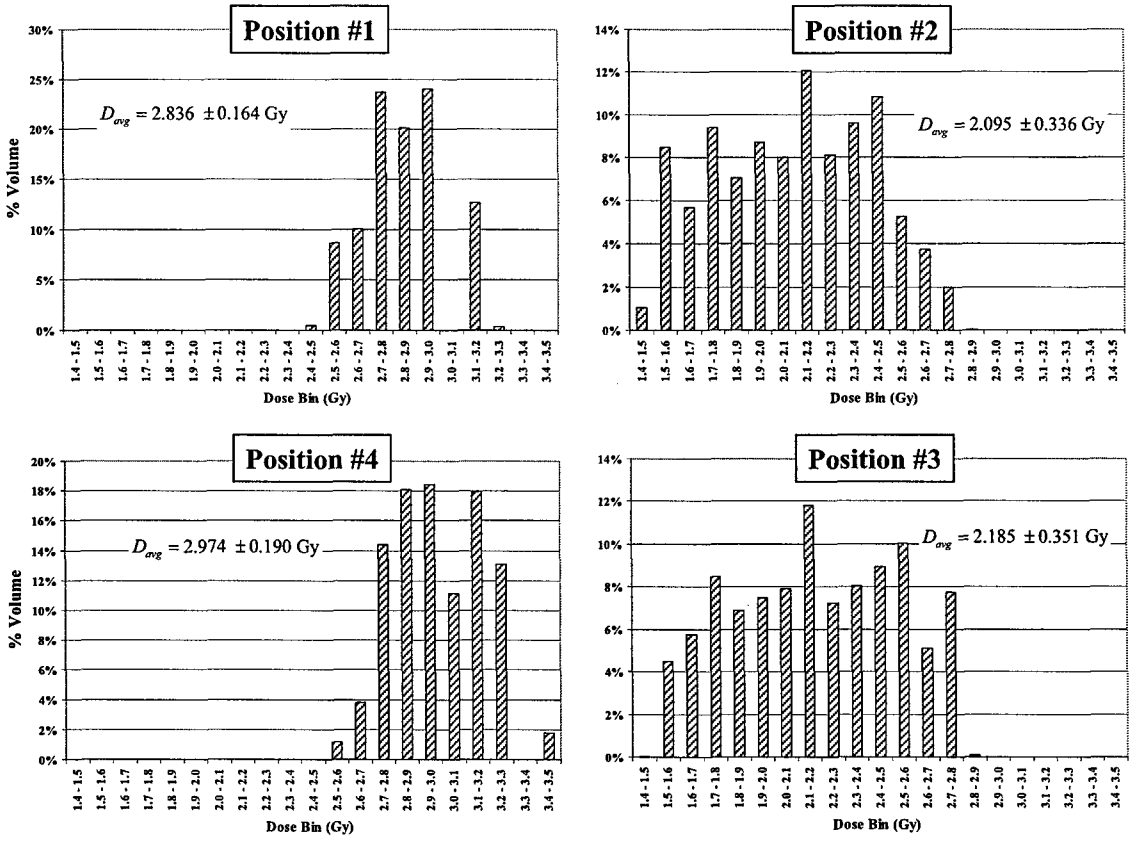

Figure 4.12. DVH for the unfiltered x-ray broad beam (Configuration A, no culture medium). A nominal 2.52 ±0.09 Gy dose (in water) was delivered to the center of the 130 kVp Faxitron beam during a 2-minute irradiation. Values for mean absorbed dose (in water) and standard deviation at each position are reported in the figure.

Configuration D: DVH for the unfiltered 130 kVp millibeam (1.64 mm of water in dish)

The image and plot below continue to demonstrate the beam irradiation patterns evident in configuration A, but with the millibeam shield installed. Positions 1 and 4 receive a larger dose evidenced by a shift in the DVH. The standard deviation remains high and indicates the continued presence of the heel effect. The penumbra around each of the millibeams was quite small (i.e. ~500 pixels out of ~800,000) and most of these were filtered out due to their negligible effect on the energy deposition in the region of interest.

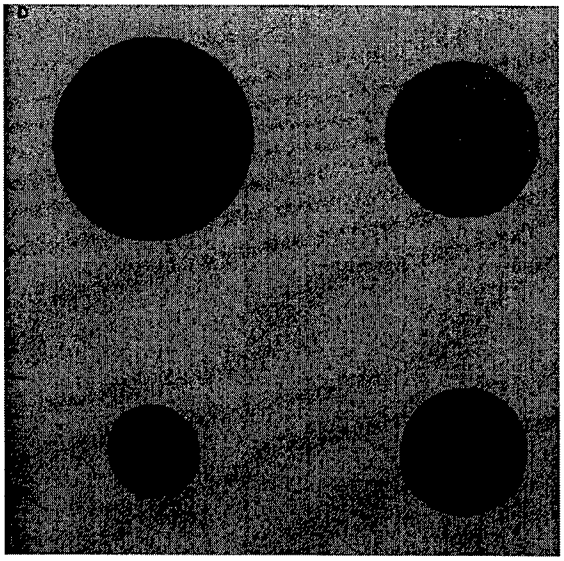

Figure 4.13. Irradiation patterns produced on the EBT film by the 130 kVp millibeam with Cu filtration (Configuration D, with 1.64 mm culture medium on top of the film).

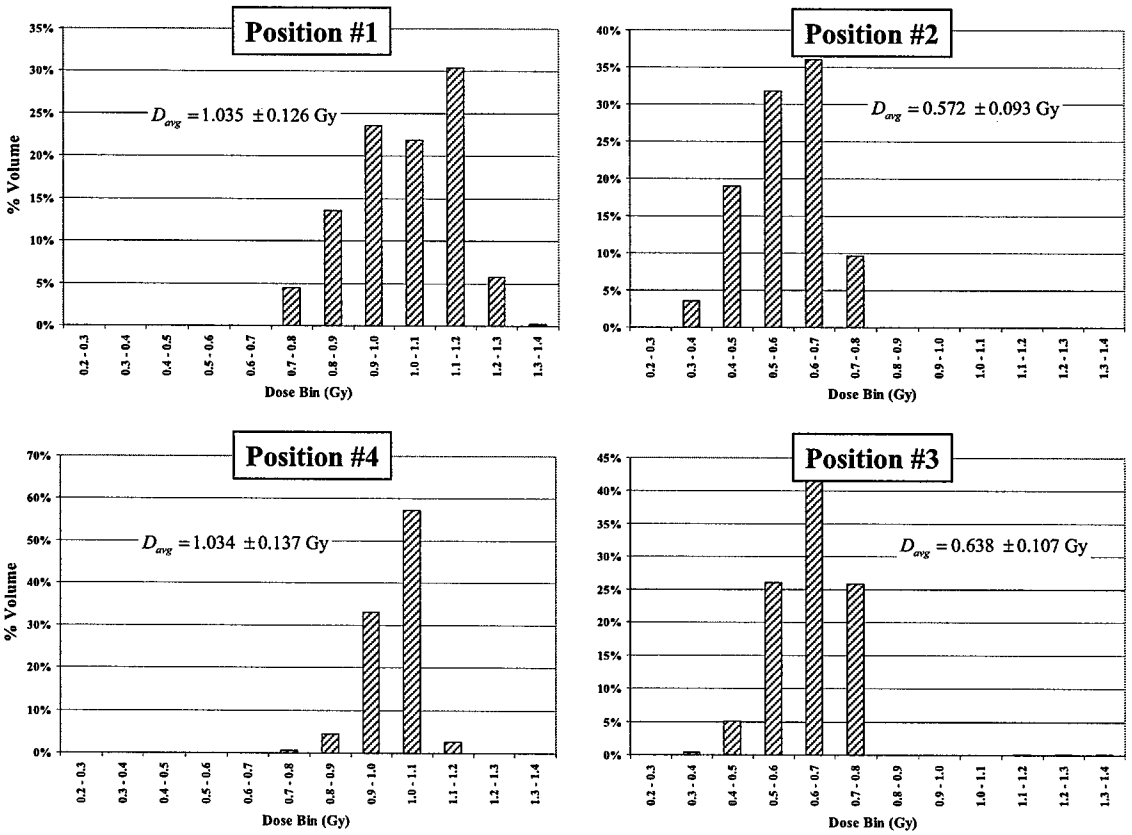

Figure 4.14. DVH for the unfiltered x-ray millibeam (Configuration D, with 1.64 mm culture medium, i.e., water). A nominal 0.956 ±0.0341 Gy dose (in water) was delivered to the center of the 130 kVp Faxitron beam during a 2-minute irradiation (62.11% attenuation through dish and water). Values for mean absorbed dose (in water) and standard deviation at each position are reported in the figure.

Configuration E: DVH for the Cu filtered 130 kVp broad beam (no culture medium)

Figure 4.15 shows the distribution of dose produced in the EBT film by the 130 kVp broad beam with the 0.4 mm Cu filter in place. Attenuation of the beam in the plexiglass is much less pronounced because low-energy photons are preferentially absorbed while passing through the Cu filter. The low-energy x-rays are the primary cause of the heel effect and the inhomogeneous dose distribution. The mean absorbed dose at each culture dish location varies by less than 2.5%, i.e., highly uniform beam.

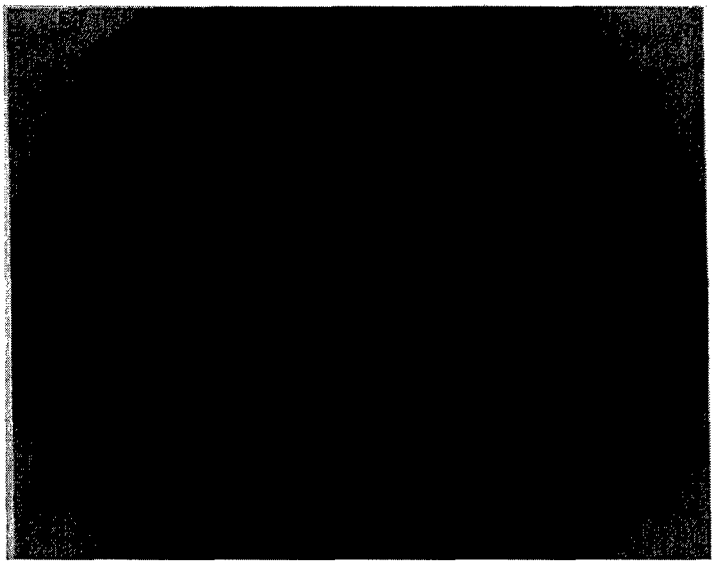

Figure 4.15. Irradiation patterns produced on the EBT film by the 130 kVp beam with Cu filtration (Configuration E, no shield or culture medium).

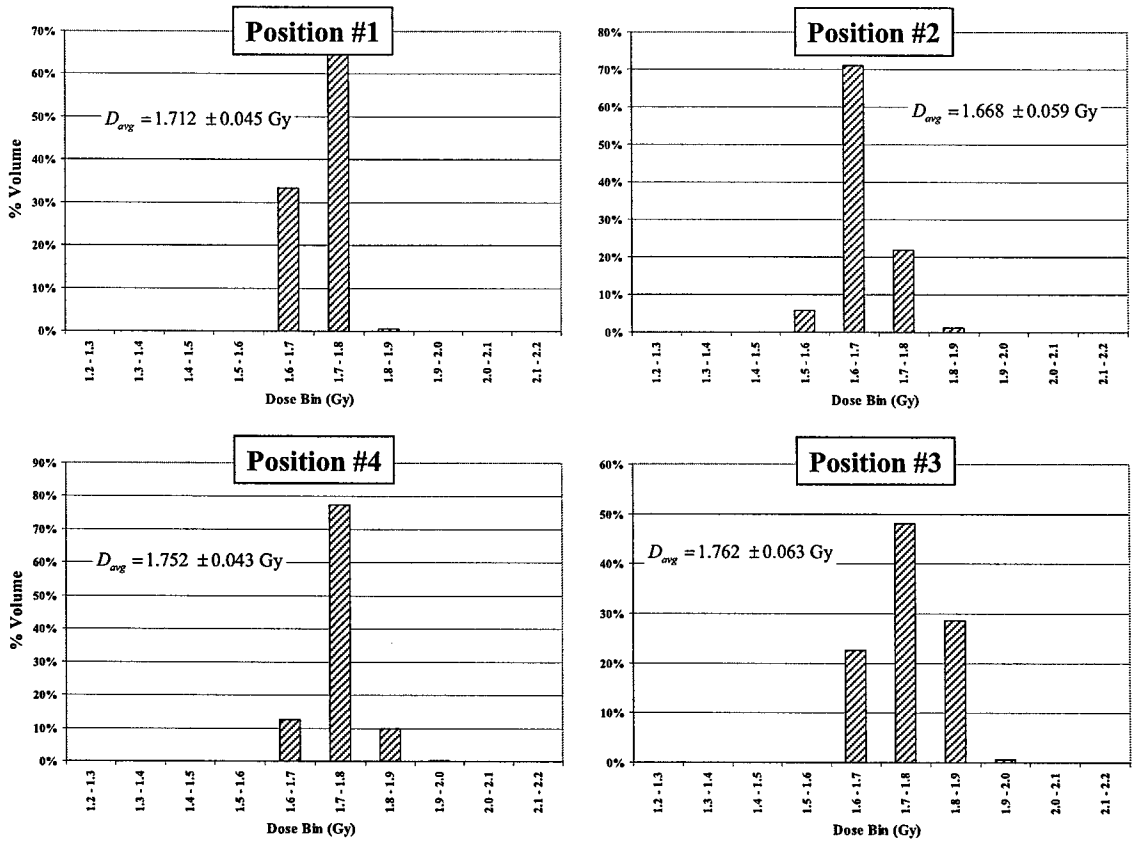

Figure 4.16. DVH for the Cu filtered x-ray broad beam (Configuration E, no culture medium). A nominal 1.72 ±0.074 Gy dose (in water) was delivered to the center of the 130 kVp Faxitron beam during a 59-minute 59-second irradiation. Values for mean absorbed dose (in water) and standard deviation at each position are reported in the figure.

Configuration H: DVH for the Cu filtered 130 kVp millibeam (1.64 mm of water in dish)

Figures 4.17 and 4.18 shows the distribution of dose produced by the 130 kVp millibeam with the 0.4 mm Cu filter in place. Standard deviation from the mean absorbed dose is relatively small. The Cu filter significantly reduces the heel effect, and results in greater beam uniformity and thus a smaller standard deviation. The penumbra around each millibeam has a negligible effect on the energy deposition in the target regions. The mean absorbed dose is smaller than Configuration D because of the attenuation caused by the 1.64 mm layer of water.

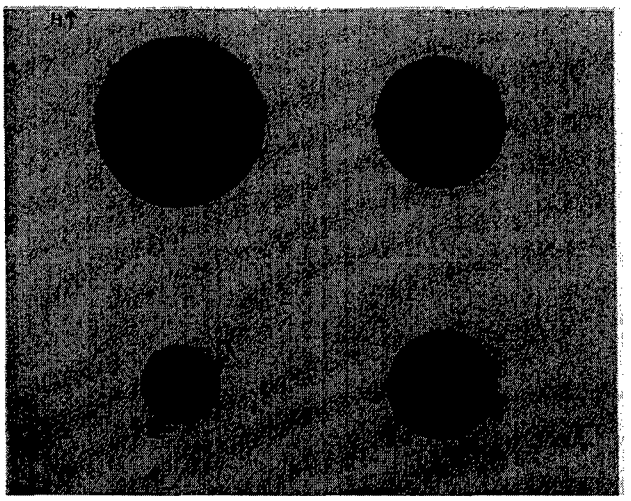

Figure 4.17. Irradiation patterns produced on the EBT film by the 130 kVp millibeam with Cu filtration (Configuration H, with 1.64 mm culture medium on top of the film).

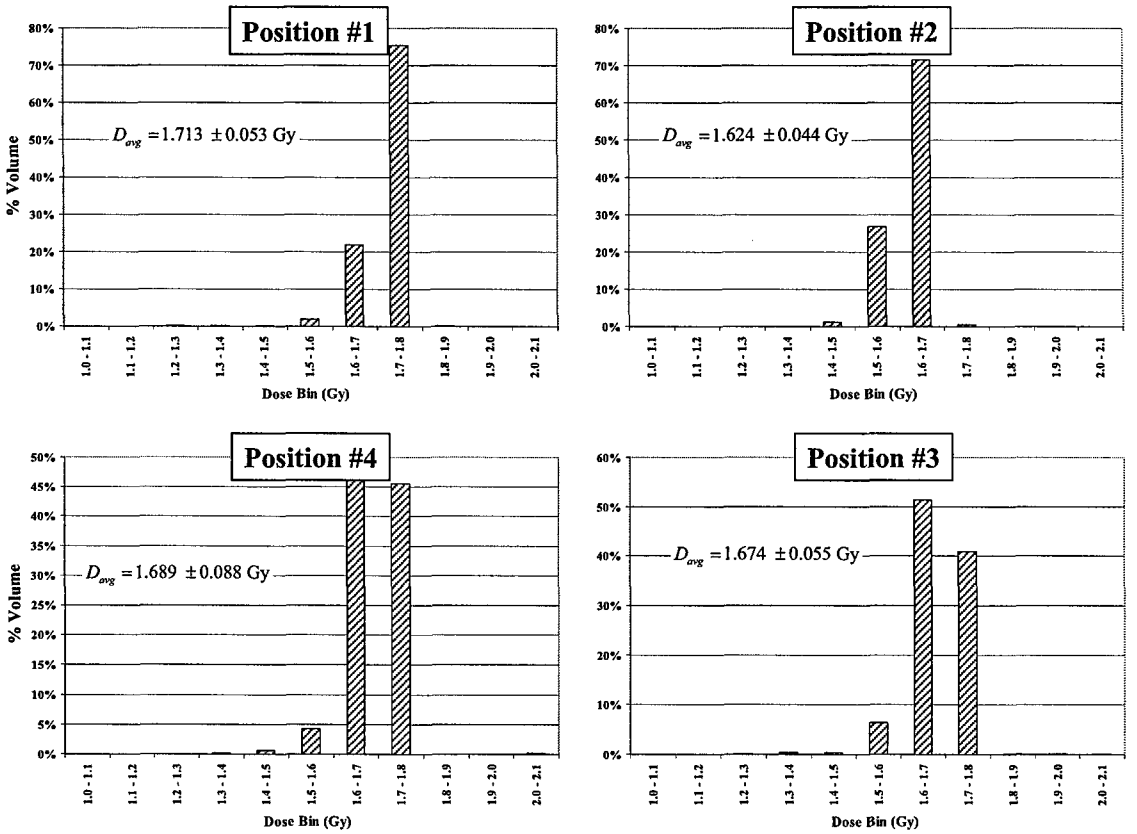

Figure 4.18. DVH for the Cu filtered x-ray millibeam (Configuration H, with 1.64 mm culture medium, i.e., water). A nominal 1.684 ±0.073 Gy dose (in water) was delivered to the center of the 130 kVp Faxitron beam during a 59-minute 59-second irradiation (2.32% attenuation through dish and water). Values for mean absorbed dose (in water) and standard deviation at each position are reported in the figure.

5. SUMMARY AND CONCLUSIONS

The Hewlett-Packard (HP) 43855B Faxitron generates an x-ray beam that, for the top irradiation shelf, targets a disk-shaped region with a cross sectional area of 532.4 cm^2 (26.035 cm in diameter). The Faxitron x-ray tube draws approximately 3 mA of current and maintains an output voltage from 10 – 130 kVp (peak x-ray energy is 130 keV). The Faxitron produces a circular beam of x-rays that are emitted at a 30-degree angle through a 0.64 mm beryllium window. The Faxitron has a removable 0.4 mm Cu filter that can be used to harden the x-ray beam. The average energy of the 130 kVp x-ray spectrum with and without the copper filter is 69.2 and 54.1 keV, respectively. The Cu filter is also effective at eliminating the so-called heel effect (Section 2.2.4 and Figs. 4.3 and 4.4). The heel effect produces up to a twelve-fold variation in the absorbed dose along on the anode side of the beam (left-right axis) but has a negligible (~ 1%) effect on beam uniformity along the other axis (front to back).

A multi-layer shield composed of steel and lead was designed to collimate the x-ray beam so that 14 – 64% of a 9-cm culture dish can be targeted with a precise dose of radiation. The regions of the culture dish that are not targeted by the x-ray millibeam receive about a million times less dose than the targeted regions (e.g., 1 μGy vs. 1 Gy). Measurements confirm that the absorbed dose delivered to non-targeted regions is indistinguishable from zero-dose (background) measurements. The ability of the millibeam to target small portions of a culture dish will provide novel capabilities for future studies that aim to examine the effects of intercellular communication on the radiation response of monolayer cell culture systems. Effective absorbed dose rates for the filtered and unfiltered 130 kVp Faxitron beam are summarized in Tables 5.1 through 5.4, and the absorbed dose for selected irradiation times are summarized in Tables 5.5 through 5.8.

For the unfiltered x-ray beam, the doses tabulated in Tables 5.5 through 5.8 need to be corrected for the attenuation of soft x-rays within the culture medium. Dose estimates may be too high by 20 – 60% if this correction is not made (see Figure 4.8).

Overall, the Faxitron provides a reproducible platform for cell culture irradiation. For the filtered x-ray beam, the absorbed dose rate (in water) at the center of the beam is 1.724 Gy/h. For the unfiltered x-ray beam, the absorbed dose rate at the center of the beam is 75.68 Gy/h. Without the filter, the dose rates for cell culture dishes at positions 2 and 3 are lower than the dose rates at the center of the beam or at positions 1 and 4 because of the heel effect. For the 130 kVp Cu-filtered x-ray beam, dose rates range from a low of 1.657 Gy/h (position 2) to a high of 1.767 Gy/h (position 1). The ratio of the maximum to minimum dose rate for the Cu-filtered beam is 1.066 (6.6%). For the unfiltered x-ray beam, dose rates range from a low of 56.01 Gy/h (position 2) to a high of 94.19 Gy/h (position 4). The ratio of the maximum to minimum dose rate for the unfiltered beam is 1.68 (68%). The large difference in the dose rates among cell culture positions 1 to 4 is due to the heel effect. The dose rates for the unfiltered beam are 50-fold larger than the dose rates for the filtered beam because of the contribution of low-energy x-rays (see 2.14 and related discussion). Heel effects have a larger impact on dose rates when the Faxitron is used in the millibeam configuration than when it is used in the broad beam configuration, e.g., compared dose rates in Table 5.1 and 5.3 (filtered beam) and Tables 5.2 and 5.4 (unfiltered beam).

Because cells are only a few micrometers thick and because cells in monolayer cultures are attached to the bottom of the dish, x-rays are attenuated within the culture medium before they reach the cells. That is, the dose at the surface of the culture medium is larger than the dose rate at the bottom of the culture medium. For the Cu-filtered x-ray beam, dose rates with and without corrections for attenuation within a layer of culture medium 0.82 mm thick (5 mL of medium in a 9-cm dish) are within about 1% of each other. For the unfiltered x-ray beam, dose rates to cells located beneath the 0.82 mm of culture medium are 50% lower than the dose rate at the surface of the dish. To correct for

attenuation within cell culture medium, Eq. (4.2) should be used be used to compute an appropriate dose reduction factor (DRF) for the specific dish size and amount of culture medium. The dose rates listed in Tables 5.1 and 5.2 (no culture medium) should then be multiplied by this DRF factor to estimate the dose rate to a monolayer of cells attached to the bottom of the dish. This correction is especially important for the unfiltered x-ray beam, although it is recommended that the correction also be applied to the filtered beam.

The maximum possible irradiation time without resetting the Faxitron timer is 59 minutes and 59 seconds. For the filtered x-ray beam, whole-dish doses up to about 1.76 Gy are possible without restarting the x-ray machine. Alternatively, 13.7% (position 4), 26% (position 3), 37% (position 2), or 63% (position 1) of the area of a 9-cm Petri dish can be targeted with a maximum dose of about 1.76 Gy without resetting the machine. For the unfiltered 130 kVp beam, doses in the range from about 62.9 to 89.2 Gy can be delivered in a single shot. For the millibeam configuration, the peak doses in the range from 56.0 to 94.2 Gy are possible. Tables 5.5 through 5.8 list the average absorbed dose for culture-dish positions 1 through 4 for selected irradiation times from 1 to 60 seconds. At the low-end of the dose range, doses of about 0.5 mGy are possible with the filtered x-ray beam (Tables 5.5 and 5.7). For the unfiltered beam (Tables 5.6 and 5.8), the minimum dose that can be delivered with the Faxitron is about 25 mGy in the absence of any cell culture medium. The minimum possible dose with a nominal level of culture medium (0.82 mm) is about 10-15 mGy.

For experiments below about 100 mGy and for low dose-rate experiments (dose rates < 1.76 Gy/h), the filtered x-ray beam is recommended in order to increase beam uniformity and to reduce uncertainties in dose estimates associated with the potentially variable amounts of culture medium within a dish. For doses larger than about 1 Gy and for all high dose rate experiments (> 1.76 Gy/h), the unfiltered x-ray beam is the only viable option with the Faxitron. Because the attenuation of soft x-rays within the culture medium can be substantial (~ 50%), the dose estimates in Tables 5.6 and 5.8 need to be

corrected using a DRF (Equation 4.2 and related discussion) appropriate to the size of the culture dish and the amount of medium within the dish.

The eDonnelly Radiography Spectrum Generator (http://www.edonnelly.com/) used in this work may or may not faithfully reproduce the Faxitron x-ray spectrum, and the effort to commission the HP Faxitron for biological studies could be improved by developing a Monte Carlo (e.g., MCNP or PENELOPE) model of the x-ray machine. A Monte Carlo model of the Faxitron will provide useful information about the filtered and unfiltered emission spectrum and also facilitate future shield and millibeam design work. The Monte Carlo models could also be used to better estimate the absorbed dose at specific locations within the beam or within a culture dish and to develop more accurate calibration factors for various radiation detectors, including the ionization chamber, film, and TLD chips. The accuracy of dose estimates derived from the EBT Gafchromic film could also be improved by investigating alternative calibration curves for the filtered 130 kVp x-ray beam (see Figure 3.14). Studies to characterize doses and dose rates within the broad beam and millibeam for voltages other than 130 kVp could further enhance the usefulness of the Faxitron for biological and other experimental studies.

A few modifications to the shield geometry could improve the accuracy and precision of the millibeam and facilitate subsequent analyses of the results of biological experiments. Initial design work relied on the assumption that the x-ray was a broad-parallel beam, and so the holes in the shield were cut directly over (centered above) the culture dishes. Figure 4.10 illustrates how the beam actually has a slight cone shape, which results in an off-center irradiation pattern away from the center of the beam. Given a relatively uniform dispersal of seeded cells on a culture dish, the millibeams at positions 2, 3 and 4 deliver a precise dose of radiation to a subset of the dish. However, the millibeam for position 1 overlaps with the edge of the dish and is less suitable for biological experiments than the other positions. To improve the geometry, several options are possible. The legs of the shield can be shortened or the dishes can be raised to minimize the gap between the holes and the culture dishes, or the alignment of the holes and/or

dishes can be modified to account for the angle of the beam. The first two options provide the most cost-efficient and least time consuming corrective measures.

The plexiglass holder provides a consistent framework to target the culture dishes or a portion of a dish and is essential for accurate dosimetry. Although the cutouts in the plexiglass holder are appropriate for a 9-cm Petri dish, the cutouts need to be enlarged slightly to hold 9-cm cell culture dish. When the plexiglass holder is used with cell culture dishes, the culture medium within the dish tends to slosh to one side or the other and preferentially attenuates low energy x-rays in the side of the dish containing more medium. For the unfiltered x-ray beam, the preferential attenuation of x-rays within the culture medium can increase or decrease the dose to part of the dish by factors on the order 20-50% (or more). It is recommended that the cutouts in the plexiglass holder be increased in size by about 0.5 mm so that Petri dishes and cell culture dishes remain level during irradiation.

While the heel effect is measurable using the detection methods outlined in Chapter 3, it results in excessive variation from the mean dose delivered to the center of the beam, as shown in Figure 4.12. To wit, there is a 12-fold increase in absorbed dose in the right-to-left direction across the broad beam. Similarly, because of the heel effect, dish positions 2 and 3 receive 50% of the dose delivered to positions 1 and 4. The heel effect is eliminated by the 0.4 mm Cu filter; however this reduces the dose 50 fold. Some possible alternatives to eliminate or reduce the heel effect could include manually rotating the culture dishes between irradiations or installing a slow-rotating (i.e. 1 rpm) electric turntable. These two methods are limited by a minimum irradiation threshold necessary to ensure the entire dish receives the same amount of radiation. Also, rotation of the dishes is undesirable from a biological perspective because it may dislodge the cells. Perhaps a better option is to use the smaller 52.5 mm diameter culture dishes for irradiations and position them on the cathode (left) side of the beam where the dose gradient due to the heel effect is negligible (refer to Figure 4.4). In this case, the smaller

dish could easily fit in the region of the beam where there is a negligible decrease in dose (i.e., good uniformity exists), and where the energy deposition rate is close to 100 Gy/h.

Table 5.1. Average absorbed dose rate (in water) produced by the **130 kVp Cu-filtered broad beam** at dish locations 1 through 4. Nominal dose rate (center of the beam) is 1.724 Gy/h.

	Absorbed Dose Rate (Gy/h)			
	No Culture Medium		0.822 mm of Culture Medium	
Position	Mean	Std. Dev.	Mean	Std. Dev.
1	1.712	0.045	1.695	0.044
2	1.668	0.060	1.652	0.059
3	1.763	0.063	1.746	0.062
4	1.753	0.043	1.736	0.043

Table 5.2. Average absorbed dose rate (in water) produced by the **130 kVp Unfiltered broad beam** at dish locations 1 through 4. Nominal dose rate (center of the beam) is 75.68 Gy/h.

	Absorbed Dose Rate (Gy/h)			
	No Culture Medium		0.822 mm of Culture Medium	
Position	Mean	Std. Dev.	Mean	Std. Dev.
1	85.08	4.9	57.06	3.3
2	62.86	10.1	42.16	6.8
3	65.55	10.5	43.96	7.1
4	89.23	5.7	59.85	3.8

Table 5.3. Average absorbed dose rate (in water) produced by the **130 kVp Cu-filtered millibeam** at dish locations 1 through 4. Nominal dose rate (center of the beam) is 1.724 Gy/h.

	Absorbed Dose Rate (Gy/h)			
	No Culture Medium		0.822 mm of Culture Medium	
Position	Mean	Std. Dev.	Mean	Std. Dev.
1	1.767	0.038	1.750	0.038
2	1.657	0.041	1.641	0.040
3	1.721	0.060	1.704	0.059
4	1.751	0.088	1.734	0.087

Table 5.4. Average absorbed dose rate (in water) produced by the **130 kVp Unfiltered millibeam** at dish locations 1 through 4. Nominal dose rate (center of the beam) is 75.68 Gy/h.

	Absorbed Dose Rate (Gy/h)			
	No Culture Medium		0.822 mm of Culture Medium	
Position	Mean	Std. Dev.	Mean	Std. Dev.
1	93.96	4.9	63.02	3.3
2	56.01	7.1	37.57	4.7
3	58.55	6.6	39.27	4.4
4	94.19	5.5	63.17	3.7

Table 5.5. Absorbed dose (in water) produced by the **130 kVp Cu-filtered broad beam** at dish locations 1 through 4. Eq. (4.2) should be used to correct absorbed dose estimates for attenuation in culture medium (water). Nominal dose rate (center of the beam) is 1.724 Gy/h.

	Absorbed Dose (mGy)							
	Position 1		Position 2		Position 3		Position 4	
	1.712 Gy/h		1.668 Gy/h		1.763 Gy/h		1.753 Gy/h	
Irradiation Time (s)	Mean	Std. Dev.	Mean	Std. Dev.	Mean	Std. Dev.	Mean	Std. Dev.
1	0.476	0.012	0.463	0.017	0.490	0.017	0.487	0.012
2	0.951	0.025	0.927	0.033	0.979	0.035	0.974	0.024
3	1.427	0.037	1.390	0.050	1.469	0.052	1.461	0.036
4	1.902	0.049	1.853	0.066	1.959	0.070	1.948	0.048
5	2.378	0.062	2.317	0.083	2.449	0.087	2.435	0.060
6	2.853	0.074	2.780	0.099	2.938	0.105	2.922	0.072
7	3.329	0.087	3.243	0.116	3.428	0.122	3.409	0.084
8	3.804	0.099	3.707	0.132	3.918	0.140	3.896	0.096
9	4.280	0.111	4.170	0.149	4.408	0.157	4.383	0.108
10	4.756	0.124	4.633	0.165	4.897	0.175	4.869	0.120
15	7.133	0.186	6.950	0.248	7.346	0.262	7.304	0.181
20	9.511	0.247	9.267	0.331	9.794	0.349	9.739	0.241
25	11.889	0.309	11.583	0.413	12.243	0.436	12.174	0.301
30	14.267	0.371	13.900	0.496	14.692	0.524	14.608	0.361
45	21.400	0.557	20.850	0.744	22.038	0.785	21.913	0.542
60	28.533	0.742	27.800	0.992	29.383	1.047	29.217	0.722

Table 5.6. Absorbed dose (in water) produced by the **130 kVp unfiltered broad beam** at dish locations 1 through 4. Eq. (4.2) should be used to correct absorbed dose estimates for attenuation in culture medium (water). Nominal dose rate (center of the beam) is 75.68 Gy/h.

	Absorbed Dose (mGy)							
	Position 1		Position 2		Position 3		Position 4	
	85.08 Gy/h		62.86 Gy/h		65.55 Gy/h		89.23 Gy/h	
Irradiation Time (s)	Mean	Std. Dev.	Mean	Std. Dev.	Mean	Std. Dev.	Mean	Std. Dev.
1	23.633	1.369	17.461	2.802	18.208	2.928	24.786	1.585
2	47.267	2.738	34.922	5.605	36.417	5.856	49.572	3.171
3	70.900	4.108	52.383	8.407	54.625	8.784	74.358	4.756
4	94.533	5.477	69.844	11.210	72.833	11.713	99.144	6.342
5	118.167	6.846	87.306	14.012	91.042	14.641	123.931	7.927
6	141.800	8.215	104.767	16.814	109.250	17.569	148.717	9.513
7	165.433	9.585	122.228	19.617	127.458	20.497	173.503	11.098
8	189.067	10.954	139.689	22.419	145.667	23.425	198.289	12.683
9	212.700	12.323	157.150	25.222	163.875	26.353	223.075	14.269
10	236.333	13.692	174.611	28.024	182.083	29.282	247.861	15.854
15	354.500	20.538	261.917	42.036	273.125	43.922	371.792	23.782
20	472.667	27.385	349.222	56.048	364.167	58.563	495.722	31.709
25	590.833	34.231	436.528	70.060	455.208	73.204	619.653	39.636
30	709.000	41.077	523.833	84.072	546.250	87.845	743.583	47.563
45	1063.500	61.615	785.750	126.108	819.375	131.767	1115.375	71.345
60	1418.000	82.154	1047.667	168.144	1092.500	175.690	1487.167	95.126

Table 5.7. Absorbed dose (in water) produced by the **130 kVp Cu-filtered millibeam** at dish locations 1 through 4. Eq. (4.2) should be used to correct absorbed dose estimates for attenuation in culture medium (water). Nominal dose rate (center of the beam) is 1.724 Gy/h.

	Absorbed Dose (mGy)							
	Position 1		Position 2		Position 3		Position 4	
	1.767 Gy/h		1.657 Gy/h		1.721 Gy/h		1.751 Gy/h	
Irradiation Time (s)	Mean	Std. Dev.	Mean	Std. Dev.	Mean	Std. Dev.	Mean	Std. Dev.
1	0.491	0.011	0.460	0.011	0.478	0.017	0.486	0.024
2	0.982	0.021	0.921	0.023	0.956	0.033	0.973	0.049
3	1.473	0.032	1.381	0.034	1.434	0.050	1.459	0.073
4	1.963	0.043	1.841	0.045	1.912	0.067	1.946	0.098
5	2.454	0.053	2.301	0.057	2.390	0.083	2.432	0.122
6	2.945	0.064	2.762	0.068	2.868	0.100	2.918	0.147
7	3.436	0.075	3.222	0.079	3.346	0.117	3.405	0.171
8	3.927	0.085	3.682	0.091	3.824	0.133	3.891	0.196
9	4.418	0.096	4.143	0.102	4.303	0.150	4.378	0.220
10	4.908	0.107	4.603	0.114	4.781	0.167	4.864	0.244
15	7.363	0.160	6.904	0.170	7.171	0.250	7.296	0.367
20	9.817	0.213	9.206	0.227	9.561	0.334	9.728	0.489
25	12.271	0.267	11.507	0.284	11.951	0.417	12.160	0.611
30	14.725	0.320	13.808	0.341	14.342	0.500	14.592	0.733
45	22.088	0.480	20.713	0.511	21.513	0.751	21.888	1.100
60	29.450	0.640	27.617	0.681	28.683	1.001	29.183	1.467

Table 5.8. Absorbed dose (in water) produced by the **130 kVp unfiltered millibeam** at dish locations 1 through 4. Eq. (4.2) should be used to correct absorbed dose estimates for attenuation in culture medium (water). Nominal dose rate (center of the beam) is 75.68 Gy/h.

	Absorbed Dose (mGy)							
	Position 1		Position 2		Position 3		Position 4	
	93.96 Gy/h		56.01 Gy/h		58.55 Gy/h		94.19 Gy/h	
Irradiation Time (s)	Mean	Std. Dev.	Mean	Std. Dev.	Mean	Std. Dev.	Mean	Std. Dev.
1	26.100	1.372	15.558	1.963	16.264	1.825	26.164	1.516
2	52.200	2.744	31.117	3.925	32.528	3.650	52.328	3.032
3	78.300	4.115	46.675	5.888	48.792	5.474	78.492	4.549
4	104.400	5.487	62.233	7.850	65.056	7.299	104.656	6.065
5	130.500	6.859	77.792	9.813	81.319	9.124	130.819	7.581
6	156.600	8.231	93.350	11.775	97.583	10.949	156.983	9.097
7	182.700	9.602	108.908	13.738	113.847	12.773	183.147	10.613
8	208.800	10.974	124.467	15.700	130.111	14.598	209.311	12.129
9	234.900	12.346	140.025	17.663	146.375	16.423	235.475	13.646
10	261.000	13.718	155.583	19.626	162.639	18.248	261.639	15.162
15	391.500	20.576	233.375	29.438	243.958	27.372	392.458	22.743
20	522.000	27.435	311.167	39.251	325.278	36.495	523.278	30.323
25	652.500	34.294	388.958	49.064	406.597	45.619	654.097	37.904
30	783.000	41.153	466.750	58.877	487.917	54.743	784.917	45.485
45	1174.500	61.729	700.125	88.315	731.875	82.115	1177.375	68.228
60	1566.000	82.305	933.500	117.753	975.833	109.486	1569.833	90.970

BIBLIOGRAPHY

BIBLIOGRAPHY

American Society for Testing and Materials (ASTM) 2005 E1026-04e1 Standard Practice for Using the Fricke Reference-Standard Dosimetry System

Attix F H, Roesch W C and Tochilin E 1966 *Radiation dosimetry* (New York,: Academic Press)

Austerlitz C 2003 Absorbed dose determination with plane-parallel chambers *Radiat Prot Dosimetry* **106** 273-6

Boone J M and Seibert J A 1997 An accurate method for computer-generating tungsten anode x-ray spectra from 30 to 140 kV *Med Phys* **24** 1661-70

Bushberg J T 2002 *The essential physics of medical imaging* (Philadelphia: Lippincott Williams & Wilkins)

Butson M J, Cheung T and Yu P K 2005 Absorption spectra variations of EBT radiochromic film from radiation exposure *Phys Med Biol* **50** N135-40

Cai Z, Pan X, Hunting D, Cloutier P, Lemay R and Sanche L 2003 Dosimetry of ultrasoft x-rays (1.5 keV Al(Kalpha)) using radiochromatic films and colour scanners *Phys Med Biol* **48** 4111-24

Devic S, Seuntjens J, Sham E, Podgorsak E B, Schmidtlein C R, Kirov A S and Soares C G 2005 Precise radiochromic film dosimetry using a flat-bed document scanner *Med Phys* **32** 2245-53

Feinendegen L E, Evidence for beneficial low level radiation effects and radiation hormesis. Br. J. Radiol. 78, 3–7 (2005).

Frame P W 2004 A history of radiation detection instrumentation *Health Phys* **87** 111-35

Frankenberg D, H. J. Brede, U. J. Schrewe, C. Steinmetz, M. Frankenberg-Schwager, G. Kasten and E. Pralle, Induction of DNA double-strand breaks by 1H and 4He ions in primary human skin fibroblasts in the LET range of 8 to 124 keV/μm. Radiat. Res. 151, 540–549 (1999).

Frankenberg-Schwager M, Induction, repair and biological relevance of radiation-induced DNA lesions in eukaryotic cells. Radiat. Environ. Biophys. 29, 273–292 (1990).

Gamboa-deBuen I, Buenfil A E, Ruiz C G, Rodriguez-Villafuerte M, Flores A and Brandan M E 1998 Thermoluminescent response and relative efficiency of TLD-100 exposed to low-energy x-rays *Phys Med Biol* **43** 2073-83

Goodhead D T, Initial events in the cellular effects of ionizing radiations: clustered damage in DNA. Int. J. Radiat. Biol. 65, 7–17 (1994).

Guo S and Ziemer P L 2004 Health Physics Aspects of Neutron Activated Components in a Linear Accelerator *Health Phys* **86** S94-S102

Hei T K, L. J. Wu, S. X. Liu, D. Vannais, C. A. Waldren and G. Randers-Pehrson, Mutagenic effects of a single and an exact number of α particles in mammalian cells. Proc. Natl. Acad. Sci. USA 94, 3765–3770 (1997).

Higson D J, The bell tolls for LNT. Health Phys. 87 (Suppl.), S47–S50 (2004).

ICRU (1960), *Radiation Quantities and Units,* Report 10 of the International Commission on Radiation Units and Measurements (Bethesda, MD).

ICRU (1970), *Radiation Quantities and Units,* Report 25 of the International Commission on Radiation Units and Measurements (Bethesda, MD).

ICRU (1979), *Radiation Quantities and Units,* Report 31 of the International Commission on Radiation Units and Measurements (Bethesda, MD).

ICRU (1980), *Radiation Quantities and Units,* Report 33 of the International Commission on Radiation Units and Measurements (Bethesda, MD).

ICRU (1984), *Radiation Quantities and Units,* Report 35 of the International Commission on Radiation Units and Measurements (Bethesda, MD).

ISP (2005), GafChromic EBT – Self-developing film for radiotherapy dosimetry (Wayne, NJ).

Klassen N V, Shortt K R, Seuntjens J and Ross C K 1999 Fricke dosimetry: the difference between $G_{(Fe3+)}$ for ^{60}Co gamma-rays and high-energy x-rays *Phys Med Biol* **44** 1609-24

Landolt-Bornstein (1991), New Series: Units, ed. J Bortfeldt and B Kramer.

Little J B 2000 Radiation carcinogenesis *Carcinogenesis* **21** 397-404

Ma C M and Nahum A E 1993 Dose conversion and wall correction factors for Fricke dosimetry in high-energy photon beams: analytical model and Monte Carlo calculations *Phys Med Biol* **38** 93-114

Ma C M, Rogers D W, Shortt K R, Ross C K, Nahum A E and Bielajew A F 1993 Wall-correction and absorbed-dose conversion factors for Fricke dosimetry: Monte Carlo calculations and measurements *Med Phys* **20** 283-92

Mack A, Mack G, Weltz D, Scheib S G, Bottcher H D and Seifert V 2003 High precision film dosimetry with GAFCHROMIC films for quality assurance especially when using small fields *Med Phys* **30** 2399-409

Martin C J, The LNT model provides the best approach for practical implementation of radiation protection. Br. J. Radiol. 78, 14–16 (2005).

Mayneord, WV. The use of x-rays and gamma rays in medicine. Rep. Prog. Phys.. 5, 284-301 (1938).

McKeever S W and Moscovitch M 2003 On the advantages and disadvantages of optically stimulated luminescence dosimetry and thermoluminescence dosimetry *Radiat Prot Dosimetry* **104** 263-70

Mersseman B and De Wagter C 1998 Characteristics of a commercially available film digitizer and their significance for film dosimetry *Phys Med Biol* **43** 1803-12

Mothersill C and C. Seymour, Medium from irradiated human epithelial cells but not human fibroblasts reduces the clonogenic survival of unirradiated cells. Int. J. Radiat. Biol. 71, 421–427 (1997).

Muniz J L, Delgado A, Gomez Ros J M and Brosed A 1995 Application of glow curve analysis methods to radiotherapy mailed dosimetry with LiF TLD-100 *Phys Med Biol* **40** 253-68

Nagasawa H and J. B. Little, Induction of sister chromatid exchanges by extremely low doses of α-particles. Cancer Res. 52, 6394–6396 (1992).

NCRP, Evaluation of the Linear-Nonthreshold Dose-Response Model for Ionizing Radiation. Report 136, National Council on Radiation Protection and Measurements, Bethesda, MD, 2001.

Nelson J M, A. L. Brooks, N. F. Metting, M. A. Khan, R. L. Buschbom, A. Duncan, R. Miick and L. A. Braby, Clastogenic effects of defined numbers of 3.2 MeV alpha particles on individual CHO-K1 cells. Radiat. Res. 145, 568–574 (1996).

Preston R J, The LNT model is the best we can do--today. J. Radiol. Prot. 23, 263–268 (2003).

Prise K M, O.V. Belyakov, M. Folkard and B. D. Michael, Studies on bystander effects in human fibroblasts using a charged particle microbeam. Int. J. Radiat. Biol. 74, 793–798 (1998).

Schulz R J, deGuzman A F, Nguyen D B and Gore J C 1990 Dose-response curves for Fricke-infused agarose gels as obtained by nuclear magnetic resonance *Phys Med Biol* **35** 1611-22

Seibert J A 2004 X-ray imaging physics for nuclear medicine technologists. Part 1: Basic principles of x-ray production *J Nucl Med Technol* **32** 139-47

Seibert J A and Boone J M 2005 X-ray imaging physics for nuclear medicine technologists. Part 2: X-ray interactions and image formation *J Nucl Med Technol* **33** 3-18

Shapiro J 1990 *Radiation protection : a guide for scientists and physicians* (Cambridge, Mass.: Harvard University Press)

Shultis J K and Faw R E 2002 *Fundamentals of Nuclear Science and Engineering* (Dekker & CRC Press)

Shultis J K and Faw R E 2005 Radiation shielding technology *Health Phys* **88** 297-322

Simpkin D J 1995 Transmission Data for Shielding Diagnostic X-Ray Facilities *Health Phys* **68** 704-709

Trosko E J, C. C. Chang, B. L. Upham and M. H. Tai, Low-dose ionizing radiation: induction of differential intracellular signaling possibly affecting intercellular communication. Radiat. Environ. Biophys. 44, 3–9 (2005).

Upton C, National Council on Radiation Protection and Measurements Scientific Committee 1-6. The state of the art in the 1990's: NCRP Report No. 136 on the scientific bases for linearity in the dose-response relationship for ionizing radiation. Health Phys. 85, 15–22 (2003).

Ward J F, DNA damage produced by ionizing radiation in mammalian cells: identities, mechanisms of formation, and reparability. Prog. Nucleic Acid Res. Mol. Biol. 35, 95–125 (1988).

Weinstein M, German U, Dubinsky S and Alfassi Z B 2003 On the determination of the post-irradiation time from the glow curve of TLD-100 *Radiat Prot Dosimetry* **106** 121-30

Zoetelief J, Broerse J J, Davies R W, Octave-Prignot M, Rezvani M, Vergara J C and Toni M P 2001 Protocol for X-ray dosimetry in radiobiology *Int J Radiat Biol* **77** 817-35

APPENDICES

A. Operational Guidelines for the Hewlett-Packard Faxitron X-ray System

A.1. System Description

- Model: 43855B Part Number: 5081-9519
- Self-contained, radiation-shielded cabinet X-ray system
- High resolution radiographs of small-sized objects
- Designed for scientific and industrial X-ray inspection, quality control, reliability, and failure analysis or other operations requiring non-destructive testing techniques
- Consists of a self-rectified X-ray generator with control circuitry mounted in a radiation-shielded cabinet, which has the shape and appearance of a small oven
- Cabinet door is equipped with dual interlocks to prevent X-ray generation when the door is open
- All cabinets are designed to limit X-ray leakage to 0.5 mR/hour or less at 5 cm from any external surface
- Can be used in occupied areas w/no additional shielding

A.2. Specifications

- Self-rectifying, thermionic X-ray tube regulated~3 mA
- Output voltage continuously variable from 10-110 kVp
- Features automatic exposure control, in addition to the standard manual controls (helps operator select best kVp and determine correct exposure time)
- An ion chamber under film shelf monitors the X-rays penetrating the object and reaching the film; terminates X-ray when proper exposure has been achieved
- With the automatic exposure control, good pictures are more consistently obtained by inexperienced operators

A.3. Regulatory Guidance

- Indiana State Department of Health, Indoor and Radiologic Health has primacy IAW IC 16-41-35-29
- Policy Directive: 410 IAC 5
- Registration normally must be made within 30 days of acquiring each such source
- Contact Purdue Radiological and Environmental Management (REM) for further guidance

A.4. Training Requirements and Personnel Monitoring

- Radiation Safety Training (REM)
  - X-Ray Safety Video
  - Powerpoint Training
  - Verify User's Training
- Operator's Training
  - Based on Operator's Manual

- Each operator should read (as a minimum) Section 3 and Section 4 of manual

– Hewlett-Packard recommends the use of a radiation film badge for individual personnel monitoring

A.5. Radiation Leakage and Shielding

– Check for radiation leakage during installation, after extensive maintenance, periodically (not to exceed six months), and after moving the system
– Geiger-Mueller and certain other scintillator-type radiation meters are not acceptable
– Serious injury (both physical and genetic) can result if all X-ray shielding is not properly replaced or interlocks are not operating after maintenance
– Proper shielding replacement and interlock operation can only be confirmed by performing a radiation survey before placing the system in operation, and before use whenever the system is moved or serviced

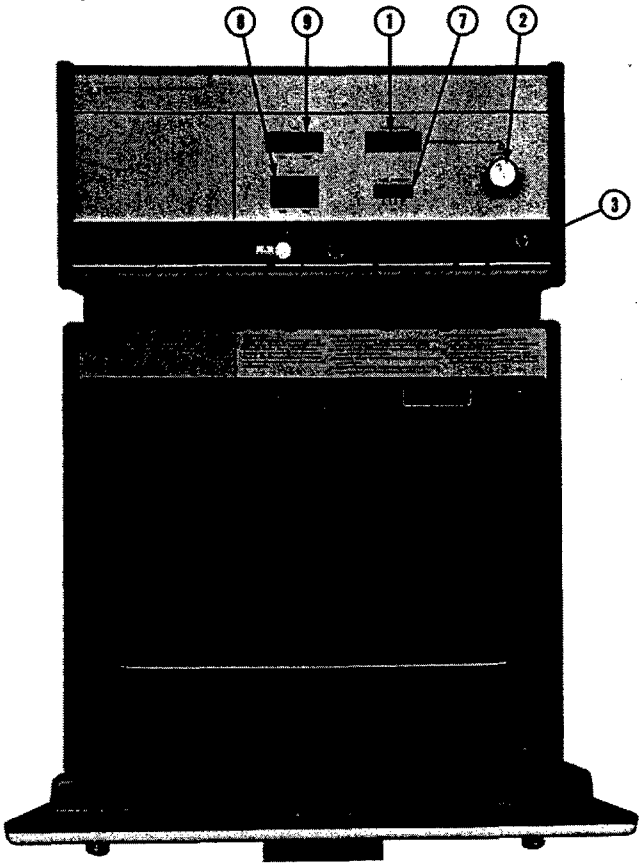

Figure A.1. Faxitron cabinet x-ray (view of irradiation shelf)

A.6. System Design and Exposure Levels

– Radiation shielded cabinet: Compartment door equipped with dual safety interlocks - each compartment door and drawer on dual cabinet and table systems;

Exposure Levels: Less than 0.5 mR/h at 5 cm (2 in.) from exterior surface at maximum voltage output of the system (110 kVp or 130 kVp)

- X-Ray Tube: X-ray source size: 0.5 mm as measured per Federal Standard No. 83; Beryllium Window Thickness: 0.64 mm (0.025 in.)
- Voltage Output to X-Ray tube: Standard; Continuously variable 10 to 130 kVp (option A04)
- Duty Cycle: Continuous
- X-Ray Tube Current: ~3 mA continuous
- Film to Source Distance (FTSD): 121 cm (48 in.) maximum for 43855B Dual Cabinet System

A.7. Radiation Safety Procedures

- Turn the kVp CONTROL to zero immediately after each exposure and leave it there between exposures
- Keep the door closed at all times except during brief loading periods
- Turn POWER switch to OFF position whenever the system is not going to be used for an extended period
- Always monitor the X-RAY ON and TUBE CURRENT indicators to be certain the light is out and the bar graph meter is at zero after each exposure
- A radiation survey should be performed every six months and when unit is moved or serviced, using competent instrumentation and personnel

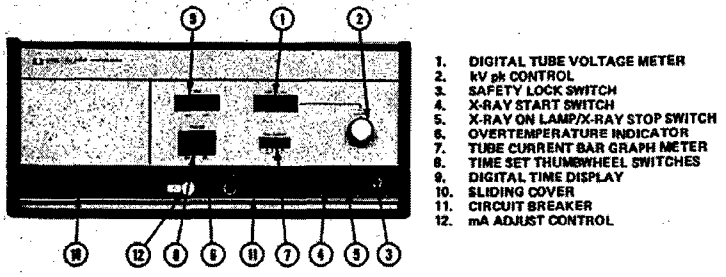

Figure A.2 Faxitron operator control panel.

A.8. Operation: Front Control Panel

- Safety Lock Switch (3): Prevents unauthorized use of the x-ray equipment
- X-Ray START Switch (4): Closes the main power relay energizing the x-ray tube high voltage transformers (the relay remains closed until the exposure is terminated by the timer, the automatic exposure circuit, or by opening an interlock)
- X-RAY STOP Switch (5): Ceases production of x-rays, and turns off the "X-Ray On" lamp
- Exposure TIME SET thumbwheel switches (8): In manual (timed) mode, pre-set any exposure from 1 sec. to 60 min
- Digital TIME display (9): Four-digit display makes up the timer (blanked out until the X-RAY START switch is pressed)
- mA Adjust (12): Allows adjustment of the maximum filament voltage which controls x-ray tube current

A.9. Operating Procedures

- Verify circuit breaker switch (hidden behind slide panel) is set to ON
- Insert key in POWER switch and turn to ON
- Verify that the X-RAY ON light is off
- Open compartment door and place film on shelf
- Remove or Insert 0.4 mm copper filter, as required
- Close compartment door completely
- Adjust kVp CONTROL for desired voltage
- Set TIME SET thumbwheels to desired duration
- Press X-RAY START button (verify X-RAY ON light and TUBE CURRENT bar graph meter both active)
- The TIME DISPLAY will light and indicate the number on the TIME SET thumbwheels; the display will count down in one second steps until it reaches zero
- At "zero", the display will blank out and the exposure will terminate.

A.10. Radiation Safety Design

- Faxitron systems are designed IAW Title 21, Chapter 1, Subchapter J, Part 1020
- Checked prior to shipment to ensure that radiation leakage is below 0.5 mR/h at 5 cm from any external surface
- Leak checks should be conducted after installation, and after maintenance
- Do not operate system above max kVp indication on the TUBE VOLTAGE meter
- Internal lead shielding reduces external radiation
- Safety interlock switches minimize the possibility of exposure if the compartment door is not completely closed
- Radiation is shut off when the door opens
- Restart is not possible until the door is closed and the X-RAY START button is again pressed

A.11. How to Conduct a Radiation Survey

- Pre Survey: Check calibration date, battery, and source
- Survey:
  - Determine the lowest value of background reading
  - Place 1-gal water jug on 18" FTSD shelf. Make certain there is no filtration in the direct beam
  - Wedge the door open (just before the interlock actuates)
  - Adjust the system to maximum kVp and 3.0 mA
  - Slowly scan the door, four sides and top of system
  - If the system is on a table, the bottom of the unit should be surveyed (remove all attenuation)
  - Be certain to survey adjacent rooms, if applicable
- Post Survey: Complete Battery/Source Checks

B. Scanner and Image Analysis Procedures for Calibration of EBT Film and Faxitron Millibeam (includes DVH Preparation)

Film Calibration and Analysis Procedures (Ispcorp EBT GafChromic Film)

B.1. Film Preparation

1. Don lab gloves
2. Select 8" x 10" sheet of GAF chromic EBT film (note: film is UV and heat sensitive.. avoid prolonged exposure to office lighting)
3. Cut sheet in 35 mm strips (only cut the minimum number of strips to avoid clutter and confusion)
4. Cut each 35 mm strip into 35mm x 37mm rectangles
5. Safely store the 35mm x 37mm films for use

B.2. Documentation

1. For calibrations with 35 mm slides, film should be stored in a "Slide Saver Vue All" (similar to a plastic page protector). Several boxes are in the Health Sciences admin storage area. The Slide Saver is usually in a 4 x 6 grid and allows 24 films per sheet. White backing pages may be used, if desired, to provide better contrast.
2. It is recommended that each film be given an index # which correlates to a database, spreadsheet, and/or log. The database should contain the following parameters: exposure time (i.e. minutes), kVp (i.e., 130 kVp), mA (i.e., 3mA), location of film during irradiation (i.e., plexi-center if film was irradiated in well of plexiglass), use of filters (i.e., 0.4mm Cu), shelf position (i.e., top shelf), date/time of irradiation (i.e., yyyymmdd hhmm). See sample calibration form.

B.3. Irradiation

1. Important: Users must obtain x-ray training from REM prior to using x-ray system. See x-ray procedures for details on operating system.
2. Set shelf at desired height setting (usually top or bottom)
3. Select and insert the plexiglass template with 35mm x 37mm center well
4. Insert or remove radiation filters, as required
5. Make sure system is on (i.e., circuit breaker powered "on" and key control "on")... Note: It is preferable to use a continuous power supply to avoid interruptions during irradiation
6. Set kVp and timer to desired settings
7. Don lab gloves
8. Place 35mm x 37mm film in rectangular well (use plexiglass template)
9. Document settings in calibration log
10. Irradiate for desired time
11. Don lab gloves, if necessary

12. Remove film
13. Label back of film (i.e., sample #) along a 37mm edge. Print size should be no taller than 3mm. This is now the top of your film, and is helpful for orienting the film during the scan procedures.
14. Store film in calibration binder; label as appropriate

B.4. Film Loading Procedure

1. Ensure scanner is powered 'ON' and connected to the computer via USB cable
2. Open scanner lid and carefully remove the white reflective padding from the bottom of the scanner lid (this enables 16-bit grayscale quality images)
3. Gently clean the glass surfaces using photographic lens cleaner and a lint free soft cloth
4. Load plastic template for 35mm Strip on to the flat window and ensure notches fall into precut positions
5. Load 35mm x 37mm films into the correct position (see Figure B.1)

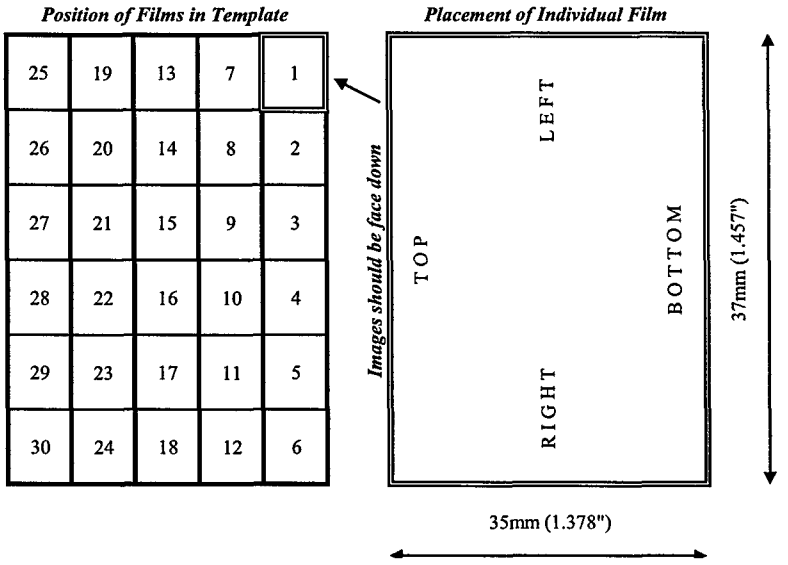

Figure B.1. Loading procedures for 35mm x 37mm films.

6. Ensure all films are properly labeled within 0.25" of the 'TOP' or 'BOTTOM' edge. This margin will ensure film labels do not interfere with scan.
7. Close lid

B.5. Scan Images

1. Load PhotoStudio 5.5
2. Select... File... Acquire {Shortcut: Alt-F... Q}. *This will open ScanGear CS, the scanning application for the CanoScan9950F.*
3. Ensure the following options are selected
   Select Source: Color Positive Film
   Film Size: 35mm Strip

Color Mode: Grayscale (16bit)
Output Resolution: 150 dpi
All Image Settings should be set to either OFF or NONE

4. Click on Preferences, and ensure the following options are selected… then click OK

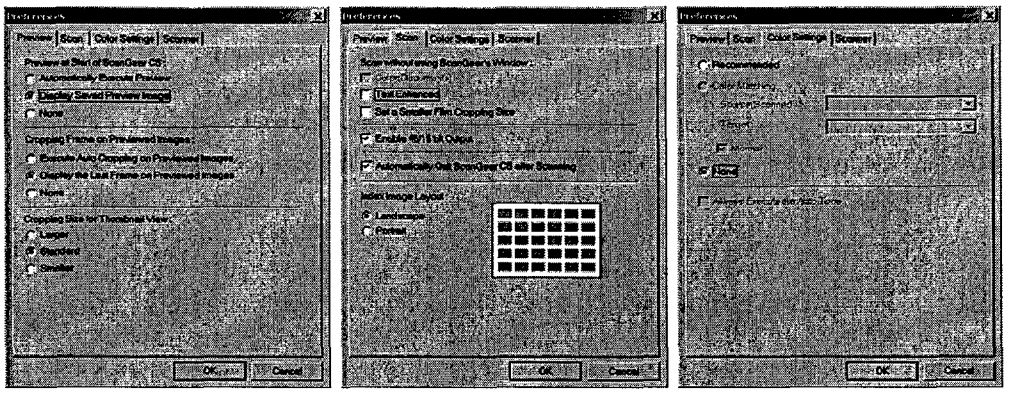

5. Preview image.
6. In the upper left hand corner of ScanGear CS, click the 2nd button from the left, "Display all cropping frames in the selected film size". *All films should now be selected.*

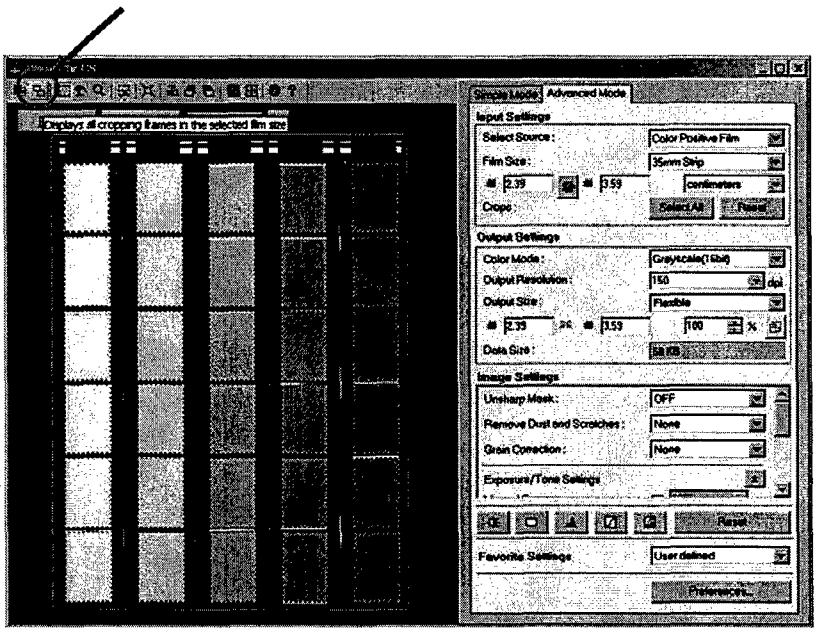

7. Click SCAN. *The resulting batch scan should take approximately 10 minutes.*

B.6. Save Images

1. When scanning is complete, the ScanGear CS window will disappear, and you will be left with the ArcSoft PhotoStudio Application. *All 30 images will be on the screen (some will be hidden).*

2. One at a time, close out of the images and be sure to save the image with it's appropriate file name. *My recommendation is to index your photos by number (ex. 01,02,03...28,29,30).*
3. After all images are saved, exit the ArcSoft PhotoStudio application.

B.7. Crop Images

1. Open the NIH ImageJ application.
2. Open Windows Explorer in a window (i.e., not full screen). Find and select your recently saved images. *If all images are in a single folder, they are easy to select by pressing Ctrl-A (edit.. select all).*
3. Ensure the selected images are highlighted, then drag and drop them onto the ImageJ application. *All 30 images should be simultaneously opened.*
4. Click on the ImageJ window
5. Select: Image... Stacks... Convert Images to Stack. *Now all images should be in one collection. You can view the collection by typing ">" (forward) or "<" (backward). Alternatively, you can use the horizontal scroll bar to view each image.*
6. Now drag the mouse over the stack of images, and you will see a crosshair. Form a vertical rectangle with dimensions w=0.65 and h=1.00. You can view these dimensions at the bottom of the ImageJ window. *If your dimensions are not exact, you can make adjustment after you form the rectangle by grabbing a side or corner of the rectangle and making the desired adjustment.*
7. Click: Image.... Crop. *You will notice the entire stack is now the same size.*

B.8. Obtaining Intensity Measurements and Calculating OD

1. Click on the ImageJ window
2. Select: Analyze... Measure. *This will open a Results window.*
3. In the Results window, select: Edit... Set Measurements
4. Make the following selections... then click OK

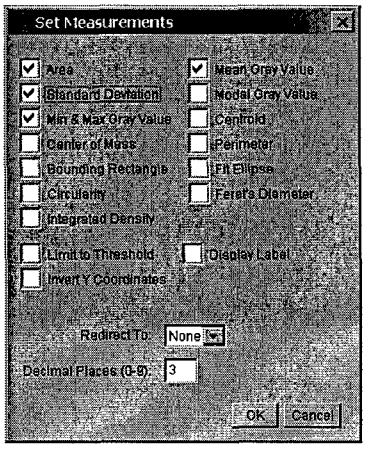

5. Now click: Edit... Clear Results... Don't Save
6. At this point, you need to cycle through your stack of images, and record your measurements. You can do this quickly using the following procedure:
    a. Click on your stack of images

b. Go to the first image (i.e., hold down '<')
c. Type Ctrl-A (select entire image)
d. Type Ctrl-M (measure image)
e. Type '>' (only enter a single keystroke)
f. Repeat steps 'd' and 'e' until all images are measured. *Be careful to avoid mistakes; otherwise your data will have errors, and you may need to Clear your results and start over.*

7. After recording all measurements, click: File… Save As… (in the results window)
8. Type in an appropriate file name (default is 'results.txt'). *This file can be opened in nearly any application, or imported into Excel. Alternatively, you could click Edit.. copy all... in the results window, and simply paste into a spread sheet.*
9. The 'mean' value in your dataset is the intensity and can be used to compute the optical density or absorbed dose. To do this you must measure the intensity of film that has not been irradiated, and compute the optical density as: $OD=log_{10}(I_o/I)$.

Faxitron Millibeam Calibration and Analysis Procedures (and DVH Preparation)

Scanner and Image Analysis Procedures for Millibeam and DVH

1. Turn on Scanner
2. Clean both glass scan surfaces with photolens cleaner and a cloth
3. Load Photostudio
4. Click acquire scan image to activate ScanGear CS
5. Run a minimum of 10 blank scans to warm up the scanner. This reduces the error from the scanning filament heating up.

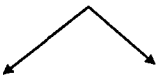

- Reflective Scan (8-bit)
  - Ensure white reflective pad is installed
  - Options:
    - Select Source: Platen
    - Paper Size: Full platen
    - Color mode: Color
    - Output Resolution: 300 dpi
  - Place film on scanner and preview
  - Select scan region with dynamic rectangle tool
  - Scan

- Transmission Scan (16-bit)
  - Remove white reflective pad
  - Options:
    - Select Source: Color positive film
    - Paper Size (select after preview):
      - 120 format (6x6) OR
      - 4 x 5 {for a larger ROI}
    - Color mode: Color(48-bit)
    - Output Resolution: 300 dpi
  - Place film on scanner and preview
  - Select scan region with dynamic rectangle tool
  - See transmission scan tips…

Transmission Scan Tips

- Scan one 4x5 image at center of scan bay to get Io "without" film. Used later to obtain mean, SD, and uniformity.
- Scan one 4x5 image at center of scan bay to get Io "with" 8x10 EBT film in place. Used later to obtain mean, SD, and uniformity.
- 8x10 EBT films should normally be placed face down in the right front corner of the scan bed
- All scanned images will need to be rotated 90 degrees counter clockwise later
- Scan large hole (position #1) with 4x5 "film size"
- Scan 3 smaller holes (position #2, 3, and 4) with 120 format (6x6)
  - Note: There is no need to preview the image each time, just grab and drag the scanning frame to your region of interest.
- Scan the center of each film (position #5) with 120 format (6x6) to test effectiveness of shield and compare with control film(s)

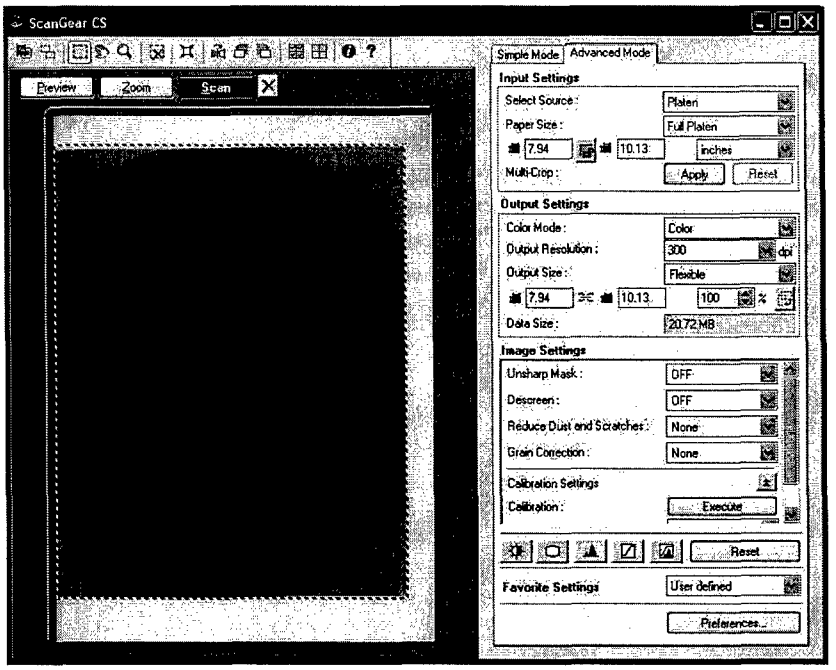
ScanGear CS
Preview
Zoom
Scan
Simple Mode
Advanced Mode
Input Settings
Select Source :
Platen
Paper Size :
Full Platen
7.94
10.13
inches
Multi-Crop :
Apply
Reset
Output Settings
Color Mode :
Color
Output Resolution :
300
dpi
Output Size :
Flexible
7.94
10.13
100
%
Data Size :
20.72MB
Image Settings
Unsharp Mask :
OFF
Descreen :
OFF
Reduce Dust and Scratches :
None
Grain Correction :
None
Calibration Settings
Calibration :
Execute
Reset
Favorite Settings
User defined
Preferences...

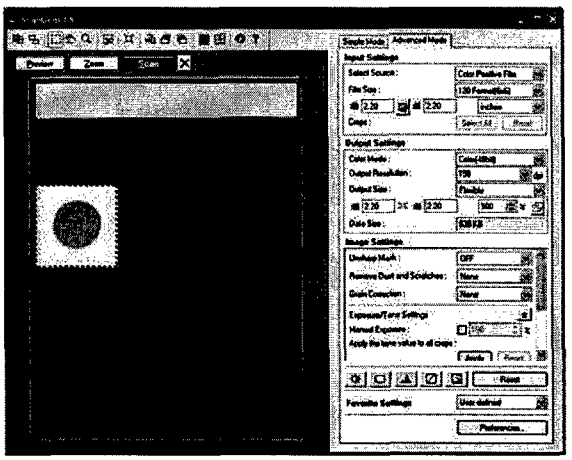

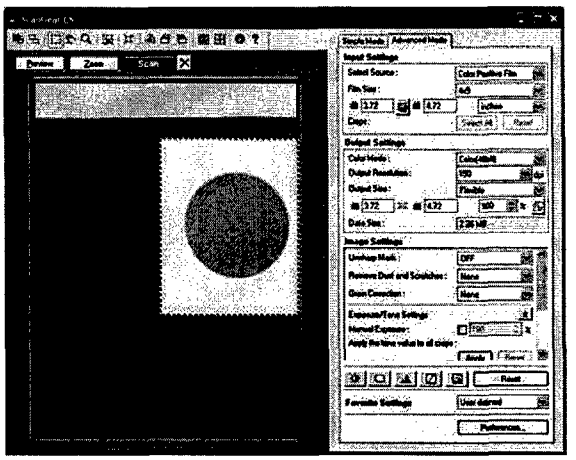

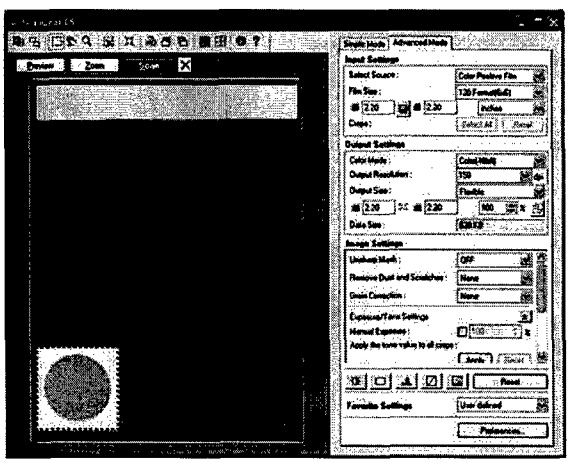

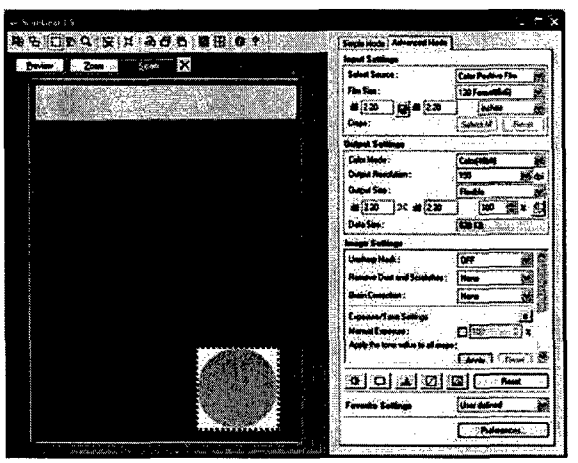

ImageJ Tips

•Open ImageJ
•Open Windows Explorer in a medium-sized window (so you can see the ImageJ window)
    •Select all the files you want to analyze, and drag them into the ImageJ window
•If you scanned the images in 48-bit color mode, you should notice that each image has three channels (red, green, blue); each channel is 16-bit and the the default channel that appears on the screen is red. The ideal channel to scan EBT images is red, so there is no need to make any changes here. The greyscale intensity is an average of these 3 channels.
•From the ImageJ application window, click
    •Analyze
    •Tools
    •Save x,y coordinates
        •This enables you to save the image as a text file with fields:
            •X (the 2D spatial grid coordinate along the x-axis)
            •Y (the 2D spatial grid coordinate along the y-axis)
            •Pixel Intensity (this is the pixel intensity of your red channel
•You may need to crops some images (i.e. position one, 4x5). In this case, you can use the rectangle selection tool in conjunction with image..crop. Multiple same-size images can be cropped more quickly by first selecting Image… stack… convert images to stack. The entire stack can then be cropped together, and then separate for further analysis.

DVH Image Analysis

- Open NIH Image J
- Open image
- Set scale (note: this step is not necessary if scale already matches scanner resolution)
    - Click straight line selection
    - Click on point 1
    - Click on point 2
    - Click Analyze..set scale
    - Perform physical measurement (if not already accomplished) of distance in 'cm'
    - Update [known distance] in figure with measured distance, and ensure unit of length is in 'cm'
    - Click global
    - Click ok (see screenshot below)

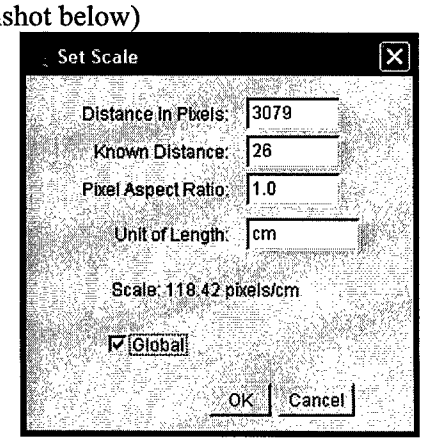

- Select region of interest (i.e., Petri dish)

    - Click oval selection
    - Press shift key
    - Draw (click and drag) circle until w and h values are equal to the diameter of Petri dish
    - Click near center of oval selection and drag to position of interest
    - Click edit… clear outside
    - Click image… crop
- Save image and text image
    - Click file.. save as… TIFF
    - Enter filename, then click ok
    - If image is a 24-bit color (i.e., RGB) image, click image… type… 8-bit, or If image is a 48-bit color image, click image… type… 16-bit (this will convert the image to grayscale)
    - Click analyze… tools… save xy coordinates… enter filename, then click ok
- Create data source for image analysis (this step uses MS Access to analyze the text file)
    - The file will be too large to open with MS Excel, therefore:
        - Open DVH Source.mdb (access database)
        - Click tables (on left)
        - Rename 'Image Data' to a desired archive name
        - Click new.. link table… ok
        - Change file type to 'text files'
        - Click on the image input file you created, click ok
        - Choose delimited… next
        - Choose Tab… next… click next again
        - For multiple images, save each link with a unique name and become familiar with query functions in MS Access (see preexisting data sources for ideas on analyzing the data)
        - Click Queries (on left)… click '3 Dose Bin Determinator'… click open
        - Type CTRL-A… CTRL-C
- Create absorbed dose bins
    - Open 'DVH Plotter.xls'
    - Click 'Import' tab
    - Click on cell A3… click CTRL-V
- Review workbook to ensure tables represent the data correctly... make adjustments as needed

C. Calibration Certificates

UW calibrations were completed for the following instruments:

- kVp meter (Radiation Measurements Model 230, SN 1154); 9 Aug 05
- RadCal parallel plate ionization chambers; 8 Aug 05
  - MDH RadCal 3036 electrometer / ionization chamber
  - MDH RadCal 10x5-180, SN 7565
  - MDH RadCal 30x6-11, SN 231
- TLDs (Co-60, Cs-137, x-rays); 11 Jul 05
  - Co-60
  - M100, M120, and M150 x-ray beam standards

Purdue Calibration Requirements

**** Irradiate all TLDs to 1 Gray. ****

UW Beam Code	Pellet Group	# of Pellets	# of Controls
UW100-M	B1	5	1
UW120-M	B2	8	1
UW150-M	B3	5	1
Co-60	A	8	1
Cs-137	C	7	1

  - Harshaw 4000 TLD reader specified in Chapter 3, Section 3.4 was used to measure the response of the calibrated TLDs (calibrated to air kerma):

	Pellet Group Response (uC/Gy)					Control Response (nC)				
	A	*B1*	*B2*	*B3*	*C*	*A*	*B1*	*B2*	*B3*	*C*
	10.35	22.27	21	19.23	10.7	3.09	2.62	2.88	3.98	2.69
	9.9	19.8	21.79	20.07	10.66					
	9.98	21.35	20.81	19.65	10.28					
	10.18	21.85	20.41	21.04	11.18					
	10.58	21.72	21.27	20.81	10.95					
	10.45		21.14		10.24					
	10.13		20.48		9.7					
	10.4		20.35							
n	8	5	8	5	7	1	1	1	1	1
mean	**10.25**	**21.40**	**20.91**	**20.16**	**10.53**	**3.09**	2.62	2.88	3.98	2.69
std dev	0.24	0.95	0.50	0.76	0.50					
rel err	2.32%	4.45%	2.37%	3.79%	4.72%					

Calibration certificates are provided in the subsequent pages.

Report No. **KVP4574**

University of Wisconsin - Madison
Department of Medical Physics
Radiation Calibration Service

This calibration report is compliant with ISO/IEC 17025-1999 and ANSI/NCSL Z540-1-1994 standards, and is accredited by the American Association for Laboratory Accreditation.

1530 Medical Sciences Center, 1300 University Ave., Madison, WI 53706
Office (608) 262-6320 Fax: (608) 262-5012

Report of Calibration for .

Diagnostic kVp Meter

Submitted by: James Schweitzer, Ph.D.
Purdue University
550 Stadium Mall Drive RM-B203
West Lafayette, IN 47907

Instrument: Radiation Measurements, Inc.
Model 230
S/N 1154

Date Received: 5/AUG/2005 Calibration Completed: 9/AUG/2005

This calibration is directly traceable to the National Institute of Standards and Technology (NIST). The expanded uncertainty of measurement as stated in the data page of this report is the standard uncertainty of measurement multiplied by the coverage factor k=2, which for a normal distribution corresponds to a coverage probability of approximately 95%.

Report No. **KVP4574**

University of Wisconsin - Madison
Department of Medical Physics
Radiation Calibration Service

kVp Measurement Data

Calibration Completed: August 9, 2005

Report Date: November 22, 2005

Radiation Measurements, Inc.

Model: 230

Serial Number: 1154

Irradiation Conditions
Picker Model G1050S (3-phase, 12-pulse) generator -- S/N 2458
Varian Model DX62 x-ray tube -- S/N 11591-U5
Machlett Dynalyzer II -- S/N 60-04-7-0094
3 mm Al HVL @ 80 kVp
UW-RCS Protocol Revision 6/1/2000
Calibration Uncertainty: 1.1%

	Calibration kVp	Instrument Reading	Error	Notes
"As Received" Results:	66.7	68.0	+1.3	
	132.3	130.6	-1.7	
Calibration Results:				
	63.6	63.3	-0.3	
	64.8	64.6	-0.2	
	78.5	78.6	+0.1	
	78.3	78.3	+0.0	
	100.7	101.0	+0.3	
	97.6	98.0	+0.4	
	119.8	119.8	+0.0	
	118.5	118.5	+0.0	
	130.9	131.3	+0.4	
	131.4	131.6	+0.2	

Note: This meter should be recalibrated within two years.

Environmental Conditions: T=21.8 C, P=738.1 Torr, RH=63 %

Calibrated by: James VanDamme, B.S.
Research Assistant
Accredited Dosimetry Calibration Laboratory

Reviewed by: Daniel R. Anderson, M.S.
Program Manager
Radiation Calibration Service

Report No. **DIA1926**

University of Wisconsin - Madison
Department of Medical Physics
Accredited Dosimetry Calibration Laboratory

Accredited Dosimetry Calibration Laboratory

This calibration is compliant with ISO/IEC 17025-1999 and ANSI/NCSL Z540-1-1994 standards, and is accredited by the AAPM and the American Association for Laboratory Accreditation.

ACCREDITED Certificate No: 1864.01

1530 Medical Sciences Center, 1300 University Ave., Madison, WI 53706
Office (608) 262-6320 Fax: (608) 262-5012

Report of Calibration for

Diagnostic Ionization Chamber

and Electrometer System

Submitted by:

James Schweitzer, Ph.D.
Purdue University
550 Stadium Mall Drive RM-B203
West Lafayette, IN 47907

Instruments:

MDH Radcal
Model 10x5-180
S/N 7565

MDH Radcal
Model 3036
S/N 36-0412

Date Received: 5/AUG/2005 Calibration Completed: 8/AUG/2005

This calibration is directly traceable to the National Institute of Standards and Technology (NIST). The expanded uncertainty of measurement as stated in the data page of this report is the standard uncertainty of measurement multiplied by the coverage factor k=2, which for a normal distribution corresponds to a coverage probability of approximately 95%.

Report No. **DIA1926**

University of Wisconsin - Madison
Department of Medical Physics
Accredited Dosimetry Calibration Laboratory

X-Ray Measurement Data

Calibration Completed: August 8, 2005

Report Date: August 9, 2005

Ionization Chamber
MDH Radcal
Model 10x5-180

Serial Number : 7565
Nominal Volume : 180cm^3
Type : Parallel Plate
Atmosphere Communication : Open

Electrometer used in Calibration
MDH Radcal Model 3036

Serial Number : 36-0412
Scale : Exposure
Range : R

Field Size	:	20 cm x 20 cm at 200 cm Source-Chamber Distance
Chamber Orientation	:	Serial Number toward beam
Chamber Reference Point	:	Center of chamber volume
Collecting Electrode Bias	:	Unknown
Charge Collected	:	Negative
Pre-Irradiation Leakage	:	None detected
Calibration Uncertainty	:	1.9 %

Beam Quality	Air Kerma Rate (mGy/s)	System Coeff. (R/Rdg)	Buildup Material
UW120-M	0.54	9.583×10^{-4}	None
UW80-M	0.47	9.739×10^{-4}	None

Comments: The reported calibration coefficients have been corrected to 22 °C and 760 mm mercury. Please refer to the appendix for a complete description of reported calibration coefficients.

Recorded in data book: XY-44 (139) Environmental Conditions: T=21.1 C, P=739.5 Torr, RH=57.4 %

Calibrated by: April A. Nunn, B.S.
Research Assistant
Accredited Dosimetry Calibration Laboratory

Reviewed by: Laboratory Director
or Designee

Report No. **DIA1925**

University of Wisconsin - Madison
Department of Medical Physics
Accredited Dosimetry Calibration Laboratory

Accredited Dosimetry Calibration Laboratory

This calibration is compliant with ISO/IEC 17025-1999 and ANSI/NCSL Z540-1-1994 standards, and is accredited by the AAPM and the American Association for Laboratory Accreditation.

ACCREDITED Certificate No: 1964.01

1530 Medical Sciences Center, 1300 University Ave., Madison, WI 53706
Office (608) 262-6320 Fax: (608) 262-5012

Report of Calibration for

Diagnostic Ionization Chamber

and Electrometer System

FILE COPY

Submitted by:

James Schweitzer, Ph.D.
Purdue University
550 Stadium Mall Drive RM-B203
West Lafayette, IN 47907

Instruments:

MDH Radcal
Model 30x6-11
S/N 231

MDH Radcal
Model 3036
S/N 36-0412

Date Received: 5/AUG/2005 Calibration Completed: 8/AUG/2005

This calibration is directly traceable to the National Institute of Standards and Technology (NIST). The expanded uncertainty of measurement as stated in the data page of this report is the standard uncertainty of measurement multiplied by the coverage factor k=2, which for a normal distribution corresponds to a coverage probability of approximately 95%.

Report No. **DIA1925**

University of Wisconsin - Madison
Department of Medical Physics
Accredited Dosimetry Calibration Laboratory

X-Ray Measurement Data

Calibration Completed: August 8, 2005 Report Date: August 9, 2005

Ionization Chamber
MDH Radcal
Model 30x6-11

Serial Number : 231
Nominal Volume : 11 cm^3
Type : Parallel Plate
Atmosphere Communication : Open

Electrometer used in Calibration
MDH Radcal Model 3036

Serial Number : 36-0412
Scale : Exposure
Range : R

Field Size	:	20 cm x 20 cm at 200 cm Source-Chamber Distance
Chamber Orientation	:	Random
Chamber Reference Point	:	Center of chamber volume
Collecting Electrode Bias	:	Unknown
Charge Collected	:	Negative
Pre-Irradiation Leakage	:	None detected
Calibration Uncertainty	:	1.9 %

Beam Quality	Air Kerma Rate (mGy/s)	System Coeff. (R/Rdg)	Buildup Material
UW120-M	0.54	0.979	None
UW80-M	0.47	0.997	None

Comments: The reported calibration coefficients have been corrected to 22 °C and 760 mm mercury. Please refer to the appendix for a complete description of reported calibration coefficients.

Recorded in data book: XY-44 (136) Environmental Conditions: T=21.1 C, P=740.2 Torr, RH=57.4 %

Calibrated by: April A. Nunn, B.S.
Research Assistant
Accredited Dosimetry Calibration Laboratory

Reviewed by: Laboratory Director
or Designee

Certificate of Irradiation

COPY

				Report Number:	IRR0743
Date Received:	11/Jul/2005	Date Irradiated:	11/Jul/2005		Page 3 of 3
Material Irradiated:	TLD Chips				
Customer:	Joe Silvers, Clinical Engineering, Health Sciences, Purdue University				
Source:	X-Ray	Source Manufacturer:	Advanced X-Ray, Inc.		
Irradiation Distance:	100 cm	Entrance Build-Up Material:	None		
Field Size:	10cm x 10cm	Temperature:	20.8 °C		

Irradiation Data

Sample [illegible]	Radiation Start	Radiation Time	[illegible]	[illegible]	[illegible]
Group B1 - M100	12:44:00 PM	12:53:04 PM	9.06	1.000	1.84
Group B2 - M120	1:00:00 PM	1:07:39 PM	7.65	1.000	2.18
Group B3 - M150	1:14:00 PM	1:22:23 PM	8.38	1.000	1.99

Comments: The TLDs listed in this report were irradiated to an Air Kerma (Ka) of 1 Gy. The TLDs were exposed on a 5 cm PMMA phantom, which requires application of a backscatter factor to determine dose of interest. Please refer to Table 2 of HPS N13.11-1993 for further details on dose calculation. The delivered air kerma during each irradiation is believed to be accurate to within +/- 2.5% at the 95% confidence interval.

Irradiated By: Cliff Hammer, B.A.
Instrumentation Specialist
Radiation Calibration Laboratory

Reviewed By: Keith A Kunugi, MBA
Associate Director
Radiation Calibration Laboratory

Certificate of Irradiation

COPY

Date Received:	11/Jul/2005	Date Irradiated:	11/Jul/2005	Report Number: IRR0743

Material Irradiated:	TLD Chips		
Customer:	Joe Silvers, Clinical Engineering, Health Sciences, Purdue University		
Source:	Cobalt 60	Source Manufacturer:	AECL El-Dorado 78
Irradiation Distance:	100 cm	Build-up Material:	5.4 mm lucite plates of density 1.176 g/ml
Field Size:	20cm x 20cm	Temperature:	22.1 °C
Exposure Rate (in air) (R/min.):	126.24	Dose Rate to Water (Gy/min.):	1.26

Irradiation Data

Sample Description	Irradiation Start Time	Irradiation Stop Time	Irradiation Time (min)	Dose Delivered to Water (Gy)
Group A	2:50:00 PM	2:50:47 PM	0.78	0.999

Comments: The sample(s) listed in this report were irradiated between two 10 x 10 cm x 5.4 mm PMMA plates. The total dose to water delivered during the irradiation is believed to be accurate to within +/- 2.5% at the 95% confidence interval.

Irradiated by: Cliff Hammer, B.A.
Instrumentation Specialist
Radiation Calibration Laboratory

Reviewed by: Keith A Kunugi, MBA
Associate Director
Radiation Calibration Laboratory

Certificate of Irradiation

COPY

Date Received: 11/Jul/2005 Date Irradiated: 11/Jul/2005 Report Number: IRR0743

Material Irradiated: TLD Chips

Customer: Joe Silvers, Clinical Engineering, Health Sciences, Purdue University

Source: Cs137 Source Manufacturer: Hopewell Designs, Inc.

Irradiation Distance: 100 cm Entrance Build-Up Material: 2.5 mm lucite plates of density 1.176 g/ml

Field Size: 10cm x 10cm Temperature: 22.3 °C

Irradiation Data

[illegible]	[illegible] Irradiation Start Time	[illegible] Irradiation Stop Time	[illegible] Irradiation Time (min)	[illegible] Air Kerma (Gy)	[illegible] Air Kerma Rate (Gy/min)
Group C	2:17:00 PM	3:25:24 PM	68.40	1.000	0.8775

Comments: The TLDs listed in this report were irradiated to an Air Kerma (Ka) of 1 Gy. The TLDs were exposed on a 5 cm PMMA phantom, which requires application of a backscatter factor to determine dose of interest. Please refer to Table 2 of HPS N13.11-1993 for further details on dose calculation. The delivered air kerma during the irradiation is believed to be accurate to within +/- 2.5% at the 95% confidence interval.

Irradiated By: Cliff Hammer, B.A.
Instrumentation Specialist
Radiation Calibration Laboratory

Reviewed By: Keith A Kunugi, MBA
Associate Director
Radiation Calibration Laboratory

D. Dose Volume Histograms for the Faxitron Broad- and Milli- beams

This appendix provides the details of the DVH plots obtained while irradiating EBT GafChromic film with the 130 kVp Faxitron for 2 minutes (for the unfiltered beam) and 59 minutes and 59 seconds (for the 0.4 mm Cu-filtered beam). Table D.1 provides a summary of the mean absorbed dose for the filtered and unfiltered x-rays. For more information on the beam configurations, refer to Chapter 4, Section 4.2.

Table D.1: Summary of mean absorbed dose imparted for filtered and unfiltered beam.

	Unfiltered Beam		
Position	D_{avg} (Gy)	$\dot{D}_{avg}$ (Gy/h)	S.D. (Gy/h)
A1	2.836	85.08	4.929
A2	2.095	62.86	10.089
A3	2.185	65.55	10.541
A4	2.974	89.23	5.708
A5	1.523	45.68	41.225
B1	3.132	93.96	4.938
B2	1.867	56.01	7.065
B3	1.952	58.55	6.569
B4	3.140	94.19	5.458
B5	0.007	0.22	0.123
C1	2.046	61.37	3.464
C2	1.118	33.54	4.468
C3	1.174	35.22	3.876
C4	1.948	58.45	3.122
C5	0.010	0.30	0.124
D1	1.035	31.04	3.767
D2	0.572	17.16	2.787
D3	0.638	19.13	3.218
D4	1.034	31.01	4.119
D5	0.013	0.38	0.175

	0.4 mm Cu filtered beam		
Position	D_{avg} (Gy)	$\dot{D}_{avg}$ (Gy/h)	S.D. (Gy/h)
E1	1.712	1.712	0.045
E2	1.668	1.668	0.060
E3	1.762	1.763	0.063
E4	1.752	1.753	0.043
E5	1.657	1.657	0.063
F1	1.766	1.767	0.038
F2	1.657	1.657	0.041
F3	1.721	1.721	0.060
F4	1.750	1.751	0.088
F5	0.067	0.067	0.014
G1	1.730	1.730	0.049
G2	1.622	1.622	0.044
G3	1.687	1.687	0.054
G4	1.723	1.724	0.088
G5	0.080	0.080	0.015
H1	1.713	1.714	0.053
H2	1.624	1.624	0.044
H3	1.674	1.675	0.055
H4	1.689	1.689	0.088
H5	0.092	0.092	0.015

Dose-Volume Histograms

DVH plots were employed below to describe the energy deposition for irradiation configurations A through H (refer to Chapter 4, Table 4.3).

Configuration A: DVH for the unfiltered 130 kVp broad beam (no culture medium)

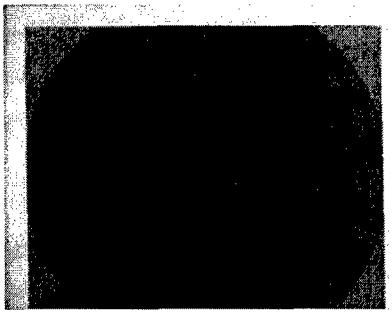

Figure D.1: Irradiation patterns produced on the EBT film by the 130 kVp broad beam with no filtration (Configuration A, no shield or culture medium) during a 2-minute irradiation.

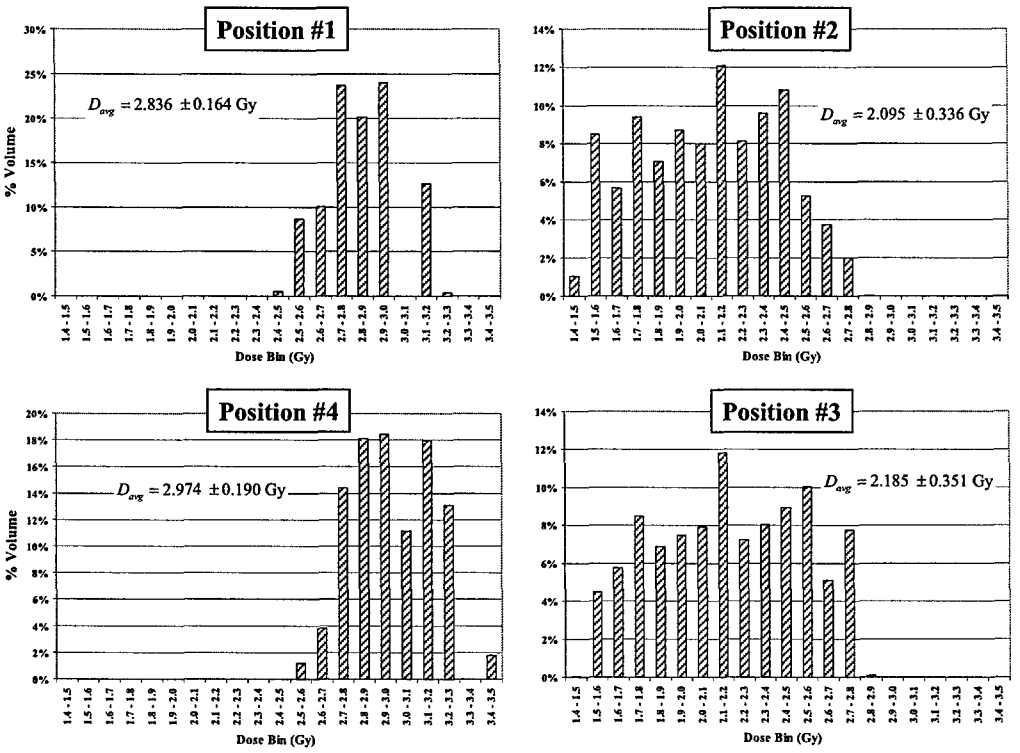

Figure D.2. DVH for the unfiltered x-ray broad beam (Configuration A, no culture medium). A nominal 2.52 ±0.09 Gy dose (in water) was delivered to the center of the 130 kVp Faxitron broad beam during a 2-minute irradiation. Values for mean absorbed dose (in water) and standard deviation at each position are reported in the figure.

Configuration B: DVH for the unfiltered 130 kVp millibeam (no culture medium)

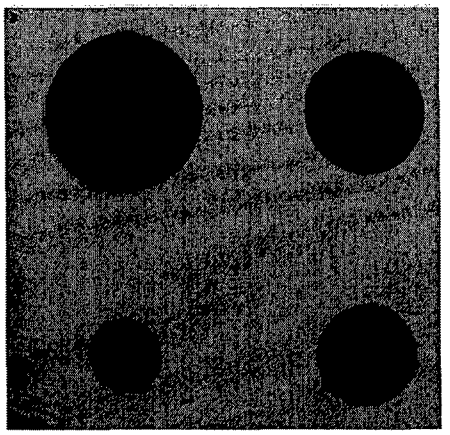

Figure D.3: Irradiation patterns produced on the EBT film by the 130 kVp millibeam with no filtration (Configuration B, no culture medium) during a 2-minute irradiation.

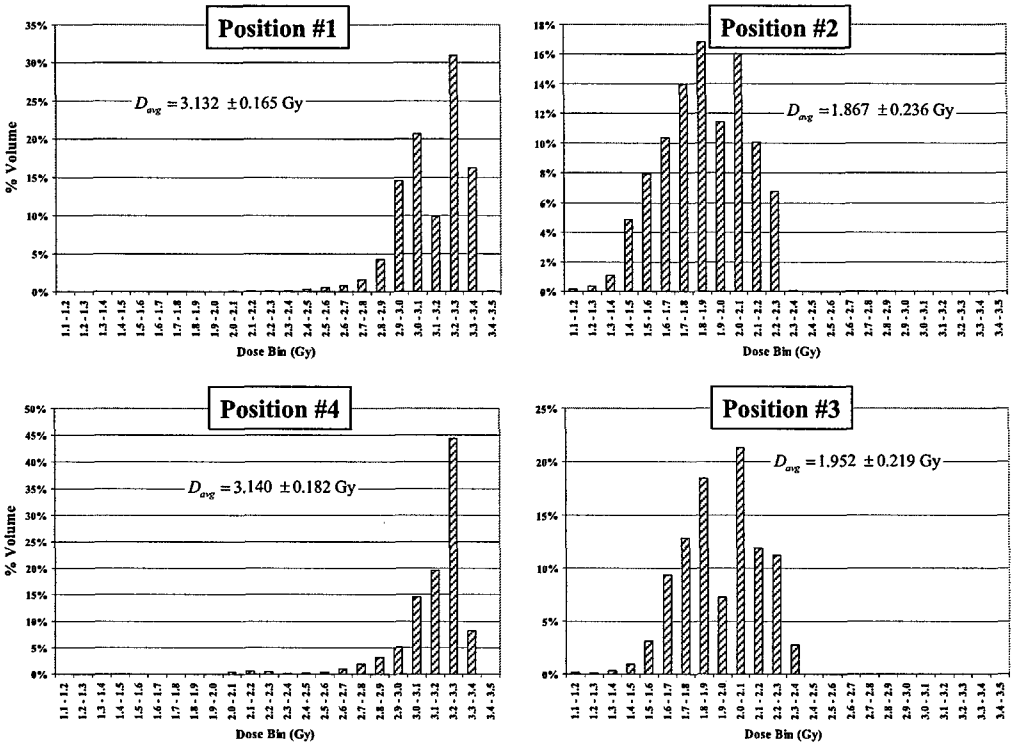

Figure D.4: DVH for the unfiltered x-ray millibeam (Configuration B) for a 2-minute irradiation (130 kVp, 3 mA).

Configuration C: DVH for the unfiltered 130 kVp millibeam (empty Petri dish)

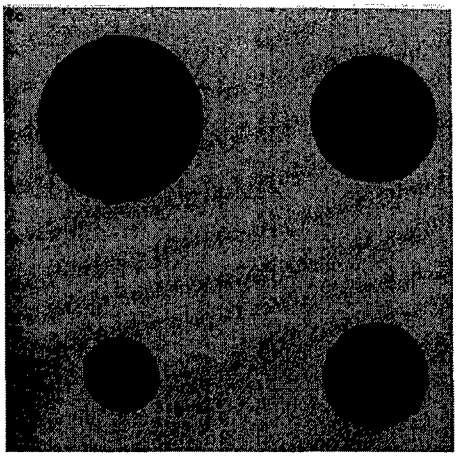

Figure D.5: Irradiation patterns produced on the EBT film by the 130 kVp millibeam with no filtration (Configuration C, empty Petri dish) during a 2-minute irradiation.

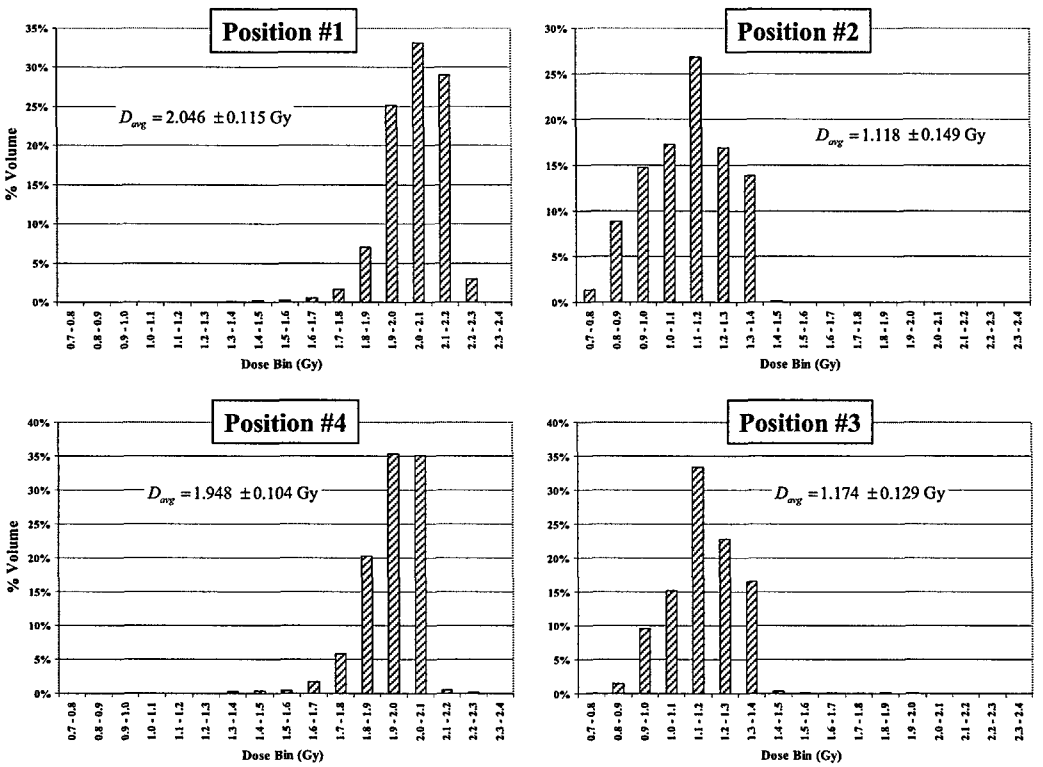

Figure D.6: DVH for the unfiltered x-ray millibeam (Configuration C) for a 2-minute irradiation (130 kVp, 3 mA).

Configuration D: DVH for the unfiltered 130 kVp millibeam (with culture medium)

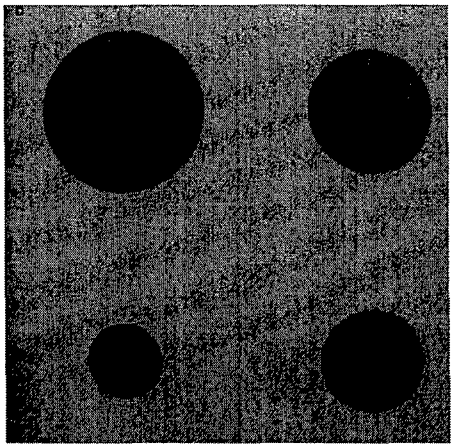

Figure D.7: Irradiation patterns produced on the EBT film by the 130 kVp millibeam with no filtration (Configuration D, with culture medium) during a 2-minute irradiation.

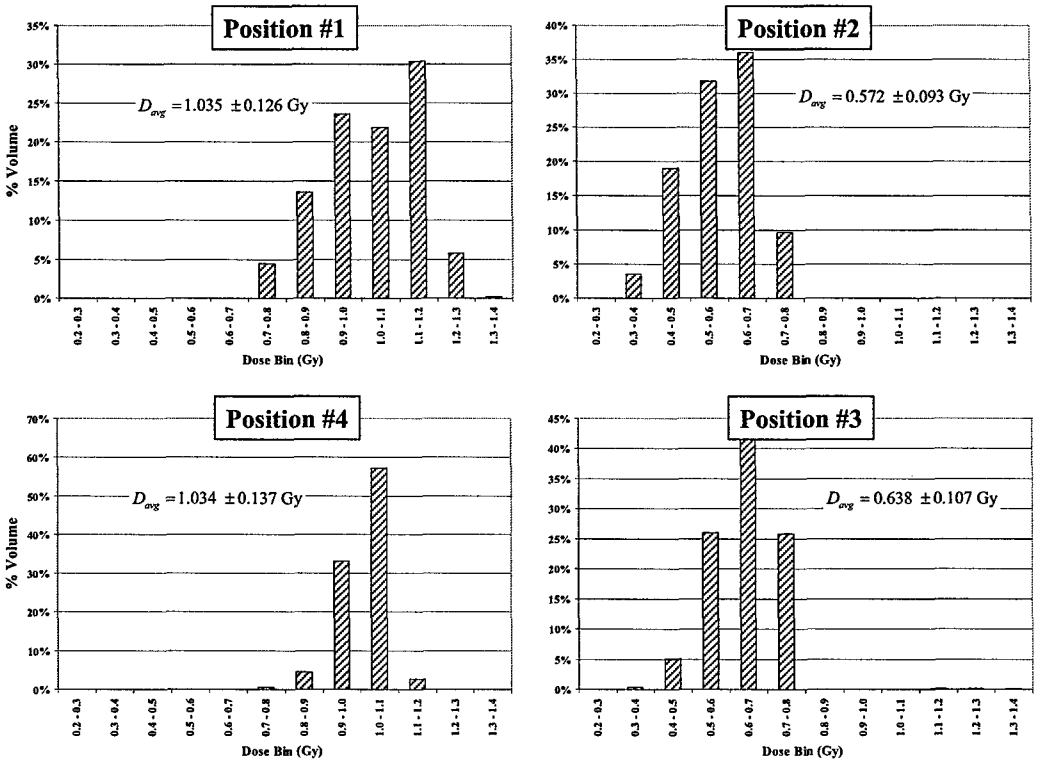

Figure D.8: DVH for the unfiltered x-ray millibeam (Configuration D, with 1.64 mm culture medium, i.e., water). A nominal 0.956 ±0.0341 Gy dose (in water) was delivered to the center of the 130 kVp Faxitron beam during a 2-minute irradiation (62.11% attenuation through dish and water). Values for mean absorbed dose (in water) and standard deviation at each position are reported in the figure.

Configuration E: DVH for the Cu filtered 130 kVp broad beam (no culture medium)

Figure D.9: Irradiation patterns produced on the EBT film by the 130 kVp broad beam with 0.4 mm Cu filtration (Configuration E, no culture medium) during a 59-minute and 59-second irradiation.

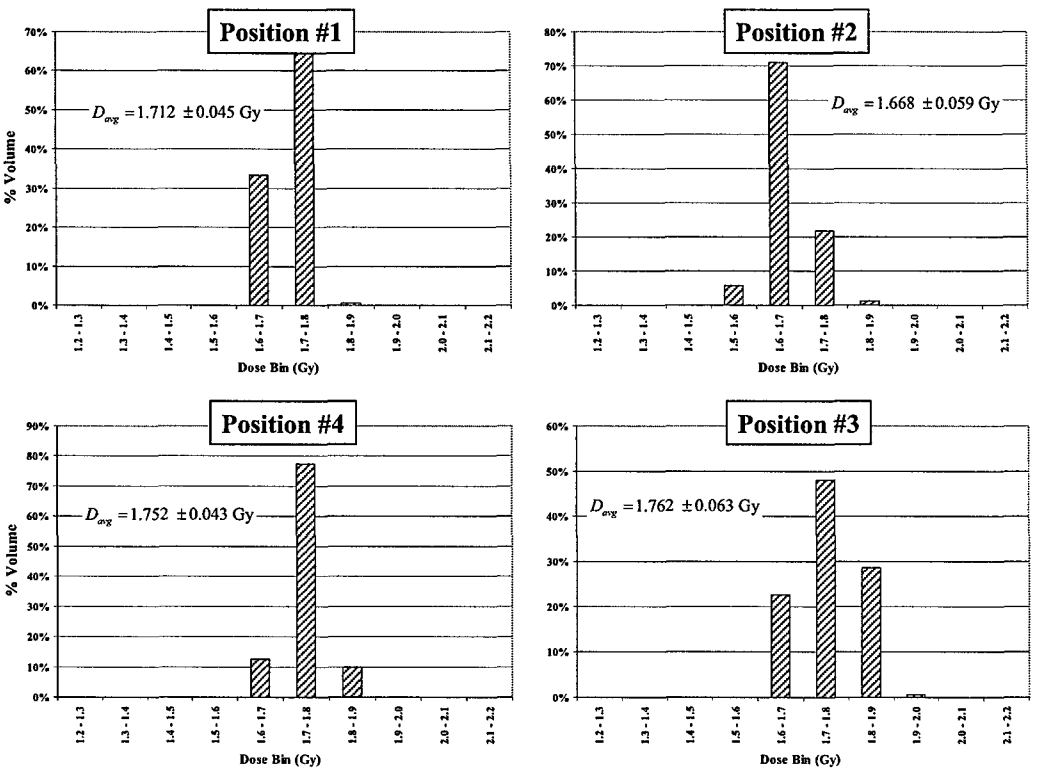

Figure D.10: DVH for the Cu filtered x-ray broad beam (Configuration E, no culture medium). A nominal 1.72 ±0.074 Gy dose (in water) was delivered to the center of the 130 kVp Faxitron beam during a 59-minute 59-second irradiation. Values for mean absorbed dose (in water) and standard deviation at each position are reported in the figure.

Configuration F: DVH for the Cu filtered 130 kVp millibeam (no culture medium)

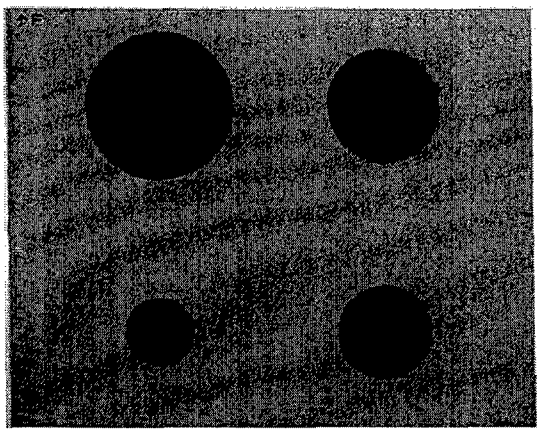

Figure D.11: Irradiation patterns produced on the EBT film by the 130 kVp millibeam with 0.4 mm Cu filtration (Configuration F, no culture medium) during a 59-minute and 59-second irradiation.

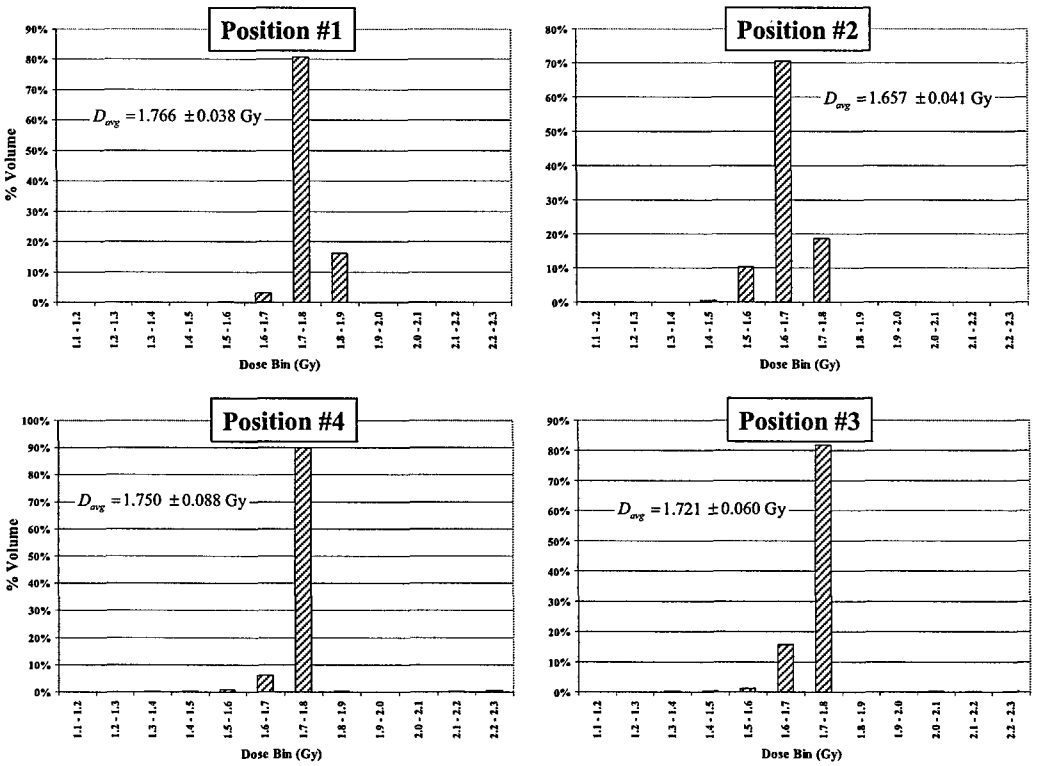

Figure D.12: DVH for the Cu filtered x-ray millibeam (Configuration F) for a 59-minute and 59-second irradiation (130 kVp, 3 mA).

Configuration G: DVH for the Cu filtered 130 kVp millibeam (empty Petri dish)

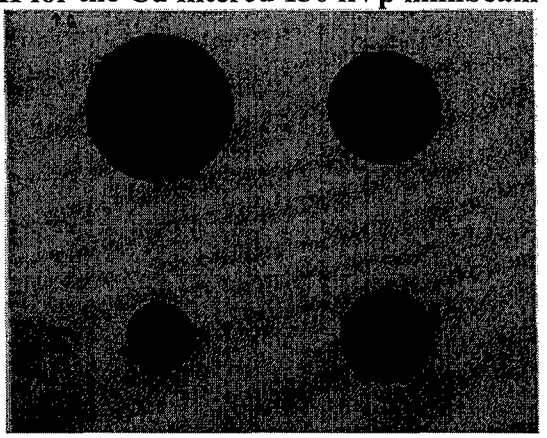

Figure D.13: Irradiation patterns produced on the EBT film by the 130 kVp millibeam with 0.4 mm Cu filtration (Configuration G, empty Petri dish) during a 59-minute and 59-second irradiation.

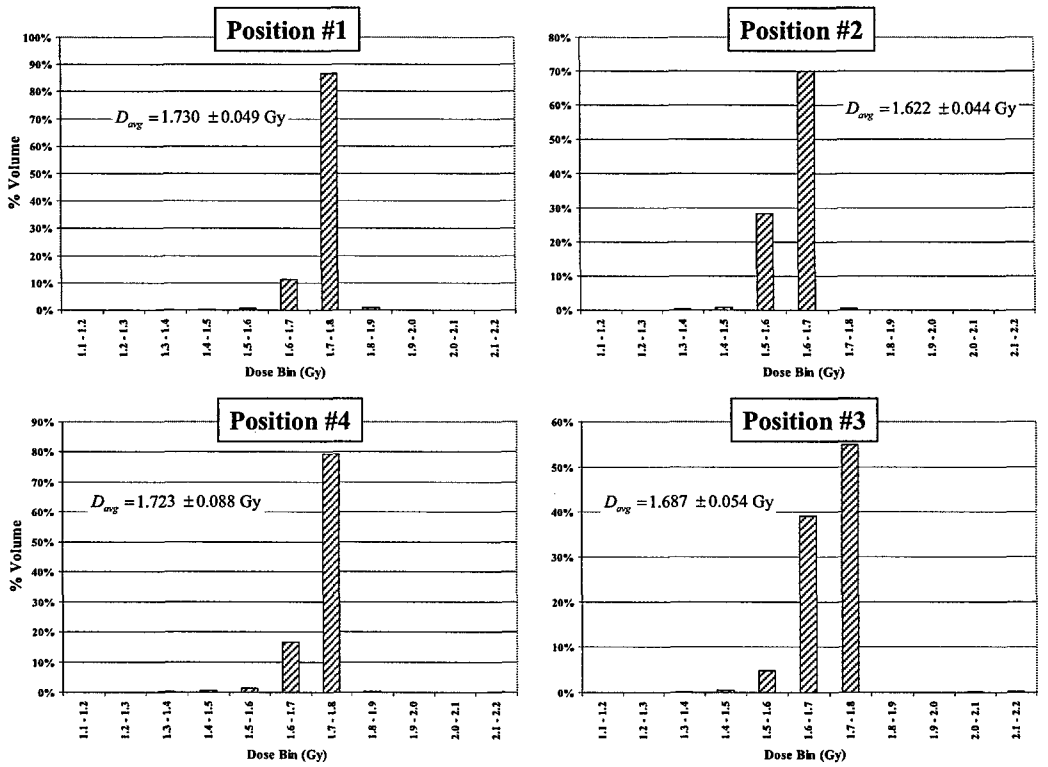

Figure D.14: DVH for the Cu filtered x-ray millibeam (Configuration G) for a 59-minute and 59-second irradiation (130 kVp, 3 mA).

Configuration H: DVH for the Cu filtered 130 kVp millibeam (with culture medium)

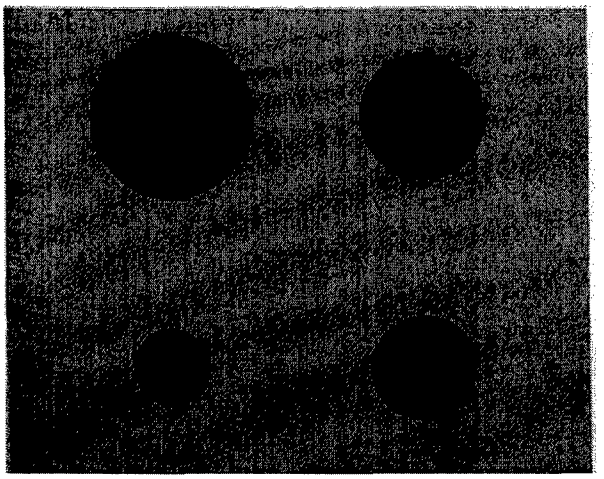

Figure D.15: Irradiation patterns produced on the EBT film by the 130 kVp millibeam with 0.4 mm Cu filtration (Configuration H, with culture medium) during a 59-minute and 59-second irradiation.

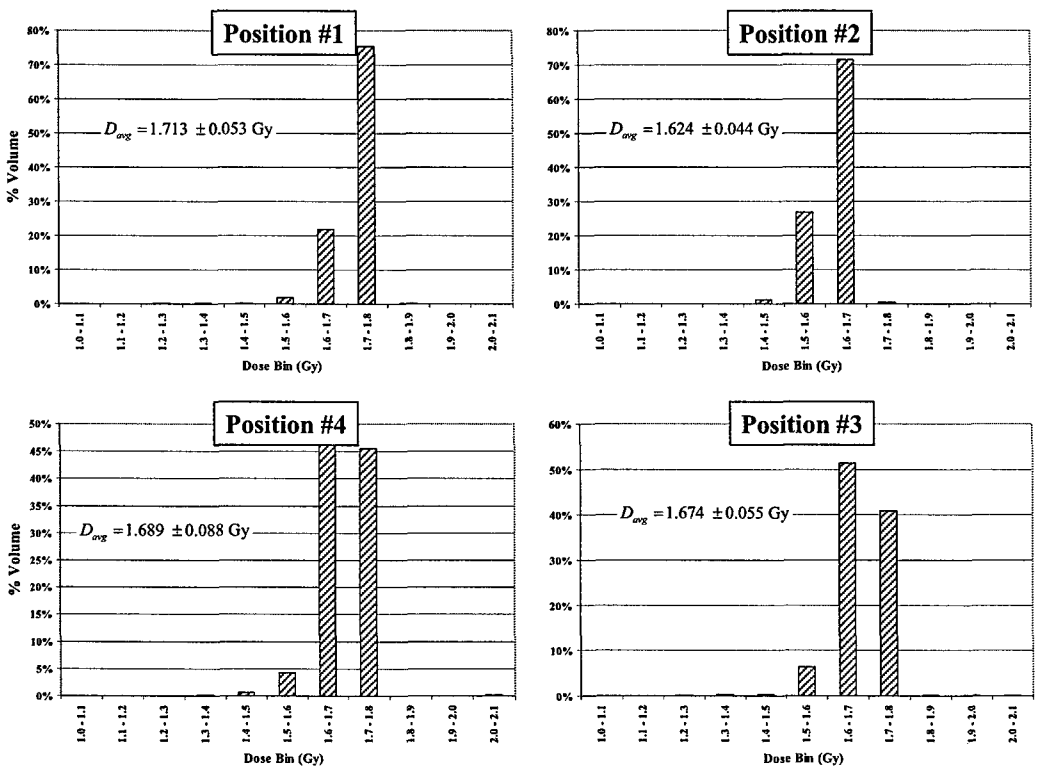

Figure D.16: DVH for the Cu filtered x-ray millibeam (Configuration H, with 1.64 mm culture medium, i.e., water). A nominal 1.684 ±0.073 Gy dose (in water) was delivered to the center of the 130 kVp Faxitron beam during a 59-minute 59-second irradiation (2.32% attenuation through dish and water). Values for mean absorbed dose (in water) and standard deviation at each position are reported in the figure.